ANL/NSE-22/27

Analysis of HolosGen Sub-Scale Simulator with Plant Dynamics Code

Nuclear Science and Engineering Division

About Argonne National Laboratory
Argonne is a U.S. Department of Energy laboratory managed by UChicago Argonne, LLC under contract DE-AC02-06CH11357. The Laboratory's main facility is outside Chicago, at 9700 South Cass Avenue, Lemont, Illinois 60439. For information about Argonne
and its pioneering science and technology programs, see www.anl.gov.

DOCUMENT AVAILABILITY

Online Access: U.S. Department of Energy (DOE) reports produced after 1991 and a growing number of pre-1991 documents are available free at OSTI.GOV (http://www.osti.gov/), a service of the US Dept. of Energy's Office of Scientific and Technical Information.

Reports not in digital format may be purchased by the public from the National Technical Information Service (NTIS):

U.S. Department of Commerce
National Technical Information
Service 5301 Shawnee Rd
Alexandria, VA 22312
www.ntis.gov
Phone: (800) 553-NTIS (6847) or (703) 605-6000
Fax: (703) 605-6900
Email: **orders@ntis.gov**

Reports not in digital format are available to DOE and DOE contractors from the Office of Scientific and Technical Information (OSTI):

U.S. Department of Energy
Office of Scientific and Technical Information
P.O. Box 62
Oak Ridge, TN 37831-0062
www.osti.gov
Phone: (865) 576-8401
Fax: (865) 576-5728
Email: **reports@osti.gov**

ANL/NSE-22/27

Analysis of HolosGen Sub-Scale Simulator with Plant Dynamics Code

Anton Moisseytsev, Brent Patrick Hollrah
Nuclear Science and Engineering Division
Argonne National Laboratory

Claudio Filippone
HolosGen LLC

May 27, 2022

ABSTRACT

The Subcritical Power Module Sub-scale Simulator (SPM-SS) has been designed and constructed by HolosGen LLC under the ARPA-E MEITNER program to simulate the thermal-hydraulic and heat transfer behavior of the full-scale Holos-Quad Subcritical Power Modules (SPMs). Four coupled SPMs, each rated at 5.5MW, form the Holos-Quad gas-cooled microreactor design. The SPM-SS represents a substantially scaled-down system with a power rating less than 40 kW, equipped with an electrically heated fuel cartridge heat exchanger, an electrically heated compressor heat exchanger, and a valve actuated turbine heat exchanger, in addition to a recuperator and a cooler heat exchanger. The fuel cartridge represents a portion of the full-scale SPM core, the compressor heat exchanger mimics the temperature changes resulting from the compressor's turbomachinery inefficiencies, the turbine heat exchanger mimics the expansion process normally occurring through the turbine, while the recuperator and cooler heat exchangers complete the subscale simulator loop. The heaters equipping the fuel cartridge and the compressor heat exchangers are electronically controlled to simulate normal and off-normal SPM operating conditions. The full-scale Holos-Quad SPM design eliminates the traditional balance of plant and executes thermal-to-electric energy conversion by means of an intercooled Brayton cycle with decoupled compressor-turbine turbomachinery. The Holos-Quad full-scale design is equipped with a multi-stage axial Low- and High-Pressure compressor, and a multistage axial turbine. The SPM-SS is designed for testing and validation of selected components which are instead coupled by a traditional balance of plant. The SPM-SS is not equipped with turbomachinery (compressor and turbine) as the development of these components were excluded from the scope of work under the ARPA-E MEITNER funding program. The SPM-SS balance of plant enables modifications, replacement and testing of individual components with different working fluids and is designed to include the turbo-machinery components that will be developed in future research . The SPM-SS can be operated with different gases, variable mass-flow-rates, pressures, and temperatures to obtain test data for selected components, whose performance can be scaled to validate the computer model of the full-scale SPM at various conditions (e.g., start-up, transients conditions). The SPM-SS can operate at the maximum Holos-Quad design pressure of 7 MPa, and a maximum temperature limited to 650 °C by the electrical heaters. Several SPM-SS tests have been conducted and analyzed with the Plant Dynamics Code (PDC) developed at the Argonne National Laboratory (ANL). These tests aimed at validating the PDC modeled predictions of the full-scale Holos-Quad design with data from selected SPM-SS components. In order to address SPM-SS specific characteristics, such as components heat losses and absence of turbomachinery components, some modifications to the PDC have been implemented to factor the design differences from the full-scale Holos-Quad SPM to the SPM-SS. As the PDC offers capabilities to analyze systems with different working fluids, air, nitrogen, and helium were utilized as the SPM-SS working fluids. Air was utilized to fine-tune the SPM-SS Systems Structures and Components (SSCs), nitrogen was utilized to pressure test the SPM-SS loop at the SPMs design maximum pressure of 7MPa. Helium was utilized as the working fluid circulating through the SPM-SS SSCs for specific tests to validate the PDC predictions of the fuel cartridge heat exchanger. SPM-SS tests data were also analyzed with both the steady-state and transient analysis capabilities offered by the PDC.

This report describes the PDC analysis of the SPM-SS tests data, including the necessary code modifications and comparison of the code results with the experimental data. Based on the results, a discussion is presented on how the analysis supports design and transient calculations of the full-scale Holos-Quad microreactor. Also based on the results of this work, recommendations are made for future optimizations of the SPM-SS components and PDC model development needs.

TABLE OF CONTENTS

1 Introduction

The thermal-hydraulic analysis of the Holos-Quad microreactor design performed under the HolosGen-ARPA-E MEITNER project [1] involved the design calculations of the helium Brayton cycle [2] as well as the transient calculations of the load following analysis [3]. Both these sets of calculations were carried out using the Plant Dynamics Code (PDC) [4] developed at the Argonne National Laboratory. The PDC was originally developed to model steady-state and transient analysis of supercritical carbon dioxide (sCO_2) Brayton cycles. During the code development, a significant effort was devoted to validation of the code models. Because the primary application of the PDC was focused on sCO_2 cycles, code validations were based on testing of components and loops designed to operate with carbon dioxide as working fluid [5-12].

In order to validate the PDC features specific for the Holos-Quad design, whose working fluid is helium, the Subcritical Power Module Sub-scale Simulator (SPM-SS), has been designed to operate with helium at the full-scale Holos-Quad design pressure ratios.

Figure 1.1 shows a perspective rendered view of the full-scale Holos-Quad micro-reactor formed by four coupled SPMs fitting within the dimensional constraints of a shipping ISO container, and a semi-transparent view of a single SPM, illustrating the layout of the main Brayton cycle components integrated with the Fuel Cartridge.

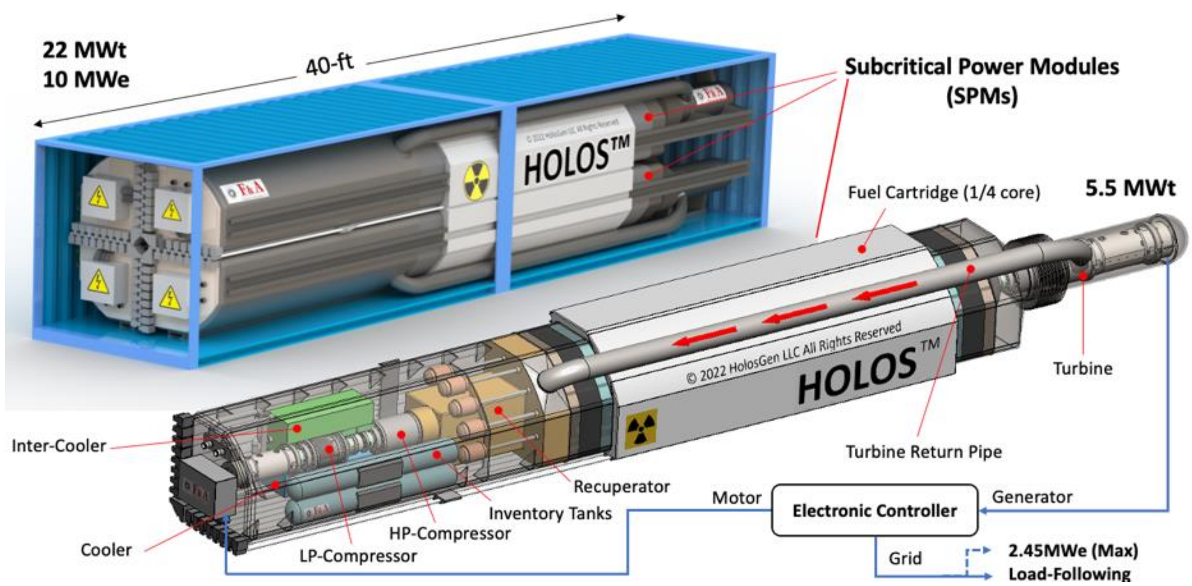

Figure 1.1. HolosGen Holos-Quad 10MWe Microreactor and SPM Internals.

Figure 1.2 shows the top-views of the main SPM-SS Systems Structures and Components (SSCs) with the layout of main components, including the locations for instrumentation and data sampling utilized for comparisons with the PDC predictions. Figure 1.3 shows the operational SPM-SS loop with the balance of plant and components thermally insulated to lower components heat losses with the surrounding environment. The thermal-hydraulic parameters utilized during operations at full SPM-SS design conditions are shown in Figure 1.4. The SPM-SS SSCs form a thermal-hydraulic loop whose specific characteristics and effect on the PDC validation activities are discussed below.

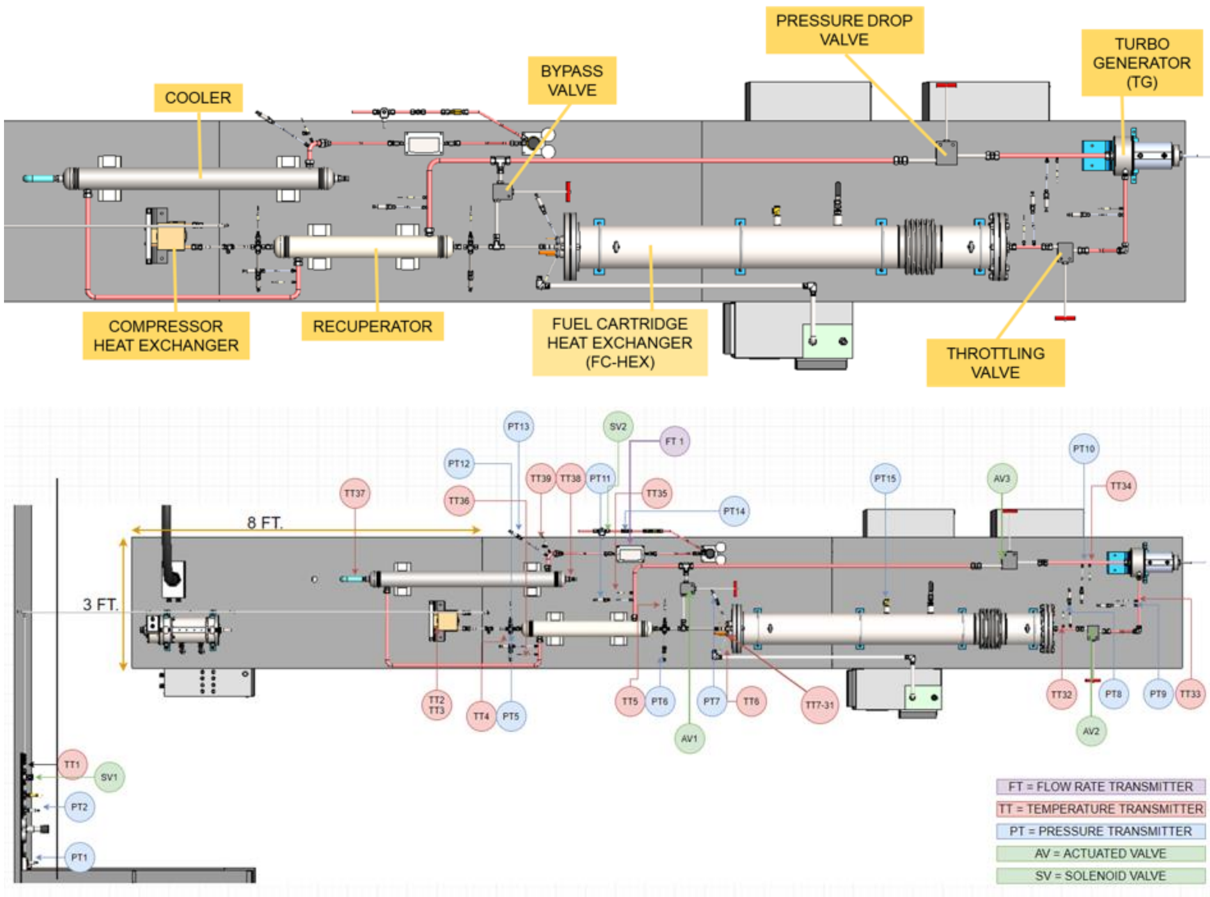

Figure 1.2. HolosGen Subcritical Power Module Sub-scale Simulator (SPM-SS).

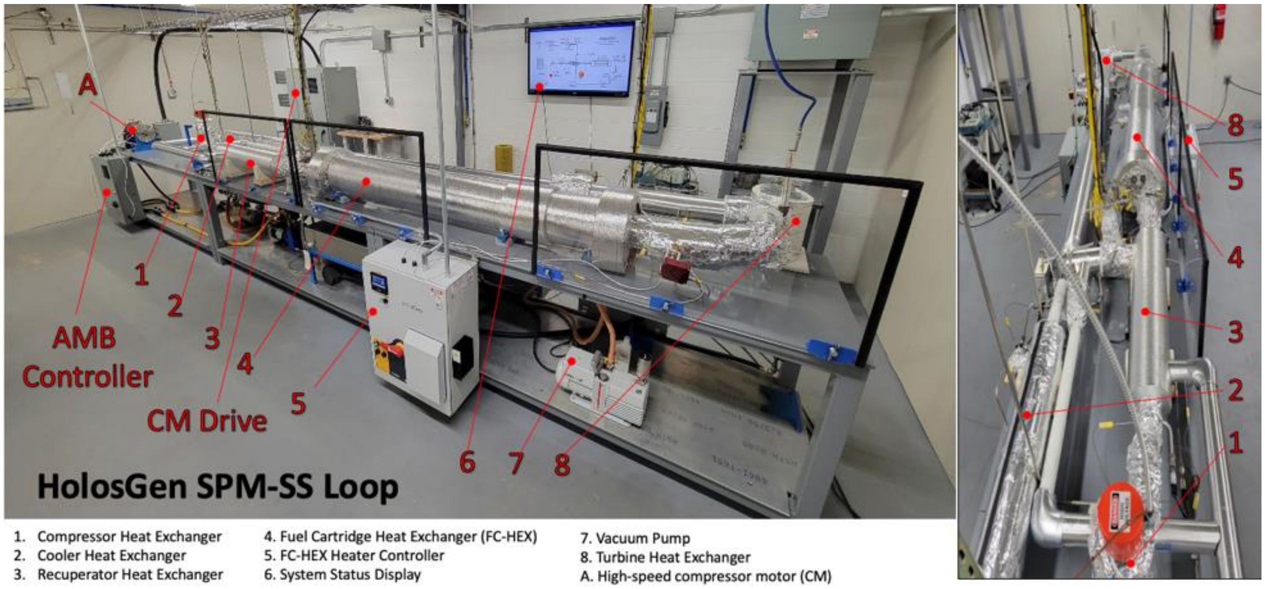

Figure 1.3. Photograph of the SPM-SS Operated at HolosGen's Test Facility.

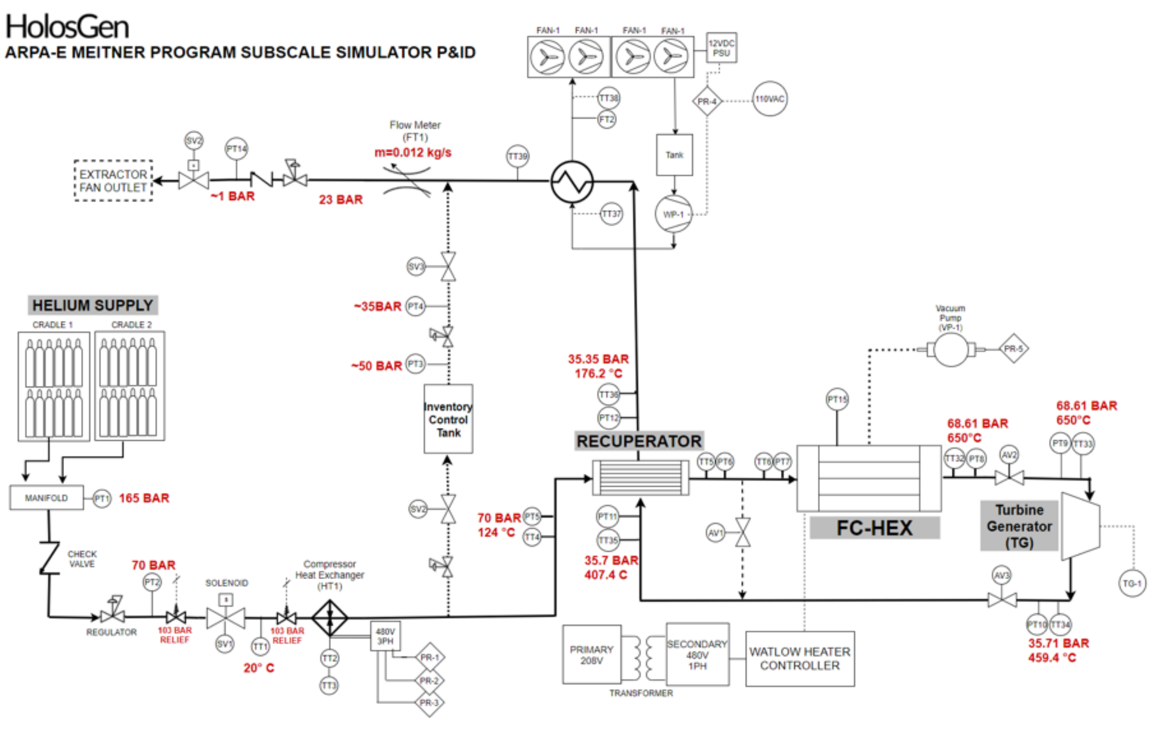

Figure 1.4. P&ID of the SPM-SS Loop with Operational Parameters.

1.1 Subcritical Power Module Sub-scale Simulator Specifics

The SPM-SS SSCs design utilizes off-the-shelf equipment and custom-made components thermal-hydraulically coupled by a traditional balance of plant formed by high-pressure tubing interconnected by pressure fittings. The SPM-SS is equipped with electronic controllers, networks of sensors and computer interfaces to regulate the electric power supplied to the heaters embedded with the FC HEX and the compressor heat exchanger. The electronic controllers regulate and monitor the actuation of sets of the high-pressure and high-temperature valves also shown in Figure 1.4. These valves can be actuated to configure the SPM-SS prior to executing tests, or during operations to simulate, for example, loss of coolant accident scenarios, increased backpressure through selected components (e.g., at the surrogate turbine discharge). The Turbine Generator (TG) shown in Figure 1.2 and Figure 1.4 was initially equipping the SPM-SS. This component was formed by an off-the-shelf micro-turbine coupled to a high-speed motor/generator actively cooled by a water-jacket. After a series of initial SPM-SS tests, it was determined that the heat losses represented by heat conduction between the subscale turbine volute and the water-cooled motor/generator complicated PDC predictions validations. Additionally, the TG motor/generator was operated at the full Brayton cycle pressure of 7 MPa which caused challenges for power and data cables crossing the TG pressure boundary. To increase data sampling accuracy in the components coupled to the TG, and decrease heat losses, the TG assembly was replaced by the turbine heat exchanger (component 8, Figure 1.3), which simulates the working fluid thermodynamic conditions as it were expanding through turbomachinery. The Compressor Motor (CM) (A, Figure 1.3) was initially coupled to the SPM-SS loop. As for the full-scale SPM design, the CM was equipped with active magnetic bearings (AMBs). For the purposes of SPM-SS testing this component was coupled to two full-scale compressor blisks. The CM and the radial and thrust AMBs were tested and successfully operated as part of the ARPA-E project milestones. Due to COVID 19 pandemic impact on the project schedule, especially for long-lead components of the compressor assemblies, CM and blisks were replaced by a dedicated heat exchanger (“compressor heat exchanger” 1, Figure 1.3). This component simulates the thermodynamic states occurring to the working fluid as it undergoes compression. The full development of turbomachinery for the SPM-SS compressor and turbine was excluded from the project mainly due to poor scalability of these components from sub-scale SPM rated at 40kW to full-scale SPM rated at 5.5MW. The SPM-SS can switch working fluid by actuating selected valves to isolate portions of the balance of plant to generate vacuum (7, Figure 1.3) and recharge portions of the balance of plant, or the whole SPM-SS loop, with a different gaseous working fluid. Overall, sets of actuated valves shown in Figure 1.4 and Figure 1.5 were controlled by a computer user interface (CUI) to configure the SPM-SS to mimic operational and off normal conditions of selected components forming the full scale SPM by simulating transient events, load-following with variable power-up/power-down ramp rates, passive and active decay heat removal, various types of loss of coolant accident scenarios, and station black out. Figure 1.5 shows various portions of the uninsulated balance of plant forming the SPM-SS. Figure 1.6 shows the complete SPM-SS loop, with equipment surrounded by thermal insulating materials, and the clustered tanks of working fluids (e.g., helium and nitrogen) utilized for testing.

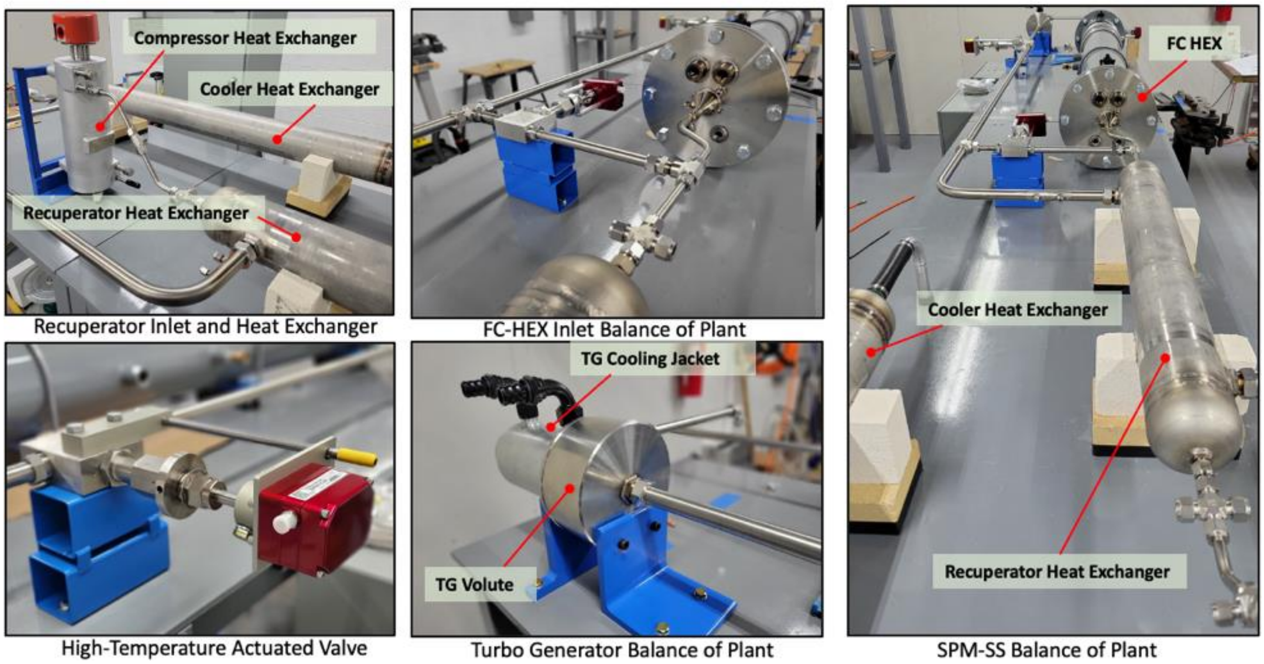

Figure 1.5. *SPM-SS* Balance of Plant.

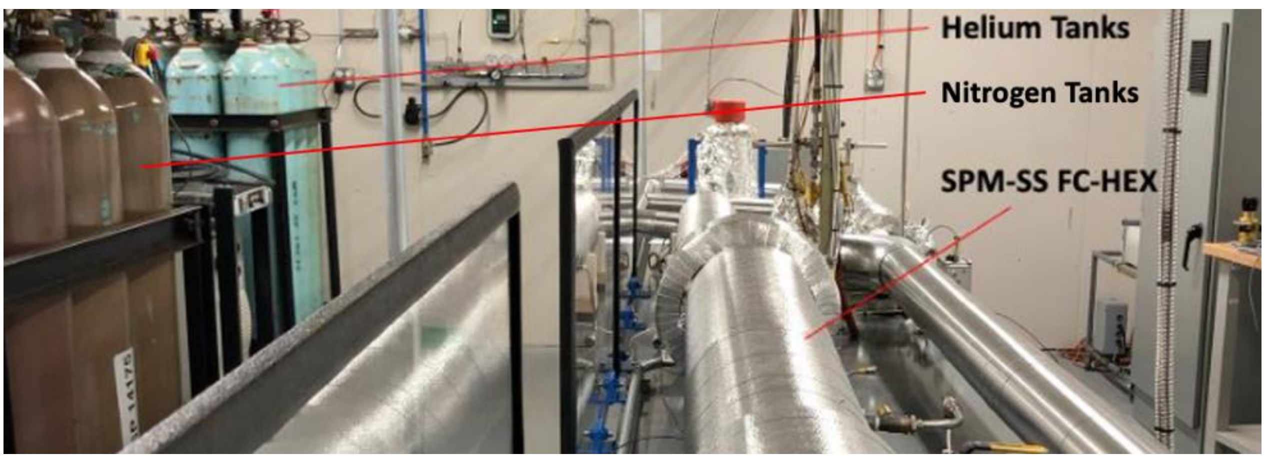

Figure 1.6. *SPM-SS* Multiple Working Fluids Capabilities.

Figure 1.7 provides a perspective view of the SPM-SS loop with detailed views of the high-speed Compressor Motor (CM), two full-scale stages of the axial compressor, and TG assemblies initially equipping the loop. The high-speed CM included Active Magnetic Bearings (AMBs). As it will be described in following sections, this component was designed, manufactured, and tested to demonstrate functionality of the AMBs. The two full-scale axial compressor blisks shown in this figure were also equipped with two radial and one thrust AMBs.

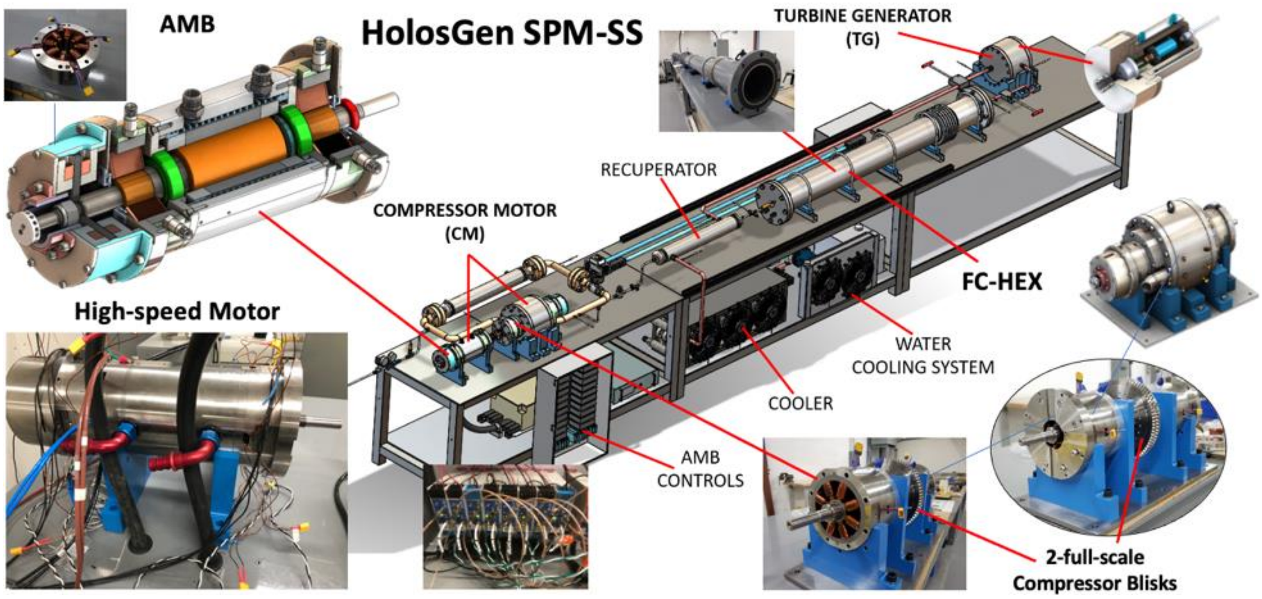

Figure 1.7. SPM-SS Components and Initial Layout.

The SPM-SS uses electrical heaters integrated with the Fuel Cartridge Heat Exchanger, also referred to as FC HX, to simulate heat generation from the nuclear fuel expected to be loaded in the full-scale SPM core. As actual nuclear fuel cannot be used for testing the subscale FC HX, the fuel performance modeling capability in PDC was not utilized, however, this has very little effect on validation of other microreactor components. The FC HX is formed by tubes through a graphite matrix comprising the electrical heaters as shown in Figure 2.2.

The simulator loop is designed for much lower power, 20 kW - 40 kW, compared to the full-scale Holos-Quad SPM rated at 5.5 MW. To keep the SPM-SS as representative as possible to the full-scale system, linear scaling with power is maintained whenever possible. For example, the number of "fuel" and coolant channels in the graphite matrix utilized as moderator is scaled linearly with power, while preserving the channel dimensions (diameters). The SPM-SS "core" graphite matrix structure is also scaled linearly. For practical reasons, the core length is reduced from 4 m to 2 m. The power scaling by itself does not present a challenge for the PDC validation, as the code results can be scaled with power and flow. However, as it will be discussed below, there are practical considerations that cannot be scaled linearly with power. The most important example of such constraints is the heat losses that represent a significantly higher portion than it would be in the full-scale 5.5MW SPM system.

Due to SPM-SS balance of plant material limitations and long lead time for high-temperature heaters, the loop maximum temperature was reduced from 850 °C, design max temperature for the full-scale Holos-Quad SPMs, to 650 °C. This change would be most noticeable for the validation of turbomachinery performance and the calculation of the cycle efficiency. However, under the ARPA-E project scope, turbomachinery and thermodynamic cycle performance of the SPM-SS was excluded, therefore, the PDC capabilities to analyze turbomachinery were not applied to the modeling of the SPM-SS. For all other SPM-SS components and loop characteristics, the effect of the reduced maximum temperature on the code validation is small. For example, a heat exchanger performance can mostly be scaled linearly with temperature change and temperature difference between two flows, rather than with the absolute temperature.

As part of the HolosGen-ARPA-E project, the high-speed motor with integrated AMBs was successfully tested and readied for coupling with two full-scale stages of the compressor turbomachinery components during the initial phases of the COVID 19 pandemic. As the project budget and schedule became gradually impacted by the pandemic, the design of the SPM-SS was simplified to eliminate high lead-time components, such as helium seals for the compressor. Therefore, the high-speed CM, coupled to the two-stage helium compressor, was bypassed, and helium (or other working fluids) was supplied to the loop at design pressure by clusters of high-pressure helium tanks as those shown in Figure 1.6. The CM and two-stage compressor were replaced by an electrically heated heat exchanger to simulate the working fluid heating resulting from compressor operations. Components by-passing or replacement in the SPM-SS balance of plant is relatively easy as the loop is equipped with flanges, ports, and pressure fittings enabling coupling/decoupling of all SPM-SS components forming various branches of the thermal-hydraulic loop.

These SPM-SS design simplifications induced limitation on the PDC predictions validation analyses. Operations of the SPM-SS two-stage compressor shown in Figure 1.7 would have enabled validation of the PDC compressor performance subroutines. Additionally, the compressor off-design performance drives the transient and control response of the cycle, as this component defines pressures and/or mass flow rate in the system.

As the helium compressor was bypassed and pressurized helium is provided by a fixed inventory of helium stored in high-pressure tanks, the SPM-SS operation with helium tests were conducted in an open loop configuration by actuating selected valves as shown in Figures 1.2 and 1.4. By configuring these valves, the SPM-SS loop can be closed or opened (e.g., by venting the working fluid via “Extractor Fan Outlet”). In the open loop configuration, helium is drawn from the supply tanks, flows through the loop once, and then is vented at atmospheric pressure. As a result, helium tests could only be executed for limited run time (e.g., proportional to the inventory stored in the tanks). As it will be shown in this report, this configuration combined with the relatively large thermal inertia represented by the SPM-SS SSCs significantly reduces the ability for the loop to reach equilibrium, thus validating the model predictions at steady-state becomes challenging. As PDC transient calculations start from steady-state conditions that define the initial conditions for the transient, the inability of establishing steady-state induces discrepancies in the transient analysis, as PDC transient calculations would start from conditions that may be different from those encountered in the tests. The effect of the difference will be discussed in the helium test analysis section of this report. On the other hand, the SPM-SS design modifications enabled the loop to run with different gases, including nitrogen and air. SPM-SS tests utilizing air as working fluid do not require supply tanks, thus these tests were run for extended time durations. When the SPM-SS was operated with compressed air, steady-state conditions could be achieved. Therefore, the validation of PDC transient analysis results was executed by operating the SPM-SS with air as working fluid. PDC predictions validation via comparison with the SPM-SS operated with air can then be extrapolated for helium by resetting the PDC to recalculate the model predictions with helium as working fluid.

In the initial SPM-SS tests, a surrogate non-optimized micro turbine was coupled to the loop (Turbine-Generator “TG”, Figures 1.2 and 1.4), however, as the SPM-SS power generation performance was excluded from the ARPA-E project scope and these components represented additional heat losses, these components were excluded from the SPM-SS loop. In later tests, the TG assembly was replaced with an air-cooled heat exchanger and a throttle valve to simulate the turbine inlet and discharge conditions. For these reasons, the SPM-SS turbine design and performance models are not considered in this work.

The full-scale Holos-Quad design uses diffusion bonded heat exchangers primarily for their compactness, effectiveness and integration capabilities within the Holos-Quad dimensional requirements represented by shipping ISO containers (see Figure 1.1). Scaling down these types of heat exchangers to the SPM-SS power rating required customization with costs and lead times for manufacturing that were beyond the scope of the project. As PDC can be configured to analyze the performance of different types of heat exchangers, the shell-and-tube heat exchanger types were adopted for the cooler and recuperator heat exchangers equipping the SPM-SS. Because the compact heat exchangers are not included in the SPM-SS testing, the models in PDC with the effect these types of heat exchangers would have on the cycle performance, both at the design conditions and in transients of the SPM-SS are not included in this work. However, PDC models of the shell-and-tube heat exchangers equipping the SPM-SS enabled validation of the PDC predictions with test data.

As mentioned above, the sub-scale loop is designed for much lower power rate compared to the full-scale system. At the SPM-SS power rating, the heat losses that could often be neglected in a full-size system become significant as they represent a much larger portion of the overall heat transfer rate. This is an unavoidable consequence of testing at the very low power rating of the SPM-SS. For the modeling validation effort, however, significant effort was spent on characterizing and simulating the heat losses in the test loop. Moreover, the heat losses for some components often could not be characterized (or derived) precisely from the test data itself, thus could not be fully simulated in the model. One such example, that will be discussed in the analysis section below, is a distribution of the heat loss in the SPM-SS FC HX in terms of losses in axial and radial directions. This distribution will play an important role in explaining this component axial temperature profiles. However, even if the PDC models were developed to account for these types of losses, they could not be properly simulated because the SPM-SS was not encapsulated within a controlled environment to measure heat transfer from each component to the surrounding environment.

It follows from the limitations of the SPM-SS test setup described above that *the primary focus of the PDC validation work presented in this report is centered on the Fuel Cartridge Heat Exchanger, as a surrogate for the full-scale SPM microreactor component, and the loop piping.*

1.2 Measurement Uncertainties

Table 1.1 presents measurement uncertainties for the sensors used in the sub-scale loop. The total values include the sensor uncertainty and the data acquisition system (DAQ) uncertainties. Figure 1.8 demonstrates the value of temperature uncertainty from Table 1.1 as a function of measured temperature. For practical reasons, the uncertainties will not be provided on the measured quantities plots when results of the PDC predictions are compared with test data. The uncertainties in temperature are small enough so the error bar would be about the size of the line thicknesses on the plots. Likewise, the coolant flow rate uncertainty is small to be shown on the plots. The pressure uncertainty, on the other hand is so large that it would dominate everything else on the plots. For example, most of the air tests were carried out at around 1 MPa pressure, with combined pressure drop across the entire loop of less than 0.1 MPa. Therefore, all measured pressures in this case would be within the uncertainty margins of 0.194 MPa in Table 1.1. The relatively high uncertainty in pressure measurement also made validation of pressure drop calculations impractical. The adoption of more sensitive differential pressure detectors would have mitigated this uncertainty, however, procurement of such detectors with operating conditions adequate for operations in the SPM-SS represented long lead times with increased schedule risks (COVID 19-induced supply chain delays). Differential pressure detectors will be adopted in future upgrades of the SPM-SS.

Table 1.1. Measurement Uncertainties

Sensor Name	Sensor Uncertainty	DAQ Uncertainty	Total Uncertainty
K Type Thermocouple (ANSI)	±2.2°C or 0.75%*	±0.77°C	**±2.97°C or ±0.75% + 0.77°C (see Figure 1.8)**
TPT Pressure Transmitter	±1.72 bar (±1% FSR)	±0.22 bar (±0.13% Reading)	**±0.194 MPa**
mini CORI-FLOW Coriolis Flow Meter	±0.5% of Flow Rate	±0.1% Signal Converter ±0.13% DAQ Reading	**±0.73% Flow Rate**
SFI-800 Sight Flow Indicator (water flow)	±6.625 LPM (±5% FSR)	±0.172 LPM (±0.13% Reading)	**±6.797 LPM (approx. ±0.113 kg/s)**
F4T Controller (Heater power)	±1.37°C ±0.251 kW	N/A	**±1.37°C ±0.251 kW**

* Whichever is greater

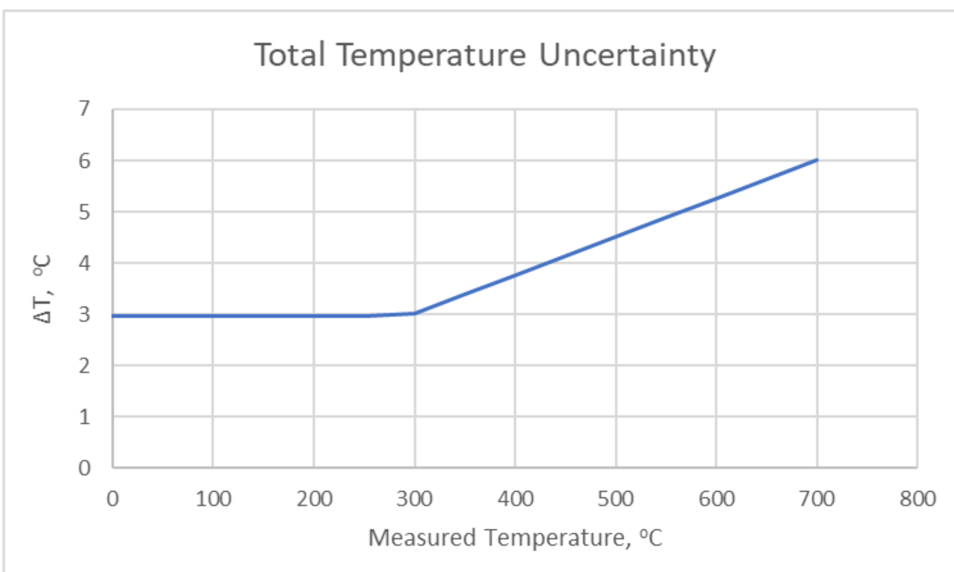

Figure 1.8. Total Uncertainty in Temperature Measurement.

In the absence of differential pressure transducers, pressure drop can be derived from the difference in absolute pressure, with uncertainty:

$$\Delta(\Delta P) = \sqrt{\Delta P^2 + \Delta P^2} = \Delta P\sqrt{2} = 0.274 \text{ MPa}$$

Again, this value far exceeds the measured changes in pressures. The pressure drop calculations thus will only be checked (rather than validated) against the difference in the measured absolute pressures.

There is another consequence of high uncertainty in pressure. All pressure readings in the test data show significant and seemingly random oscillations (noise). Although these oscillations are within the measured uncertainty levels, they created practical challenges for PDC validation and transient calculation. As it will be discussed in Section 2.6, pressure readings were used to define the boundary conditions for the loop in all transients. Direct application of measured pressure data, with oscillations, resulted in unstable solution for the code. To mitigate that effect, a 10-second averaging was applied to all pressure measurements in this report for the PDC input and/or code comparison. 10 seconds was selected as a trade-off between reduction in oscillations and delays in transient data. But even with such 10 second averaging, oscillations in pressures are only smoothed out to some degree, but not eliminated completely. As a result, the compressor and turbine maps still could not be defined based on the pressures alone. Therefore, for all transient calculations presented in this report, the measured flow rate will be used as a boundary condition for the "compressor flow", along with the "compressor-inlet" pressure (rather than defining both inlet and outlet pressures). Since uncertainty on the flow measurement was relatively smaller, defining flow rate (and calculating pressure drops) resulted in a more stable solution for PDC (than defining the pressures and calculating flow rate based on pressure difference).

1.3 SPM-SS Loop as Modeled

Since PDC was developed for the analysis of Brayton cycle for nuclear power plant applications, the cycle configuration in the code assumes a closed loop with at least one turbine and at least one compressor. The code solves conservation equations, both in steady-state and transient models, including a conservation of mass in a closed loop. Additionally, the working fluid mass flow rate in transients is calculated in the code from the performance of a compressor (or compressors). Therefore, both the closed loop configuration and a presence of turbine and compressors are required in the PDC modeling. However, the subscale simulator loop was not equipped with turbomachinery components. Subsequently tests were executed with the working fluid pressurized through sets of high-pressure tanks to supply a finite amount of working fluid inventory and pressurize the components forming the loop in place of a compressor. To mimic the turbine, the loop was equipped with a network of valves operated to regulate flow-rate and pressure through various heat exchangers at desired design conditions. After circulating through the loop's components, the working fluid was vented to atmosphere, thus testing were executed in "open-loop configuration". To enable the code to run without turbine and compressor, a series of methodologies were implemented to compensate.

Figure 1.9 shows the sub-scale simulator loop as modeled in PDC for all analyses presented in this report. All components outside the pressure relief or regulator valves are not included in the model. Instead, the loop *is assumed* to be closed with a line shown in red in Figure 1.9. This line includes an artificial compressor (as required for PDC modeling). The compressor heat exchanger (HT1) is also not included in the model. Instead, the measured heater-outlet conditions (temperature TT4 and pressure PT5) are provided to PDC as pre-determined compressor-outlet conditions for both the steady-state and transient calculations. The cooler outlet pressure (PT13, not shown in the figure) is specified as the compressor-inlet pressure for both steady-state and transient calculations. The cooler-outlet temperature (TT39) defines the compressor-inlet temperature in the steady-state calculations and the target compressor-inlet temperature for water flow rate control in the cooler for transient analysis.

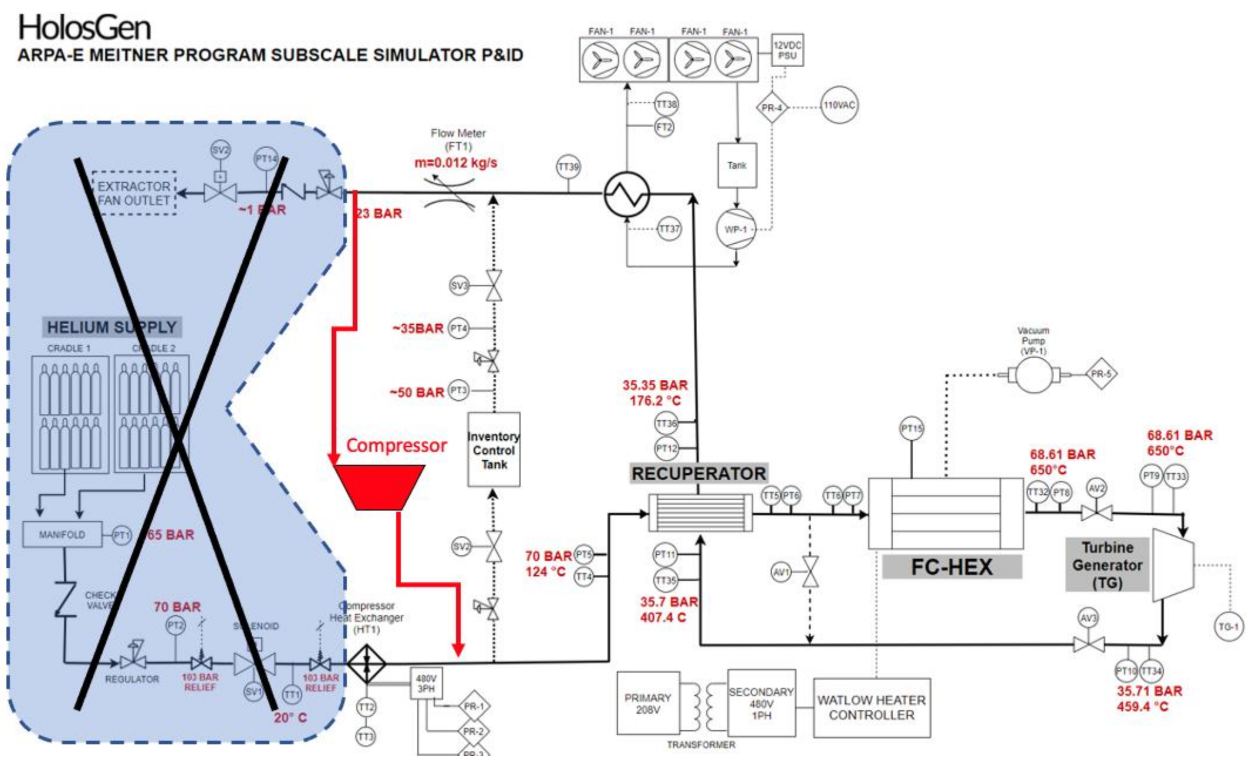

Figure 1.9. HolosGen Sub-Scale Simulator Loop as Modeled in PDC.

To satisfy the code requirement for the inclusion of at least one turbine, the PDC model includes a fictitious turbine, even for the SPM-SS tests with the turbine replaced by a heat exchanger and a throttling valve. Similar to the compressor modeling, the turbine-outlet temperature (TT34) is provided directly to the code for both steady-state and transient calculations. For the transient calculations, the combined pressure change in the surrogate turbine and any of the actuated AV2 or AV3 valves is provided to PDC as the turbine pressure change as a function of time.

The Fuel Cartridge Heat Exchanger (FC HX or FC-HEX) is modeled as a reactor component with electrically heated rods. In the PDC, the difference between electric heating and the reactor fuel is the material properties for the rod/fuel – in these calculations stainless steel properties are used for the “reactor fuel” channel. The power deposition in the fuel/rod is an external input for the PDC calculation and does not depend on the fuel/rod type. Since the heater rod power is directly specified for the PDC, auxiliary heater components shown in Figure 1.9 (transformer and vacuum pump) are not included in the PDC model.

On the cooler side, the water inlet temperature (TT37) is provided as the boundary conditions. The water flow rate is calculated by the code to match the target "compressor" inlet (cooler outlet) temperature on the fluid side. The water thermodynamic conditions are assumed at atmospheric pressure at all times. In this treatment, modeling of other water loop components shown in Figure 1.9 is not needed.

The model also includes all branches in the loop, such as the turbine bypass line with the AV1 valve and the inventory storage line with the tank shown in Figure 1.9. Note that in all tests conducted with the subscale simulator loop for the purposes of this report, neither the turbine bypass line nor the inventory line was activated, as the inventory branch will be utilized in future tests. Therefore, the presence of these lines (high-pressure tubing) has no effect on the results described in this report (except for a small working fluid inventory accumulated in the closed lines). The PDC model also includes the recuperator bypass line installed on the hot side (from the turbine discharge) of the recuperator (not shown in Figure 1.9). This line was activated in the loop heat-up phase and is included in the simulation of some transients analyzed in this report.

The input information for the PDC model includes all the design information available for each component and the loop piping, such as tube/pipe diameters, thicknesses, lengths, and number of bends (for each loop pipe), as well as material selection for components and piping. For the FC HX, information was provided on the coolant channels and heater rod dimensions, cross-section of the graphite blocks with number and diameters of holes for coolant and heater channels, and length. For the recuperator and cooler heat exchangers, the number and dimensions of the coolant tubes was provided, as well as the number and dimensions for baffle plates and the external shell. For all valves, the flow coefficient for fully open valve is provided. However, for the flow rates utilized in all tests, it was found that the effect of the pressure drop of open valves is very small, thus have not been included in the PDC model. The pressure-drop in the turbine throttling valve, if activated, is included in the "turbine" pressure change as described above.

2 Code Modifications

This chapter describes the PDC modifications adopted to address the specifics of the subcritical power module sub-scale simulator (SPM-SS) described in previous chapters. A general approach to the code changes was to implement the minimal required modifications sufficient to simulate the tests. To the extent possible, the code modifications were implemented in a way that they would have no (or minimal) effect on the results of the code calculations for the full-scale system. One obvious example of such approach is the implementation of air properties for the working fluid when the SPM-SS was operated with air – this change does not affect the full-scale SPM results, as helium was used for the Holos-Quad full-scale SPMs calculations.

2.1 Air as Working fluid

The PDC material property functions have been extended to allow calculations with air as the working fluid for the SPM-SS cycle simulation. The majority of the air thermal-physical properties were already included in the PDC as air was used as the ultimate heat sink media for the cooler heat exchangers. The property functions for air have been extended mostly to allow using air in turbomachinery calculations, such as various formulations of entropy and other derived properties. Although the SPM-SS turbomachinery and power generation performance was not included in the scope of this project, turbomachinery design and performance calculations are still executed by the code and air properties are required for code compilation. The additional property functions implemented for air in this analysis are similar (in formulation) to the property functions implemented for helium under this project [13].

The air property formulations implemented in the PDC for this analysis are only approximate and are not of the same standard as for other fluids in the PDC. For non-ideal gasses, like CO_2 and nitrogen, detailed property formulations based on the equation of state are implemented. Calculating air properties at the same accuracy is more complicated since air is a mixture of gasses. Detailed property formulation for mixtures is not currently supported in PDC and the corresponding code modifications were outside the project scope. Instead, common fits for air properties were implemented based on available data [14]. These fits, however, are often obtained for most common air applications, at atmospheric pressure and low temperatures, such that extrapolation of these properties to high temperature (up to 650 °C as encountered in the tests) and high pressure (up to 10 atmospheres when air was utilized as SPM-SS working fluid) would require a dedicated new validation effort. Such work again was outside the project scope, and rather simplistic air property formulations were assumed to provide sufficient accuracy, unless the calculations with the code would highlight problems with air properties at some conditions (e.g., if heat balances would not match the measured data).

2.2 Shell-and-Tube Heat Exchanger with Baffle Plates

As it was discussed in previous chapters, the <40kW SPM-SS loop employs shell-and-tube heat exchangers for the recuperator and cooler components, while compact diffusion bonded heat exchanger are components selected for the full-scale 5.5MW SPMs equipping the Holos-Quad design.

General shell-and-tube heat exchangers designs are included in the PDC models, but these models assume a purely counter-flow arrangement in all heat exchangers. The SPM-SS heat exchangers, however, are custom designed with baffle plates, which define a cross-flow heat exchanger configuration. Development of accurate cross-flow heat exchanger would have required re-formulation of code equations from one-dimensional approach for the counter-flow configuration into a two-dimensional approach for the cross-flow design. As a result, a compromise solution was implemented. The flow is still assumed to be one-dimensional in a purely counter-flow configuration, but heat transfer and pressure drop correlations developed for cross-flow heat exchangers [15] were added to the code. This solution is not ideal, since the flow characteristics (flow area, velocities, etc.) calculated in the code would not necessary match those used for the development of these correlations. However, as the results of analysis presented further in this report will show, this approach provides reasonably accurate results when comparing the tube-and-shell heat exchangers design performance predictions implemented by HolosGen as well as with the test data. As the tube-and-shell heat exchangers are not used in the full-scale Holos-Quad design, the development of an accurate cross-flow shell-and-tube heat exchanger model in PDC merely for the purposes of the SPM-SS was deemed unnecessary.

2.3 Heat Loss from the Reactor (FC HX)

Analysis of test results presented further in this report revealed a significant misbalance between the heat addition to the heater rods and heat transfer to the working fluid in the fuel cartridge heat exchanger, even at steady-state conditions. Often, the heat transfer rate to the coolant was less than half the power supplied to the heaters. This difference is attributed to substantial heat losses to the environment, due to the physical setup of the FC HX with a power rating <40kW. In this case, "substantial" is intended in a relative sense as substantial heat losses are not expected for the 5.5Mw full-scale Holos-Quad. In large reactor systems, for which PDC was originally developed, typical heat losses are on the order of 1% or less of the core thermal power. For these reasons, heat losses in the SPM-SS FC-HX component were originally not included in the PDC modeling. However, as it will be shown, for reactor simulator systems characterized by relatively extended balance of plant components operating with very low power rating, the assumption of negligible heat losses, valid when applied to relatively high power rating, leads to the misbalance between the heat addition to the heater rods and heat transfer to the working fluid as determined by test data analysis.

As the sub-scale FC HX is the component that most accurately describes the full-scale Holos-Quad core, the PDC reactor module was updated to account for heat losses (again, generally neglected for larger systems). For this purpose, the following modifications were implemented in the code.

Figure 2.1 shows how the channel-type reactor model is implemented in the PDC [16,17]. In the absence of heat losses, the (radial) heat transfer rate between structures is the same at each axial elevation. For example, in Figure 2.1, the heat transfer rate (q') that defines temperature change (ΔT) in the coolant tube is the same as heat transfer rate in the matrix and the fuel.

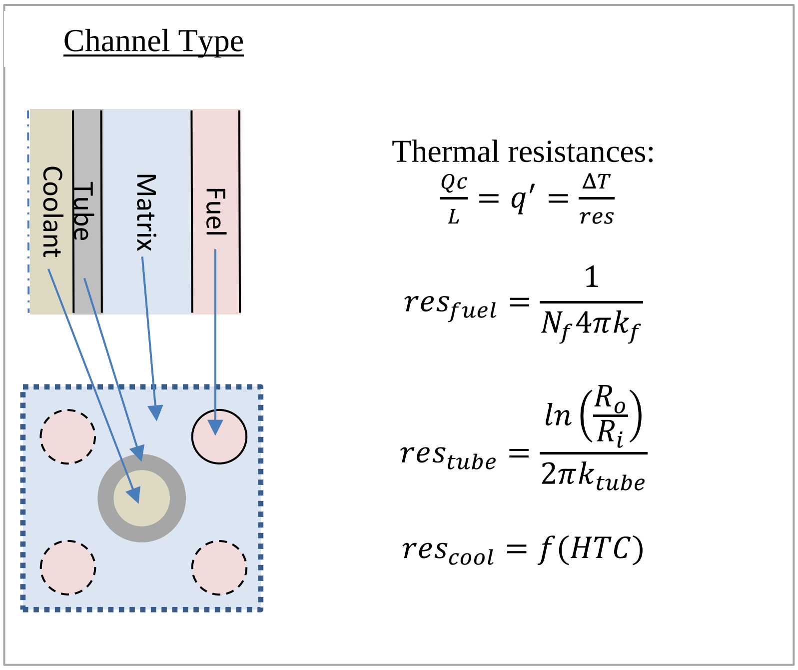

Figure 2.1. Reactor Model in PDC.

To account for the heat losses in the code reactor module, the PDC equation were adjusted. First, it is assumed that the heat loss would be occurring from the (graphite) matrix. The heat loss at each axial node is calculated as:

$$\Delta Q_{HL} = (T_m - T_{amb}) \cdot H \cdot P \cdot \Delta L \ ,$$

where

T_m, T_{amb} = matrix and ambient temperatures, respectively,

H = overall heat loss heat transfer coefficient (HTC),

P = perimeter for heat loss,

ΔL = length of axial node.

To implement the above equation, a new input for $H{\cdot}P$, heat transfer coefficient times the perimeter for the heat loss, has been added as a new input for the PDC reactor module. Note that this is a single input and thus is assumed to be the same for all axial nodes. The actual heat loss will be scaled with the matrix temperature as defined in the equation above. The input for $H{\cdot}P$ will be adjusted in the PDC simulations, further described in following chapters of this report, to match the measured difference between the heat input from the heater elements and the heat transfer rate to the coolant (calculated based on the measured inlet/outlet temperatures and flow rate). Because $H{\cdot}P$ is the user input that is adjusted to match the test conditions, the heat loss model described here is referred to as "accounting for heat loss", rather than actual calculation of the heat loss. To implement the latter, the heat transfer coefficient would need to be calculated based on the actual geometry and the FC HX insulation, including the vacuum layer (gap) between the graphite Matrix and the inner pressure vessel walls. Figure 2.2 shows a cross-sectional view of the FC-HEX internals, similarities with the channel-type reactor modeled in the PDC, and photos of key FC-HEX internal components.

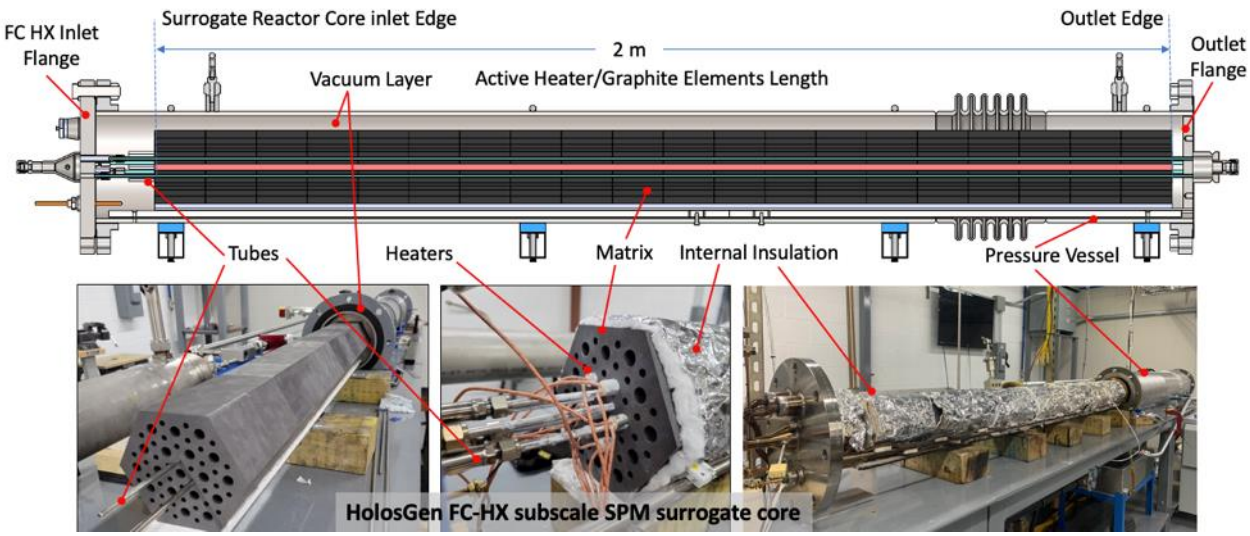

Figure 2.2. SPM-SS FC-HX Channel-Type Reactor Model.

The heat transfer equations are adjusted to differentiate between the amount of heat transfer between to coolant (tube) and matrix and between matrix and fuel:

$$q'_{f-m} = q'_{m-c} + q'_{HL}$$

$$q'_{f-m} = \frac{T_f - T_m}{\frac{res_m}{2} + res_f}$$

$$q'_{m-c} = \frac{T_m - T_w}{\frac{res_m}{2} + \frac{res_w}{2}} = \frac{T_w - T_c}{\frac{res_w}{2} + res_c}$$

$$q'_{HL} = \frac{\Delta Q_{HL}}{\Delta L}$$

where,

q'_{f-m} = linear heat transfer rate between fuel and matrix,

q'_{HL} = linear heat loss rate,

q'_{m-c} = linear heat transfer rate between matrix and coolant,

T_c, T_w, T_f = coolant (bulk), tube wall, and fuel temperatures, respectively,

$res_c, res_w,\ res_m, res_f$ = coolant, tube wall, matrix, and fuel thermal resistances, respectively – see Figure 2.1.

The equations described above were implemented into the steady-state model of the PDC reactor module. Similar modifications were introduced into the transient equations, with the only difference that the transient equations include additional terms for structure temperature derivative and thermal inertia. The inertia-times-derivative term is not affected by the changes described above, and the heat loss from the matrix is assumed to be instantaneous, meaning that any thermal inertia of the structures located between the matrix and the ambient is ignored in the PDC transient calculations (the inertia of the graphite matrix itself is included in the corresponding equations).

Out of the various PDC changes implemented in this work and described in this chapter, the account for heat loss from the reactor module is perhaps the only code change that *might* affect full-scale results. As substantial heat losses were observed in the sub-scale test, it is recommended for future analyses to re-evaluate the heat losses from the full-scale reactor system, to verify whether the assumption of negligible heat losses is still applicable to the full-scale Holos-Quad microreactor. As the Holos-Quad design eliminates the traditional balance of plant, heat losses through pipes, flanges and tubing connecting the various components forming the thermal-to-electric conversion components will be naturally lower than the heat losses produced by designs relying on extended balance of plants (e.g., thermal-hydraulically coupling components at relatively large distances from the core). Should future re-evaluations of the heat losses for the full-scale microreactor demonstrate that this assumption is erroneous, the code modifications described in this section would be readily available to compute the effect of these heat losses on the full-scale reactor performance, both for design conditions and in transients.

2.4 Account for Heat Loss in the SPM-SS Heat Exchangers

Similar to the reactor (FC HX) component, the analysis of test data presented in the next chapters revealed non-negligible heat losses in both the recuperator and cooler heat exchangers. Unlike the solutions applied to the code reactor module though, the PDC solution scheme for a heat exchanger could not be easily modified to include heat losses. The (steady-state) solution approach in PDC for heat exchanger relies on simultaneous solution of heat transfer equations for all nodes, rather than solving individual nodes. This code setting comes from the PDC original development to account for supercritical cycles, where an integrated approach was *required* to obtain a stable solution near the critical point. For the integral solution, a heat balance between the hot and cold sides, as well as through the HX wall, is postulated. For these reasons the code setting could not be changed to account for heat exchangers' heat losses, without implementing a significant revision of the entire PDC solution approach.

For these reasons, an alternative approach is adopted to account for heat losses in the sub-scale recuperator and cooler. The heat loss, assumed to primarily emanate from the HX shell, is treated externally in the PDC model. Accordingly, the model factors a short pipe added at the outlet of the shell side of the heat exchanger. The pipe material, diameter and thickness are those of the heat exchanger shell, with its length controlled to limit its effect on the cycle conditions. Then, a heat loss multiplication factor (see next section) for this pipe is manually adjusted to match the estimated heat loss from the entire heat exchanger. The advantage of this approach is that no code modification are needed to implement it – these adjustments are executed in the code input files.

The disadvantages represented by this simplified treatment of heat loss in the heat exchangers is summarized as follows. First, the heat loss is applied *after* the flow leaves the component (shell-side). Therefore, it will have no effect for the flow on the tube-side. The comparison of the code prediction with the test data presented in following chapters, however, showed that this separation of heat transfer from heat loss does not result in significant differences in the heat exchanger performance prediction. Second, the PDC does not have a provision to include any internal structure inside pipes, such as volume occupied by tubes inside a HX shell. Therefore, even though the heat loss pipe section dimension (ID and thickness) are selected to be representative of the HX shell, the flow area in this hollow pipe section would be much larger than in the HX shell with tubes. Therefore, all flow parameters important for heat transfer (velocity, Re, etc.) in that pipe would not be representative of those inside the HX shell. At steady-state condition, the difference will be compensated by adjusting the pipe heat loss factor. However, during a transient, the relationship would not necessarily hold. For example, in some transients analyzed below, the code calculates a transition from turbulent to laminar flow in the pipe, even though said transition would not be encountered in the HX shell flow in the test. This effect could not be avoided in the simulation and will affect the comparison of, most importantly, the recuperator hot-side outlet temperature between the code prediction and the test results.

2.5 Heat Loss Multiplication in Pipes

Unlike the reactor and the heat exchanger modules, the PDC equations for pipes already included provisions for the heat loss, although not in the most detailed formulation. For most components forming the full-scale reactor systems, the heat loss in the pipes is expected to be on the order of a few percent of the total reactor thermal power. Therefore, during the PDC development it was decided to not significantly complicate the code equations to add resolution to resolve few percent differences, but at the same time still provide the capability to account for heat losses in pipes. To account for the larger than expected heat losses for subscale components, the following approach was adopted in the code. The modeling has, as a reference case, equation formulations, including heat loss, for bare pipes (no insulation). Then, a heat loss multiplication factor, k_{HL}, is provided by the user for each pipe. If the user sets the code for simulation of bare pipes, then k_{HL}=1 would be used. For perfectly insulated (adiabatic) pipes, the heat loss would be excluded from the calculations if the user sets k_{HL}=0. The vast majority of PDC calculations used either of these two options. The PDC calculations for the reference full-scale Holos-Quad were carried out with no heat loss in pipes, as the design eliminates the traditional balance of plant, and the integral full-scale SPM design does not employ actual pipes. Neither of the k_{HL} options could be applied to the sub-scale simulator, as the heat losses in pipes were determined to be significant from test data, but still less than that from bare pipes due to the presence of thermal insulation surrounding the majority of the SPM-SS components (see Figure 1.4, bare pipes and HXs shells vs. Figure 1.3, insulated operational SPM-SS components). Therefore, the heat loss multiplication factors were adjusted to match the measured heat loss (temperatures change) obtained by testing. An analysis of the tests data with air revealed that a k_{HL} value between 0.5 and 0.75 is sufficient to accurately predict the heat loss in the majority of the sub-scale simulator loop piping. As mentioned, these adjustments are executed in the input file and did not require code changes.

However, to account for heat loss in heat exchangers with the adoption of pipes that simulate the HXs shell, as described in previous sections, it was necessary to extend the code capabilities to factor k_{HL} multiplication factors outside the nominal [0,1] range. The PDC modification consisted of a minor logical change in the code module addressing heat loss conditions, without affecting the overall equations. As for most code changes described in this chapter, this PDC modification was specific to the simulation of the SPM-SS and is not expected to be used in the analysis of full-scale system.

2.6 Turbomachinery Treatment and Map Option

In the absence of actual turbine and compressor in the sub-scale loop (as described in Section 1.1), the PDC was modified to continue simulating these components (as required to operate the code), but at the same time produce predictions for comparison with actual test data. The following modifications have been implemented in the code.

For steady-state calculations, the PDC features options to bypass the turbine and compressor design by providing given turbomachinery performance. These options, though, calculate the turbomachinery "performance" based on user-supplied turbine and compressor isentropic efficiency. As the SPM-SS is equipped with heat exchangers and valves to mimic turbomachinery inlet/outlet parameters and does not actually employ turbomachinery components, a definition of their efficiency does not have physical meaning. To compensate for the lack of SPM-SS turbomachinery components, this code option was extended so the turbine or compressor outlet temperature data can be directly provided in the PDC input files. Accordingly, the measured temperature values at the outlet of the SPM-SS turbomachinery surrogate components are used.

For the PDC transient calculations, regular turbomachinery maps (which are normally calculated by the code using the TM performance subroutines) will be replaced with direct input of the inlet and outlet conditions as sampled during testing. These parameters are obtained directly from the corresponding test data also listed below.

For the "compressor", the turbomachinery "map" will include, as a function of time:

- Inlet pressure = cooler outlet pressure (PT13),
- Mass flow rate = flow rate measured at cooler outlet (FT1, the only flow measurement), and
- Outlet temperature = temperature at the compressor heat exchanger outlet (recuperator inlet) (TT5).

For the "turbine", the map characteristics are (again, as a function of time):

- Pressure change = difference between turbine inlet (PT9) and outlet (PT10) pressures (but would also include throttling valve(s), if they are activated, PT8 and/or PT10), and
- Outlet temperature = temperature at turbine/HX outlet (TT34).

Note that the TM code changes described only refer to logical arrangements in the code. Since no turbomachinery components are present in the tests, the turbine and compressor design and performance subroutines in PDC are not activated as validation of SPM-SS thermodynamic performance was beyond the scope of this project. Overall, no changes are implemented in the PDC turbomachinery subroutines.

Also note that the code continues to perform general calculations for the turbomachinery components and reports the results in terms of their efficiency and work, although these values do not have physical meaning for the sub-scale simulator loop. Therefore, the results in terms of efficiency and work provided in the PDC result figures are effectively an artifact and *should be ignored* under the SPM-SS configuration analyzed in this project. The same caution is also applied to the reported SPM-SS "cycle efficiency" in the PDC output files, - because the efficiency and work are calculated based on artificial results for "turbine" and "compressor" work, *the SPM-SS cycle efficiency predicted values have no meaning*.

3 Simulation of Loop Design Conditions

Prior to applying the PDC to the measured test data, a comparison with the SPM-SS design calculations executed by HolosGen for the loop (maximum temperature, pressure, and power with helium coolant) has been carried out. The result of this comparison is shown in Figure 3.1. Note that in these calculations HolosGen did not include heat losses in the analysis. Consequently, no PDC modifications aiming to include heat loses described in the previous chapter were included in this initial analysis. The most important result to compare in these calculations is the helium flow rate. This is because PDC calculates the working fluid flow rate from all other inputs and calculations. As such, it's one of the last parameters calculated by the code, and agreement on this result could not be achieved without at least a satisfactory agreement on all other results. As Figure 3.1 shows, the PDC prediction for the helium flow rate is 0.011 kg/s, close to the design conditions at 0.012 kg/s.

The results in Figure 3.1 show that PDC underpredicts the performance of the recuperator, as the outlet temperatures for this component are lower than those shown in the HolosGen calculations. The difference was analyzed and eventually traced to how helium viscosity was used in these calculations. In PDC, a correlation for this property as a function of temperature is used, while in the design calculations a more simplistic approach with a fixed value of viscosity was used.

The cooler performance is in good agreement – both for the water flow rate (0.48 kg/s from the design vs 0.41 kg/s from PDC predictions) as well as for the water outlet temperature (28.2 °C vs 29.3 °C). These results confirm that the PDC code modifications, adopted specifically to address the SPM-SS shell-and-tube HX (the most significant code change not related to heat losses from Chapter 2), provide sufficiently accurate results.

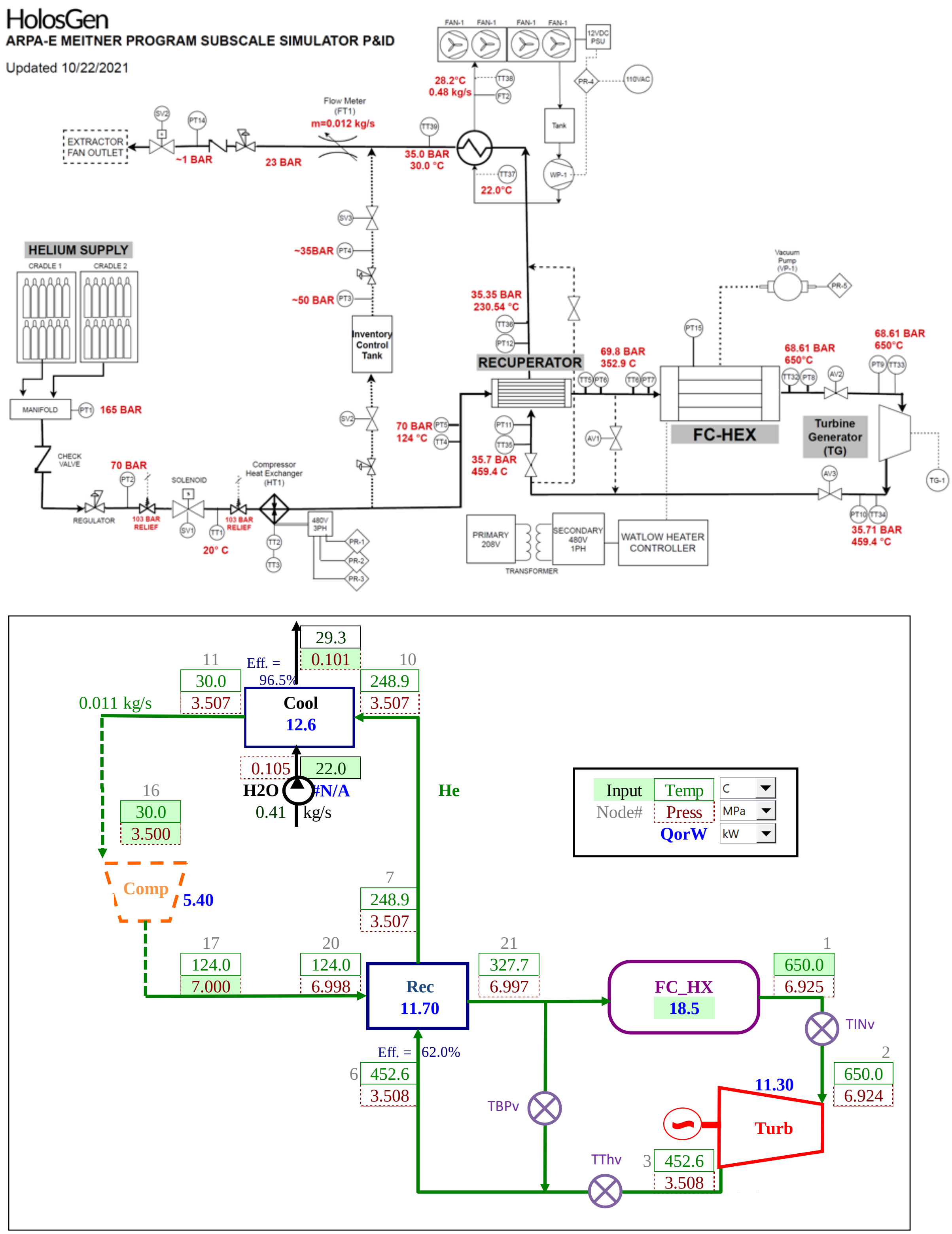

Figure 3.1. HolosGen Design Calculations (top) vs PDC Results (bottom).

4 Analysis of the SPM-SS Tests with Air

In preparation for the tests with helium, several SPM-SS tests have been conducted with air as working fluid circulating through the sub-scale loop. As discussed in Chapter 1, the main advantage of the air tests, for code predictions validation purposes, was the ability to run those tests for a prolonged time to achieve steady-state conditions. Several subs-scale air tests have been analyzed in this work with PDC, either at steady-state conditions or in transients. This report will be focusing on analysis of Test 15. This test is selected because, most of the loop troubleshooting activities were completed by improving loop deficiencies identified in previous tests. These activities overall involved the replacement of sensors to provide more accurate and repeatable readings from various SPM-SS loop, noise reductions with improved electrical grounding of instrumentation modules and sensors coupled to the computer user interface. Additional SPM-SS loop modifications were implemented to reduce damages on instrumentations caused by thermal-cycling as the loop operated for hundreds of hours with multiple cold start-up to max loop temperatures. As substantial heat losses were identified in previous tests, the loop was equipped with more effective thermal insulation. Test 15 was also selected as Tests 16 and 18 have been focusing mostly on tests with helium and the “air portions” of these tests were very similar to Test 15.

In the initial tests, bringing the loop to equilibrium at maximum temperature from cold start-up required several hours, to accelerate bringing the SPM-SS loop to temperature, the loop was modified to include a recuperator bypass line with a high-pressure, high-temperature actuated valve. Air portions means that the loop was brought to temperature by circulating air for as long as desired prior to switching to helium testing. As a target test temperature was reached at selected loop locations, the loop balance of plant was coupled to a vacuum pump to vacuum the loop and ensure that air pockets, potentially formed inside the heat exchangers and balance of plant cavities, would not mix and contaminate the helium working fluid prior to inletting this gas in the loop. The following paragraph addresses Test 15 start-up procedures in greater detail.

Test 15 (Figure 4.1) was run from starting the SPM-SS components from a cold shutdown state. After compressed air starts to flow within the loop, the FC HX electrical heaters were energized at controlled/desired power rates, and the system was operated to reach the design temperatures of 650 °C. During the start-up procedures, the recuperator bypass loop is activated to accelerate loop heating with both the primary heaters in the FC HX as well as those in the compressor heat exchanger energized. Once the target temperatures of 650 °C is achieved (measured at one of the heater rod’s surfaces via thermocouples located approximately in the middle of the FC HX), at around 1 hour, the recuperator bypass line is closed, and the heater electronic controller was switched to automatic mode to maintain the design temperatures. The loop was operated for approximately five more hours to reach steady-state conditions shortly after 6 hours; then it was shut down.

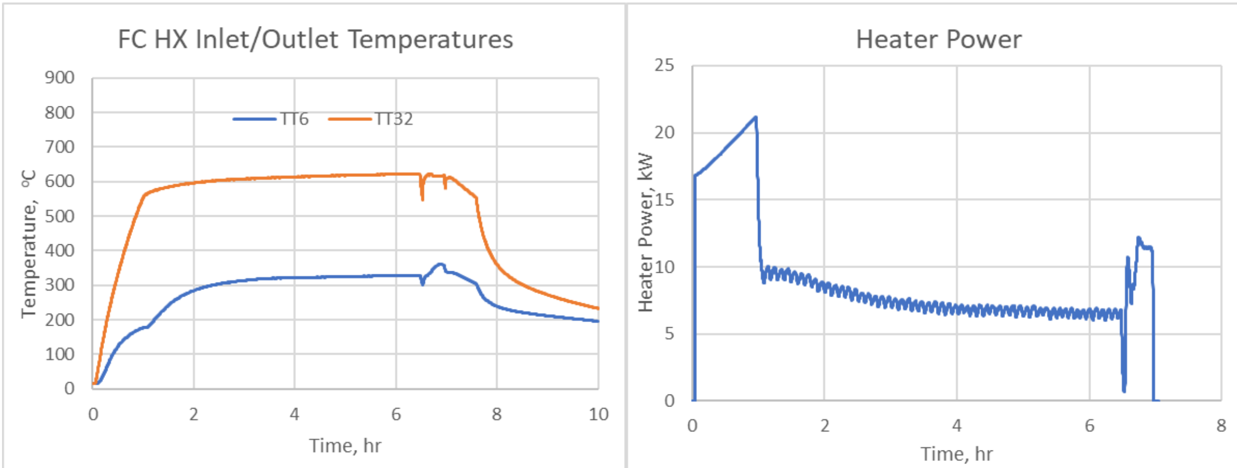

Figure 4.1. Test 15 Data with Air.

4.1 Long-Term Steady-State Conditions

The PDC analysis of Test 15 started to simulate long-term steady-state conditions at 6.3 hours. These conditions (shown in Figure 4.2) represent the best steady-state data achieved during the sub-scale loop testing (along with similar conditions in Tests 16 and 18). As shown in Figure 4.1, at 6.3 hours, the loop has operated for a relatively long time without any changes in the input, such that all the temperatures have stabilized.

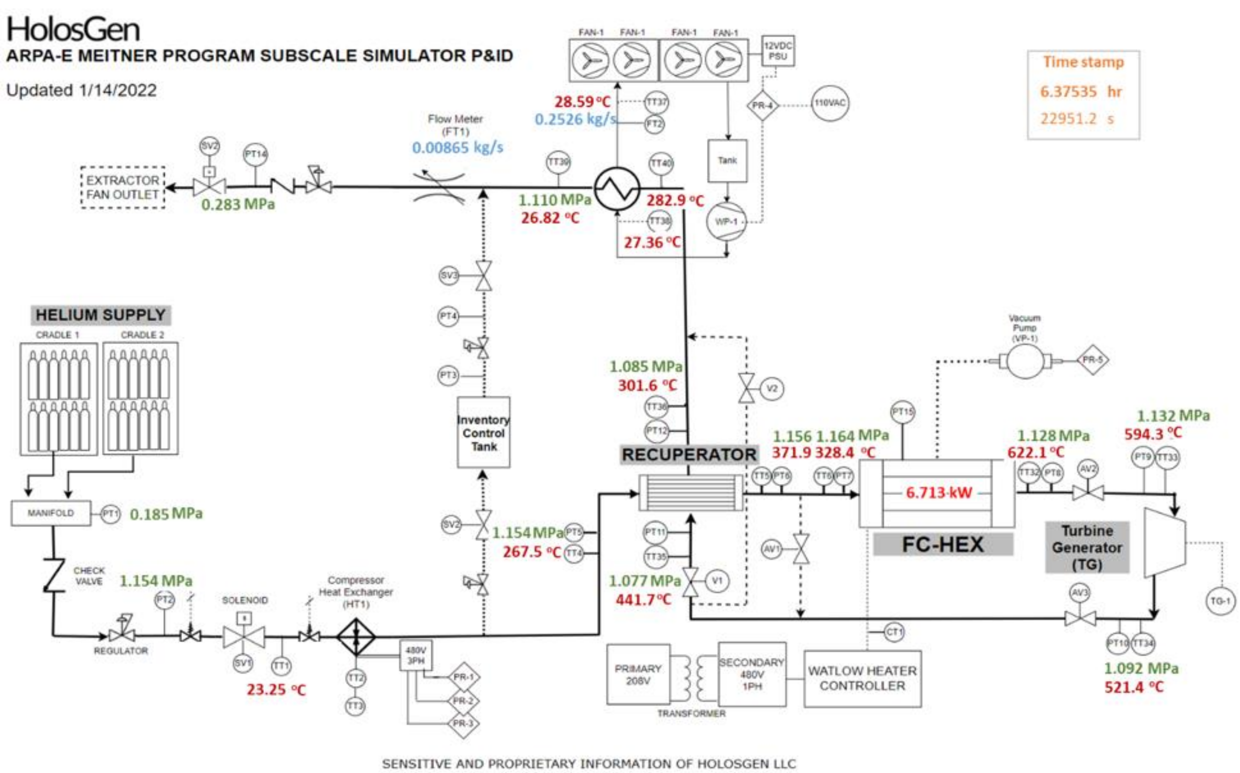

Figure 4.2. Test 15 Data with Air at 6.3 hr.

The heat balances at the 6.3 hour mark are shown in Table 4.1. In this table, the heat transfer rate for each component (or stream), dQ, is calculated based on the measured temperatures and flow rates (and heat capacity for air and water). A closed water-loop is coupled to the shell-side of the cooler heat exchanger for heat transfer with environmental air through radiators equipped with electric fans. The heat transfer rate is then compared to the values provided in the last ("To compare") column. Because all the components were at steady-state by this time, the values in the last two columns should be equal if there were no heat losses. For the FC HX, the value in the last column is the electrical input in the heater rods. Thus, the results in Table 4.1 show that of 6.7 kW heater power, only 2.6 kW was transferred to the air circulating in the loop. The remaining thermal power was transferred to the SPM-SS surrounding environment as heat loss, which represents more than 60% of the total thermal power supplied by the FC HX heaters. For the recuperator and cooler heat exchangers, "To compare" values are the heat transfer rate on the other flow of the heat exchanger. For the recuperator hot-side flow, "To compare" is the heat balance on the cold side flow of the same heat exchanger, and wise versa. For the cooler air side, "To compare" value is the heat transfer rate on the water side. For steady-state conditions without heat losses, the values in the "dQ" and "To compare" columns should be equal for all lines in Table 4.1. Therefore, data in Table 4.1 shows about 0.3 kW (~30%) of the heat loss across the SPM-SS occurs in the recuperator. The results for the cooler show approximately 1.0 kW, 50% of the total heat loss. These results were unexpected since, generally, the cooler operates at lower temperatures and thus should experience lower heat loss, compared to the recuperator. The results in Table 4.1 suggest instrumentation issues around the cooler, either on the air or water side. This hypothesis is confirmed with the test data in Figure 4.2 as it shows that the cooler air outlet temperature is below the water inlet temperature, this is not realistic, therefore an investigation on the source of data inaccuracy was recommended.

Table 4.1. Heat Balances for Test 15 at 6.3 hr

	T_in, C	T_out, C	dQ, kW	To compare kW
FC-HEX	328.4222	622.1702	2.618	6.7130
Turb	594.3955	521.4827	-0.650	
Comp	26.82184	267.5796	2.145	
Rec_hot	441.7421	301.6344	-1.249	-0.930
Rec_cold	267.5796	371.9345	0.930	1.249
Cool	282.9237	26.82184	-2.282	-1.307
Cool_w	27.36328	28.5996	1.307	2.282

The conditions of Test 15 in Figure 4.2 were simulated with the steady-state portion of PDC. The inputs for these calculations are:

- Loop configuration and design information for all components (as discussed in Section 1.3 and Chapter 2),
- FC HX power input (6.713 kW),

- FC HX helium outlet temperature (622.1 °C),
- "Compressor" inlet temperature (26.82 °C) and pressure (1.085 MPa – note that the cooler inlet pressure is used because actual cooler outlet pressure reading is showing a higher value for this measurement),
- "Compressor" outlet pressure (1.154 MPa),
- Water inlet temperature (27.36 °C) and outlet pressure (1 atm),
- Ambient temperature (not measured; 15 °C is assumed based on the cold state conditions for the same test analyzed in the next section).

The input conditions from the above list will be highlighted in the PDC result plots below as shaded in green. Based on these inputs, PDC calculates all other conditions on the loop, including:

- Performance (heat transfer and pressure drop) of heat exchangers – recuperator and cooler,
- Heat loss and pressure drop in pipes,
- Water flow rate and outlet temperature in cooler,
- Required air flow rate in the loop – based on the heat balance in the FC HX,
- Heat balances in the system – heat transfer rate in heat exchangers and heat duty of turbomachinery components.

Due to all the specifics of the sub-scale loop discussed in previous sections of this report, *significant adjustments to the PDC steady-state inputs were needed* to match the test conditions in Figure 4.2. These adjustments are described below.

Pipe heat loss (multiplication factor in PDC) for all pipes was adjusted to match measured conditions in the pipes forming the loop. This adjustment is made primarily based on the recorded inlet and outlet temperatures of the turbine-recuperator pipe. This pipe was selected because of its relatively long length and relatively high temperatures, such that the heat loss is significant and thus is well-characterized with the measured temperatures. k_{HL}=0.5 is selected based on the measurements for this pipe (meaning, halfway between bare and fully insulated pipe). The same "insulation" is applied to all other cycle pipes, except:

- FC HX-turbine pipe, where k_{HL}=0.75 is applied. This adjustment reflects different insulation in this pipe from the rest of the loop.
- Recuperator-FC HX pipe with k_{HL}=3.5. Note that this is a significant adjustment to the pipe heat loss, and it could not be explained by heat loss through the pipe insulation alone. This suggested that there was an additional heat loss through the turbine bypass line, which was connected to the recuperator-FC HX line.

Heat loss in the recuperator and cooler heat exchangers is simulated with artificial heat loss in the cycle pipes connected to the shell side outlet, as described in Section 2.4. Heat loss in the recuperator is adjusted to match the measured outlet temperature (PT12 in Figure 4.2). Heat loss in the cooler is adjusted to match the measured water flow rate on the cold side of the cooler.

Heat loss in the FC HX is adjusted by means of new HTC-times-perimeter input in the reactor model in PDC – see Section 2.3. The adjustment is made to match the air flow rate (through the FC HX and through the rest of the loop) calculated by PDC, and the heat transfer rate to air in FC HX (vs direct heat input in the heater).

Note that these adjustments are related to the heat loss which, again, was observed to be significant for the small-scale loop, but it is not expected to play a large role in the full-scale systems for which PDC was developed.

The results of the PDC prediction of the steady-state Test 15 conditions are shown in Figure 4.3. The code results are compared with the measured data (repeated from Figure 4.2)

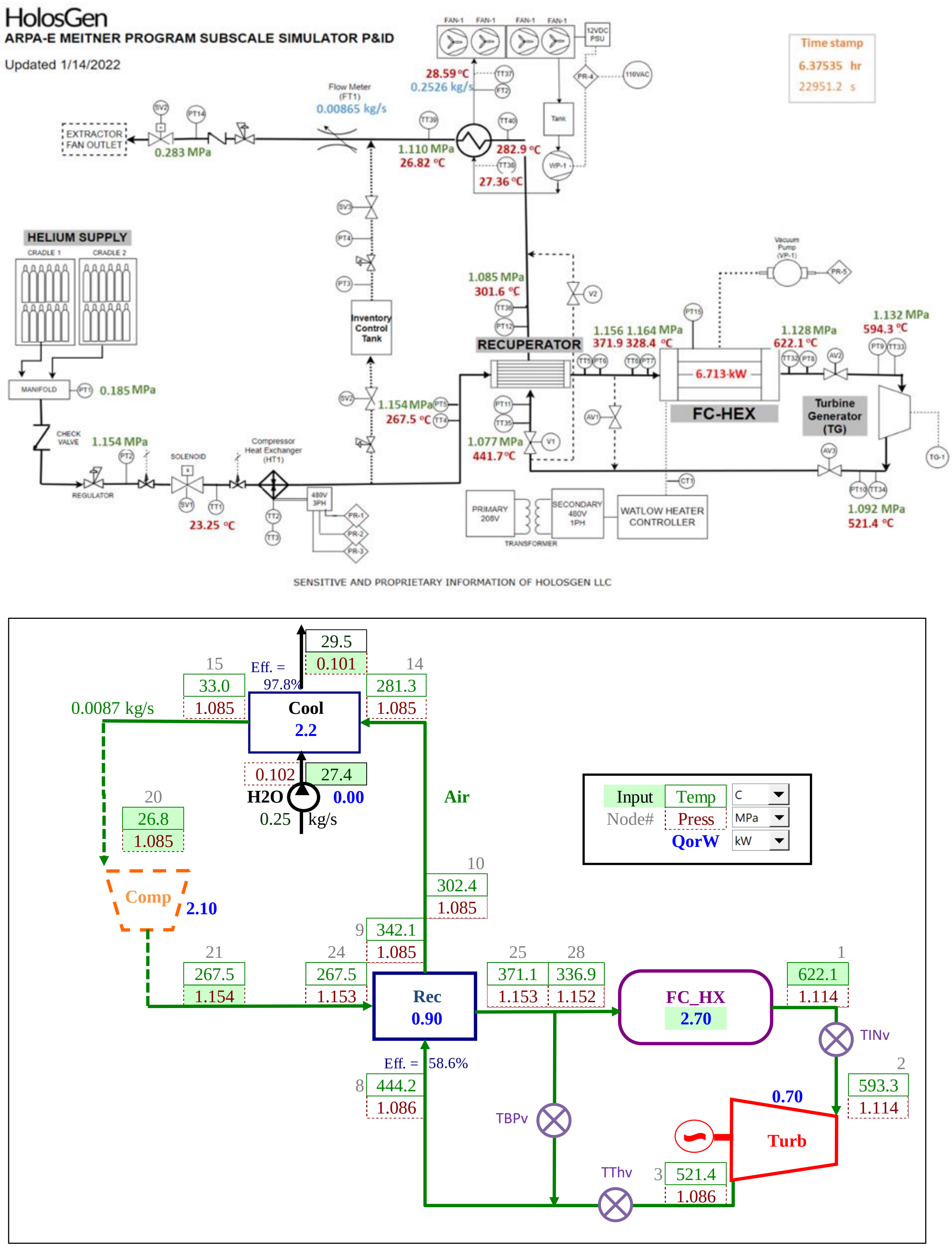

Figure 4.3. PDC Steady-State Results for Test 15 with Air.

Even though the PDC inputs were subjected to significant adjustments to directly match the measured data, *agreement between predicted and test results* could be identified in the PDC. The results shown in Figure 4.3, were not subject to the input adjustments. These results are listed below, with values shown in the “PDC/Test” format:

- Pressure drop in FC HX: 38/36 kPa (although measurement uncertainty is 274 kPa – see Section 1.2).
- Positive pressure drop across the turbine confirming pressure drops in the rest of the loop (although, again, the Δp value around 30 kPa is much smaller than the measurement uncertainty of 274 kPa).
- Recuperator cold side temperature: 371.1/371.9 °C. With the heat loss adjustment on the hot (shell) side, this result is the only one to confirm the heat exchanger performance.
- Cooler inlet temperature: 281.3/282.9 C. This result confirms heat loss in the recuperator-cooler pipe, even though no adjustment to this pipe were made (as discussed above, the k_{HL} value was applied based on the turbine-recuperator pipe data).
- Water outlet temperature: 29.5/28.6 C, although with small ΔT on the water side, difference of less than 1 °C might actually mean a significant difference in the heat transfer rate. On the other hand, the differences in water temperatures listed here are below the measurement uncertainties around 3 °C from Figure 1.8.

Overall, the PDC results in Figure 4.3 demonstrate that the steady-state part of the PDC is capable of accurately predicting the SPM-SS loop conditions with air. However, due to the adjustments in the input needed to address heat losses, the validation value of these results is diminished. For these reasons, the main purpose of the steady-state simulations for this test has shifted from the PDC validation to qualification of the heat losses in the loop. The steady-state data obtained in the test after a relatively long test is used to accurately characterize the heat losses (and thus to simulate these losses in PDC). The adjustments applied to the analysis described in this section are not repeated for all other tests (unless tests are based on additional modifications to the loop and loop components insulations). Therefore, the primary purpose of the air Test 15 steady-state conditions simulation with PDC targeted the characterization of the heat losses in the loop, and code predictions “validation” is executed in following tests.

4.2 Cold Steady-State Conditions

Because the steady-state conditions analyzed in the previous section were achieved towards the end of Test 15, these conditions could not be used as a starting point of PDC transient simulation (in PDC, transient analyses must start from steady-state calculations). Similar situations were observed in following air tests, with steady-state conditions reached at the end of those tests as well. A new starting point was needed to initiate transient simulation in PDC, therefore, the cold conditions early in Test 15 (Figure 4.4) were selected. These conditions were encountered, about 2 minutes into the test, when both the FC HX and compressor heaters were not turned on yet, while the air flow, however, was already established. As shown in Figure 4.4, the loop components temperatures at the start of the test are close to 14.5 °C, which is assumed to be an ambient temperature (the test started early in the morning). The advantages of selecting cold conditions as starting point is that there are essentially no uncertainty associated with the heat loss, as all loop components are at the same temperature as ambient temperature. For the same reasons, however, the cold conditions in Figure 4.4 could not be used to characterize the heat losses, which have already proven to be important at operating temperatures. Therefore, the analysis presented in the previous section to characterize the heat losses remains important for all other simulations presented in this report.

Early in Test 15, a recuperator bypass line (the line comprising V2 valve in Figure 4.4) was set open and the recuperator throttling valve V1 was completely closed. This was done (in this and all other tests) to avoid heat transfer in the recuperator and to use heat from the compressor heater (HT1 in Figure 4.4) to more rapidly and effectively heat-up the entire SPM-SS loop and the FC HX.

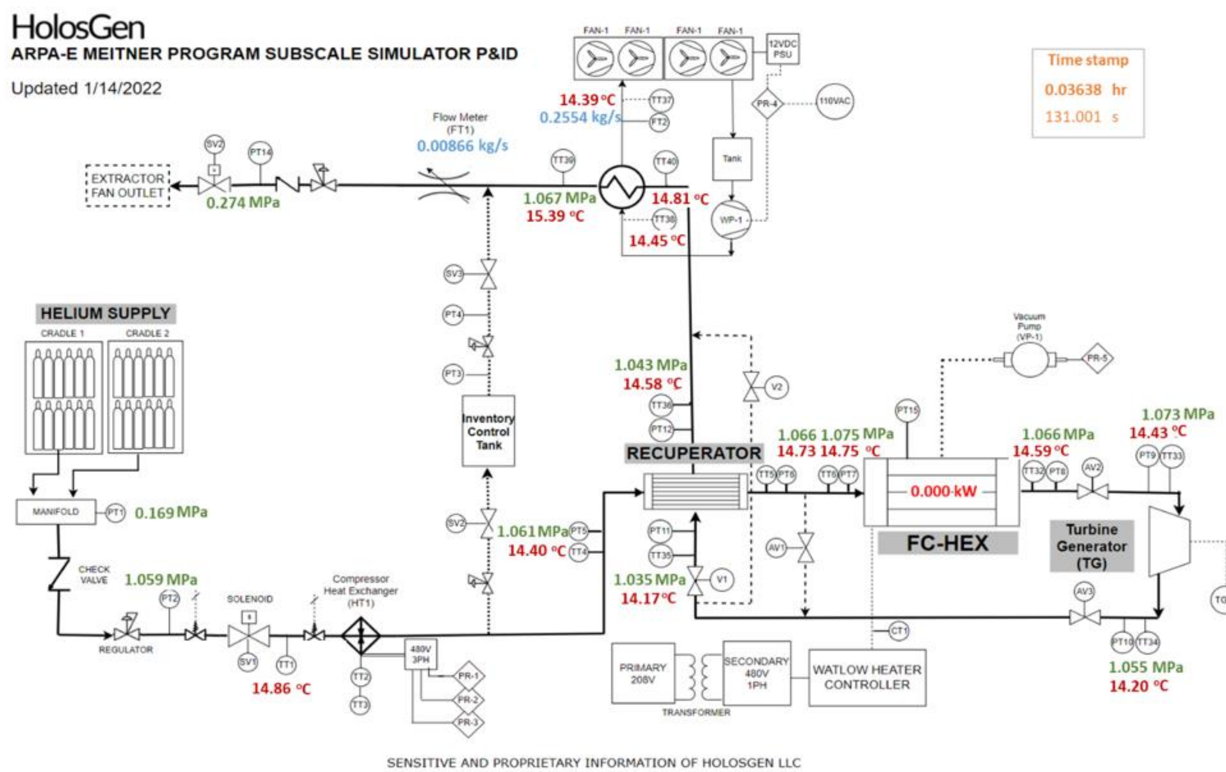

Figure 4.4. Test 15 Data with Air: Cold Conditions.

For the PDC simulation of the SPM-SS at cold conditions, no adjustments for the heat loss, similar to those described in the previous section, was needed. All the inputs (pipe heat loss, FC HX heat loss) remained unchanged. There were, however, a couple of adjustments to other inputs that were required in PDC to enable simulations of conditions in Figure 4.4 and further transient simulation of Test 15.

First, the ambient temperature was changed to 14.4 °C (from 15 °C used for hot conditions) to be consistent with average measured temperatures in Figure 4.4.

Second, as shown in Figure 4.4, the main FC HX heater was not turned on at this point. For the PDC calculations, however, zero heat input to the cycle is not allowed, since the heat balance in the main heat exchanger (or reactor core) is used to calculate the working fluid flow rate. For these reasons, a small value of 3.5 W (0.0035 kW) was used in the PDC input for the “reactor” power to initiate flow in the loop.

Lastly, the recuperator bypass action described above could not be directly implemented in PDC, as it would result in zero flow on one (hot) side of the heat exchanger. Instead, for the steady-state calculations, the recuperator bypass action was not simulated, and the full “hot” flow was allowed to circulate through the recuperator. Note that this flow would have essentially no impact on the conditions in the rest of the cycle since at this cold stage there is no heat transfer in the recuperator. In the transient simulation, though, the recuperator bypass action is simulated with some limitations as described in the transient analysis section below.

The PDC steady-state results for the cold conditions at the start of Test 15 are presented in Figure 4.5, with comparison to the measured test data. Because no heat transfer was expected at these cold conditions, the results in Figure 4.5 were not intended to validate PDC steady-state models. Limited validation of pressure drops is again confirmed in Figure 4.5, but these results are similar to those discussed previously for the SPM-SS tests at hot conditions (with some difference from effects of lower air temperature, higher density, and thus lower pressure drops). Again, the main purpose of the steady-state PDC analysis presented here is to identify and establish initial conditions for further transient simulation. Therefore, the only significant result in Figure 4.5 is that these results were obtained, meaning that the PDC steady-state solution has converged and thus the code was ready for transient simulation.

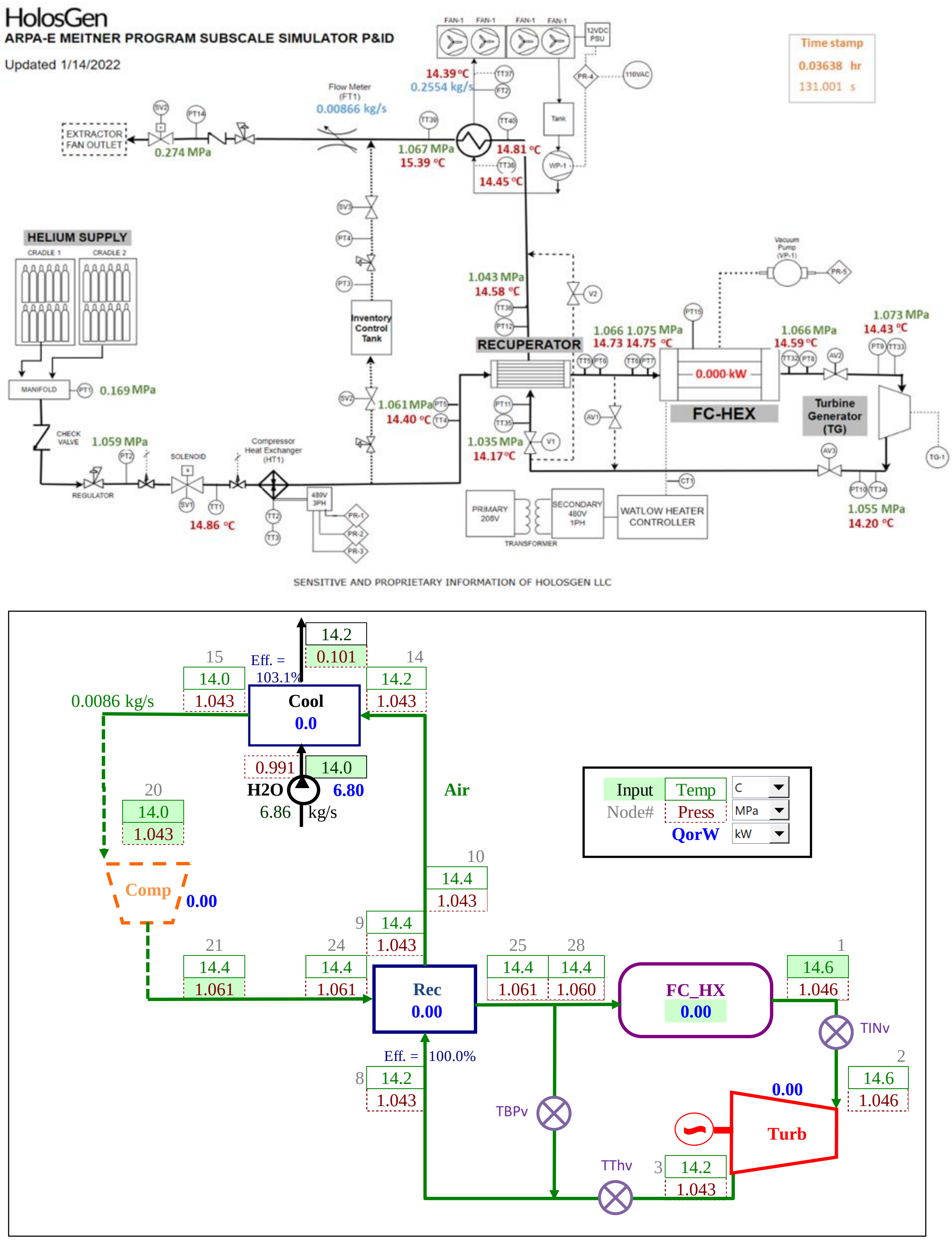

Figure 4.5. PDC Steady-State Results for Test 15 with Air: Cold Conditions.

4.3 Test 15 Transient Simulation

The description of Test 15 with air is provided at the beginning of this chapter. In general, the test was conducted to reach and maintain maximum design temperatures to achieve steady state. For this purpose, no control valve action was initiated, except for the recuperator bypass discussed in the previous section. The PDC transient simulation is carried out for almost the entire duration of the test, 22,000 seconds, or 6.1 hours. The PDC results for transient simulations is presented and compared with test on the "PDC time" scale, where t=0 represents steady-state conditions described in the previous section. Since these conditions were obtained at 131 s of test time, the test results will be shifted by 131 s. The results will also be presented in the PDC units (°C, MPa, kg/s, etc.).

The inputs for the PDC transient simulation are shown in Figure 4.6. These inputs are listed below and are obtained directly from the SPM-SS test data, as a function of time, for the PDC table input.

- FC HX heater power input,
- Working fluid flow rate,
- Cooler outlet ("compressor" inlet) pressure,
- Compressor heat exchanger outlet (recuperator inlet) temperature,
- "Turbine" pressure drop,
- "Turbine" outlet temperature, and
- Cooler water inlet temperature.

Due to limitation on some entries in selected PDC input tables, some boundary conditions from the above list were fitted with a piece-linear function (piece-linear refers to a function defined in a number of points with straight-line connection of those points). Figure 4.7 shows an example of piece linear fitting for the heater power, where the test data (orange line) was fitted with a table of 20 points (blue line). Note that Figure 4.7 shows the heater power in percent of nominal power, which is assumed to be 21 kW (exact value of maximum heater power is not important since it is also provided as PDC input, as long as it is consistent with the % values used to obtain the fit).

The recuperator bypass action was simulated in this transient as follows. For steady-state conditions prior to the transient, the bypass line is not activated (see previous section); V2 is fully closed and V1 is fully open. At the beginning of the transient (at t=0), the recuperator bypass valve, V2 is simulated to fully open in 5 seconds. The recuperator throttling valve is simulated to close during the same time-duration of 5 s. However, to avoid zero flow conditions, the V3 valve is not fully closed in the PDC calculations. Instead, it is closed to a small open fraction to allow approximately 1% flow in the recuperator. The calculations presented below demonstrated that 1% flow is small enough to have a negligible effect on the recuperator outlet temperature on the cold side, and yet it is large enough to avoid numerical stability issues at low (or zero) flow. The bypass line will remain open until 3,376 seconds (in PDC time = test time when the bypass line was closed). At that time, the bypass line will be fully closed, and the throttle valve will be fully open in 5 seconds, and both valves will remain in this state until the end of the simulation.

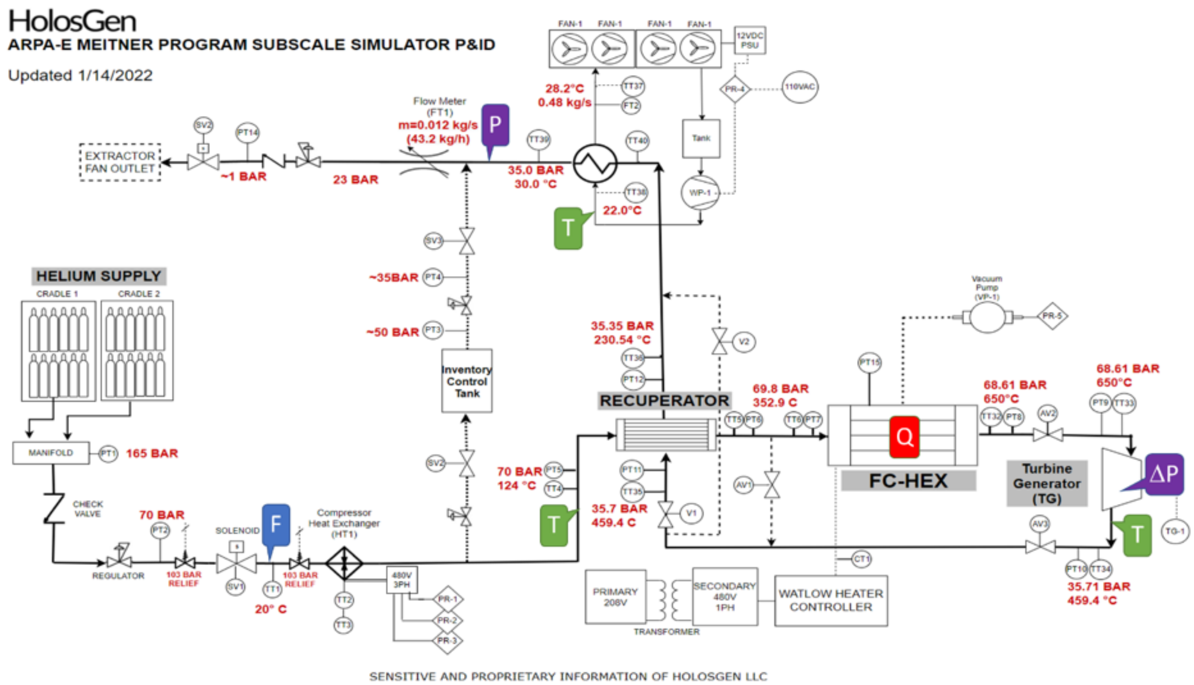

Figure 4.6. Inputs for PDC Transient Simulation.

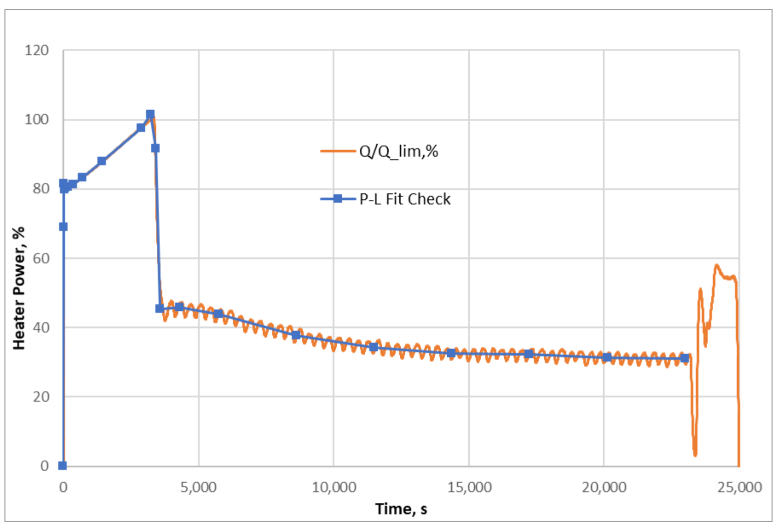

Figure 4.7. Piece-Linear Fit of the Heater Power Input for Test 15.

4.3.1 *Results with Nominal Internal Component Mass*

The main PDC results of Test 15 transient simulation are shown in Figure 4.8. In this figure, the PDC results, for which there is a direct comparison of the test data, are shown side-by-side with the corresponding test measurement. For easy comparison, the scales on both axes of the plots are selected to be the same. For multiple lines, the color-coding is preserved between the PDC results and the corresponding test data.

Overall, the results in Figure 4.8 show that PDC predicts the test conditions accurately, with some differences discussed below.

The flow rate (Figure 4.8a) were the inputs for PDC are shown here only to demonstrate that the PDC results are stable even with the noticeable oscillations in the measured air flow rate. The PDC results are shown for the turbine and compressor flow rates, which are identical in this simulation without flow branching and with negligible compressibility effects.

The pressure results in Figure 4.8b are very similar between PDC predictions and SPM-SS test data, for all loop locations. The "compressor" inlet pressure (green) lines were the input to PDC and thus are identical in both plots. The very good agreement on the orange lines (compressor outlet) show that the code predicts very accurately the pressure drop in the entire loop. This agreement is achieved even as the pressure results show significant oscillations caused by the flow rate variation. However, as discussed in Section 1.2, the uncertainty of the pressure measurements are rather large, at 0.194 MPa, such that all PDC results fall into the uncertainty range of the measured data, even of the measured compressor-inlet pressure.

The FC HX inlet and outlet temperatures in Figure 4.8c show the most significant deviation of the PDC results from the test. Even though the final (22,000 s) results are predicted with reasonable accuracy for both inlet and outlet temperatures, the trend in temperatures, especially for the outlet temperature are noticeably different between the PDC results and the test. The reasons for these differences will be discussed in the next section.

The PDC predicted recuperator temperatures in Figure 4.8d show good agreement with the SPM-SS test data. In these plots, the cold side inlet temperature (green line) is the input to PDC and thus is identical in two plots. All other temperatures are calculated by the code. Note that before the recuperator bypass line closure, around 1 hr elapsed time, the PDC hot side results (red and blue lines) should not be directly compared with the test results, because a small flow was assumed in the PDC calculations while the test results report full closure of the hot flow path. Other than this difference, the most noticeable difference is the faster increase in the cold side outlet temperature (orange line) when the bypass flow was open. The reason for this difference is discussed below.

The results for the cooler temperatures in Figure 4.8d are close in the PDC results and the test. These results however not necessary validate the cooler performance model as the cooler inlet temperature is effectively a recuperator outlet (with the pipe heat loss), while the outlet temperature is defined by the target "compressor" inlet temperature, which was the input for the PDC calculations.

PDC Test

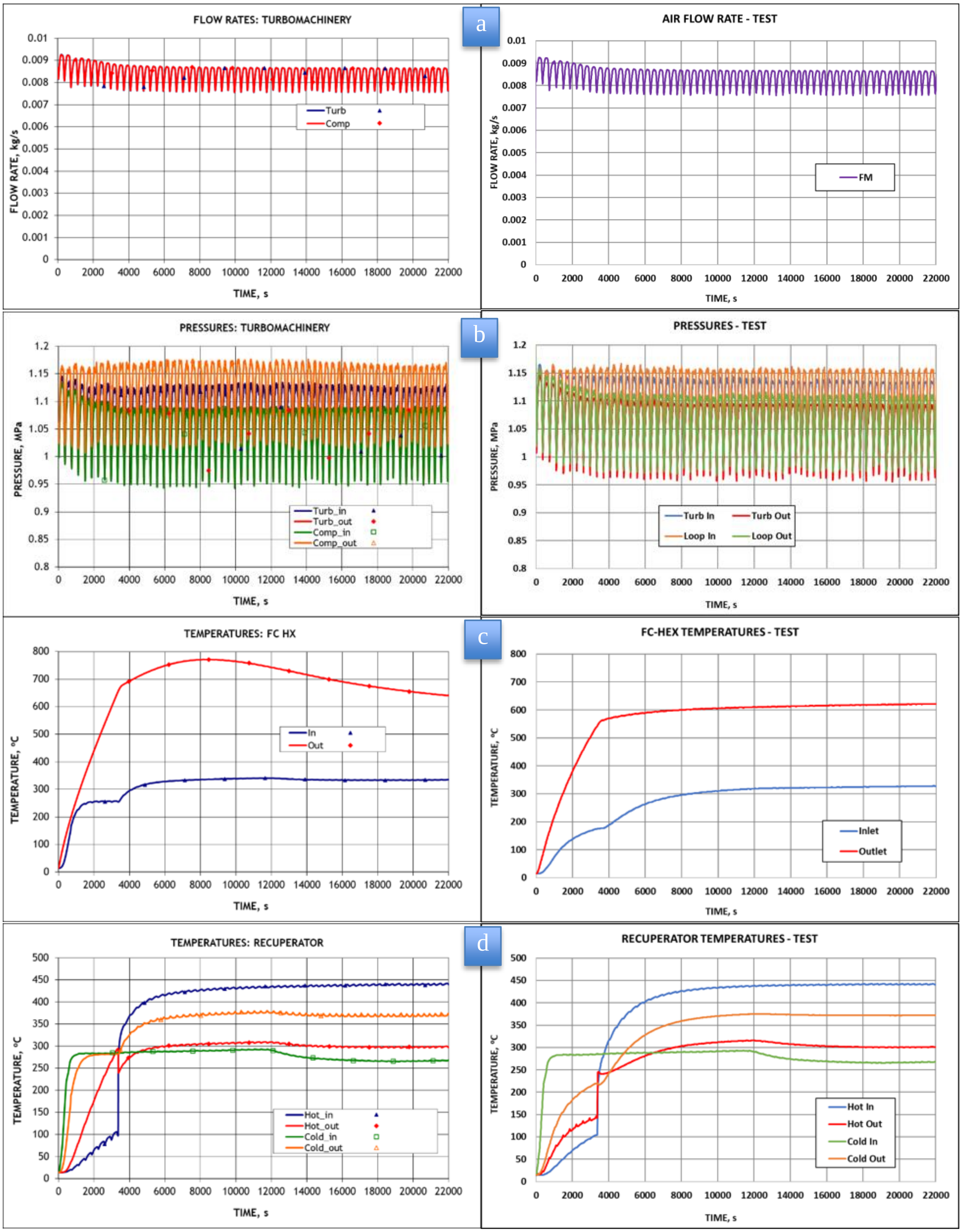
a
FLOW RATES: TURBOMACHINERY
FLOW RATE, kg/s
TIME, s
Turb
Comp
AIR FLOW RATE - TEST
FM
b
PRESSURES: TURBOMACHINERY
PRESSURE, MPa
Turb_in
Turb_out
Comp_in
Comp_out
PRESSURES - TEST
Turb In
Turb Out
Loop In
Loop Out
c
TEMPERATURES: FC HX
TEMPERATURE, °C
In
Out
FC-HEX TEMPERATURES - TEST
Inlet
Outlet
d
TEMPERATURES: RECUPERATOR
Hot_in
Hot_out
Cold_in
Cold_out
RECUPERATOR TEMPERATURES - TEST
Hot In
Hot Out
Cold In
Cold Out

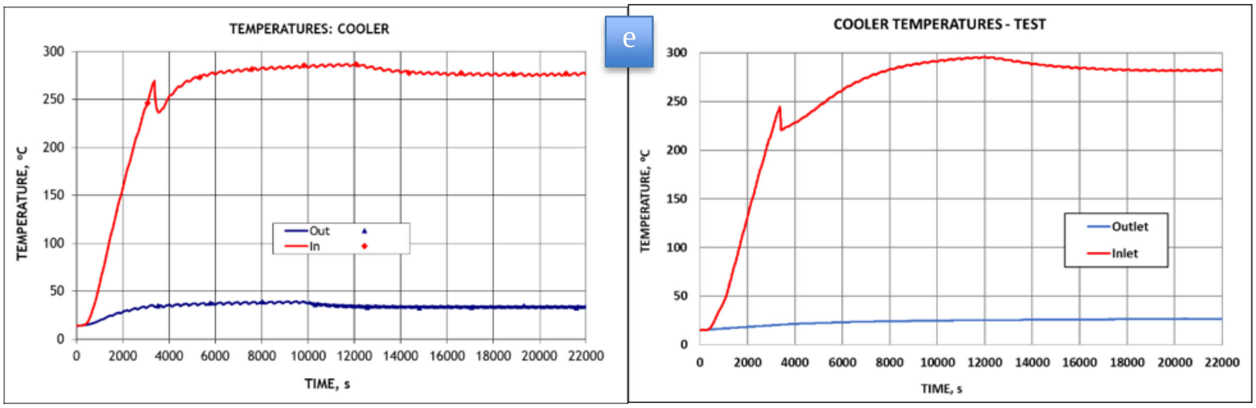

Figure 4.8. PDC Transient Results for Test 15 with Air.

4.3.2 *Results with Full Component Masses*

The PDC transient results presented in the previous section show a good agreement on the flow characteristics of the entire SPM-SS loop (pressure drop in pipes and components) and partial agreement on the heat transfer behavior of the loop (good agreement on recuperator temperatures and long-term FC HX temperatures). At the same time, there is a significant difference between the PDC results and the measured data in the short-term prediction of the loop temperatures. This difference suggests that the thermal inertia of particularly the FC HX, and also that of the recuperator, is not accurately captured in the PDC simulation.

Dynamic equations for the heat exchanger module in PDC include the mass of the material separating two flows, such as tubes for shell-and-tube heat exchangers and plates and fins for a compact heat exchanger. All other masses representing, for example, the structures and shell of the heat exchanger, headers etc., are not included in the PDC calculations, primarily because they do not participate directly in the heat transfer between two fluids. Moreover, these additional masses are generally assumed to be small compared to the tube or plate mass. For example, in the reference design of the printed circuit heat exchanger (PCHE) for the full-scale Holos-Quad recuperator, there is no shell. Each plate has a “land” or a border on each side of the plate that effectively forms a heat exchanger boundary during diffusion bonding. The land part is relatively small – out of 60 cm of plate width, the land occupies less than 2 cm on each side. This represents less than 7% of the heat exchanger mass (the rest being in the plates accounted for in the PDC equations). However, a detailed analysis of the material masses of the sub-scale recuperator (and cooler) reveled that the tube mass of the sub-scale system represents only 1/6 of the total heat exchanger metal mass, with the rest being the shell, headers, tube sheets, and baffle plates. With such significant difference, and as the PDC was designed to model larger systems, it is expected that the code would not correctly capture the thermal response of this sub-scale heat exchanger. Especially for the transients analyzed in this report when the heat exchanger altogether with its metal structures is being heated from the cold state. To account for the actual “total” heat exchangers’ mass in the PDC calculations, all of the component’s masses forming the “entire” heat exchanger mass needs to be included. For this analysis the masses of the shell, headers, tube sheets and baffle plates was included into the tubes mass. Although this assumption delays the thermal response of the tubes themselves, the results are expected to be more accurate than not including the mass of the heat exchangers’ structure into the tubes at all for the slow 6 hr transient. Therefore, for calculations presented in this section, *the* *recuperator tube mass has been increased by a factor of 6* to factor the entire heat exchanger mass. The same mass correction was applied to the cooler heat exchanger.

The PDC results in previous section also show a faster heat-up of the FC HX than what is observed in the test. Similarly, for the FC HX, the PDC "reactor" model (see Figure 2.1) only includes the internal masses, such as tubes, fuel, and graphite matrix. In a full-scale reactor, these components represent the vast majority of the reactor mass. However, as described for the recuperator and cooler heat exchangers, an analysis of the actual material mass forming the sub-scale FC HX components showed that the graphite, tubes, and heater rod masses represent only ~20% of the total FC HX mass. In fact, the majority of the test subscale component mass is in the shell, flanges, and the internal structure supporting the graphite elements. Note that these structural parts are not present in the full-scale SPMs forming the Holos-Quad microreactor, at least they would not represent a significant portion of the total mass. If the FC HX structural components' mass is included in the PDC calculations, factored as an increased graphite matrix mass, then the graphite mass is multiplied by a factor of 3.6, taking into account the difference in the heat capacities of graphite and steel for the heat exchanger shell and other structures. However, this correction leads to an overestimation of FC HX thermal inertia and thermal response. In the test (and in the reactor), the FC HX internals (graphite, heater rods, and tubes) are heated close to the maximum loop temperature of 600 °C or higher. If all FC HX mass is included into the graphite matrix, it implies that all of these masses are heated up to the same temperature as graphite. In reality, due to heat loss and external cooling, the structures outside the "reactor core", such as the shell, the inlet flange and other structural components are not expected to reach temperatures of 600 °C or higher. For the current setting of the SPM-SS instrumentation, the exact temperature of these parts in the test were not sampled. However, as a first approximation, it is assumed that all of these external structures will be heated up to roughly ½ of the graphite matrix temperature (approximately 300 °C by the end of the test). Under this assumption, *the equivalent correction factor for the graphite mass (heat capacity) of 1.8* (3.6/2) is implemented in the following calculations. Note that this correction is still not expected to result in a very accurate prediction of the complex nature of the FC HX heat up process, as different parts are expected to heat up at different rates (and to different temperatures). Applying a single correction factor for the graphite matrix implies an assumption that all structures will be heated proportionally to the graphite. Still, this simple correction leads to a reasonably accurate option to simulate the SPM-SS test conditions, without significantly modifying the PDC models to explicitly include all of the parts forming the sub-scale FC HX. Note that these considerations, resulting from testing a sub-scale physical system with very low power rating, generally indicate that microreactors with relatively low power rating need to more accurately factor the masses of components forming pressure vessels of various components and balance of plant, as their impact on heat losses and transient behavior may not be negligible as it is generally assumed for reactor designs. These simplified PDC correction factors for the masses forming the SPM-SS components were adopted as substantially modifying the PDC to accurately account for the SPM-SS subscale components heat losses was beyond the scope of the project.

The results of the Test 15 heat up transient factoring the assumed "total" component masses are shown in Figure 4.9. The simulation is the same as described in the previous section, except that a multiplier of 6.0 was applied to the recuperator and cooler tube masses, and a multiplier of 1.8 was applied to the FC HX graphite mass. The results in Figure 4.9 show that these corrections did not change the hydraulic response of the system (in terms of flow rate and pressures in plots a and b).

Also, the cooler temperatures (Figure 4.9e) are mostly unaffected by this change. However, the results for the FC HX (Figure 4.9c) and the recuperator (Figure 4.9d) show a noticeable improvement compared to previous results in Figure 4.8. Specifically, the code results no longer shows an overshoot of the FC HX outlet temperature. Under the “full mass” corrections, and as a result of improvements in the recuperator thermal response, the FC HX inlet temperature is now accurately predicted. For the recuperator heat exchanger, the cold side outlet temperature (orange line in plot d) shows a much closer agreement between the PDC predicted results and the SPM-SS test data, especially during the first hour where the recuperator bypass was active. With the corrections implemented, the code also accurately predicts the recuperator temperatures during the transition from full-bypass to full-flow.

Overall, the PDC predicted results in Figure 4.9 under the assumptions described above, show a reasonably good agreement with the test data demonstrating that the code calculates the loop behavior during the long heat up transients accurately.

At the same time, the results of the transient simulation analyzed in this section highlight the importance of capturing the heat losses and structural or external component masses. These issues, although in general specific for the small-scale SPM-SS loop, might still be present in full-scale micro-reactor systems with low power rating. Therefore, as it will be discussed in more details in the concluding (lessons learned) chapters of this report, PDC can be further optimized to capture more accurately the heat loss and thermal inertia phenomena for analysis of micro-reactor systems.

PDC Test

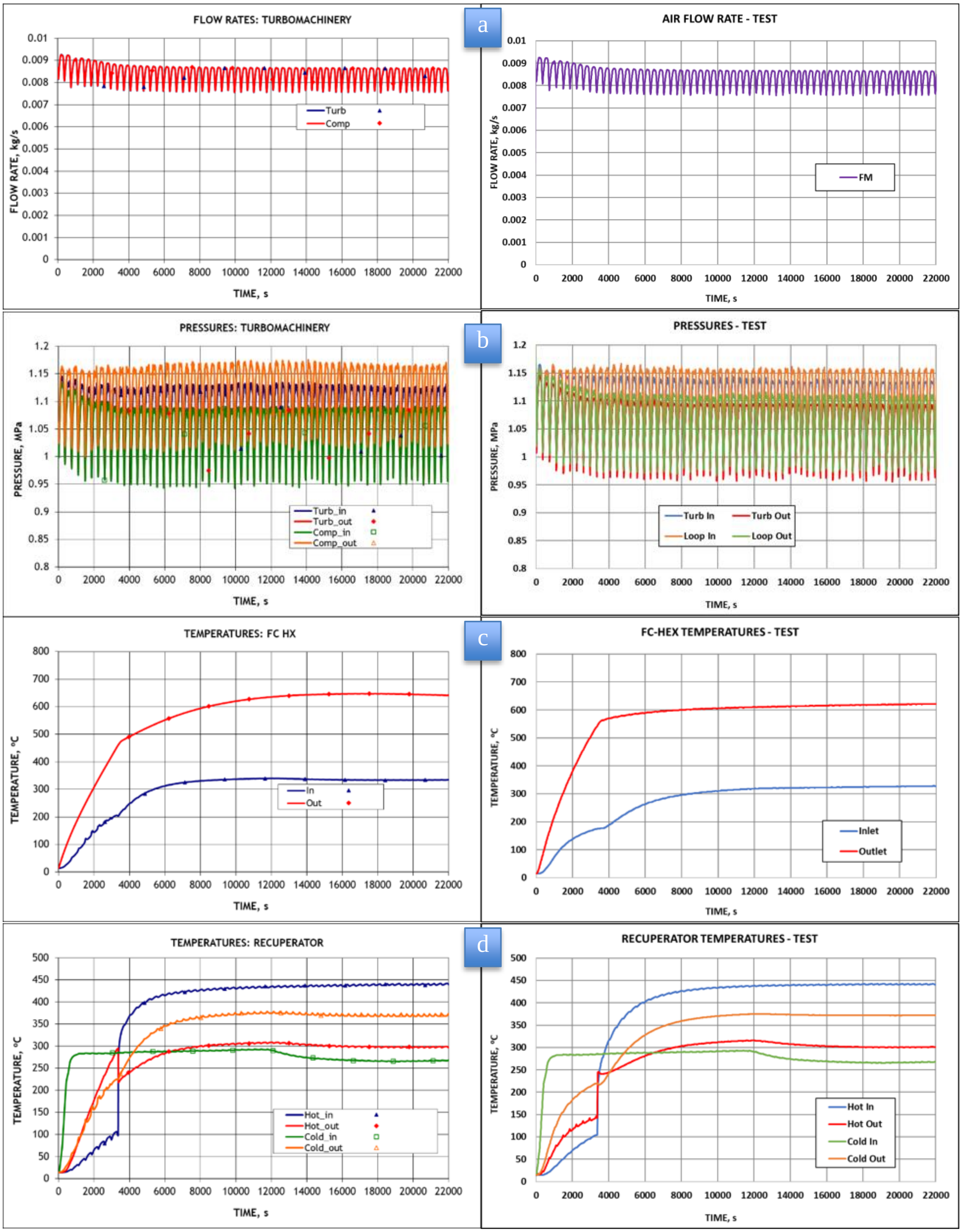
a
FLOW RATES: TURBOMACHINERY
FLOW RATE, kg/s
TIME, s
Turb
Comp
AIR FLOW RATE - TEST
FM
b
PRESSURES: TURBOMACHINERY
PRESSURE, MPa
Turb_in
Turb_out
Comp_in
Comp_out
PRESSURES - TEST
Turb In
Turb Out
Loop In
Loop Out
c
TEMPERATURES: FC HX
TEMPERATURE, °C
In
Out
FC-HEX TEMPERATURES - TEST
Inlet
Outlet
d
TEMPERATURES: RECUPERATOR
Hot_in
Hot_out
Cold_in
Cold_out
RECUPERATOR TEMPERATURES - TEST
Hot In
Hot Out
Cold In
Cold Out

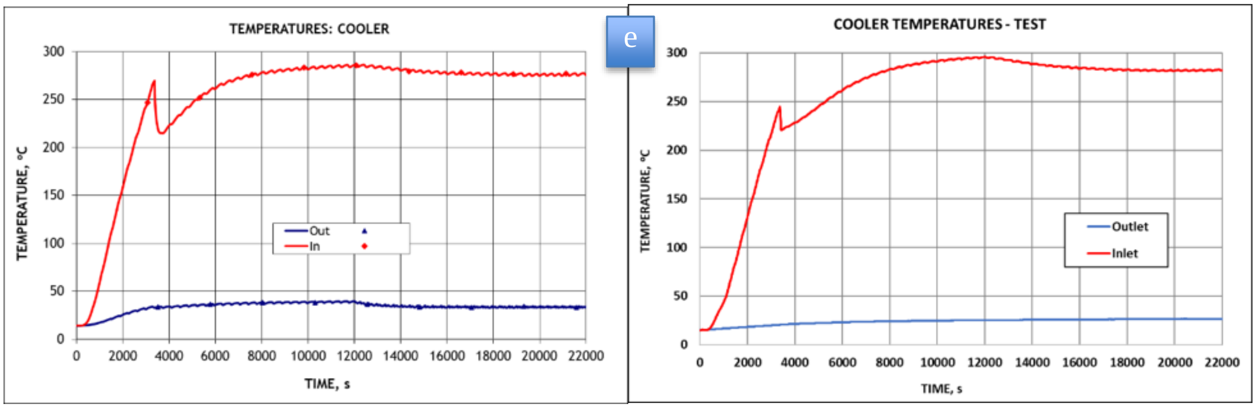

Figure 4.9. PDC Transient Results for Test 15 with Air: Full Component Masses.

4.4 Additional Air Tests

As discussed in previous sections, testing results when utilizing air for all tests starting from Test 15 are very similar. For this reason, complete analysis of air tests beyond Test 15 has not been carried out with PDC. However, some limited simulation of subsequent tests has been executed mostly to reflect loop modifications including improvements in insulation, sensors additions, troubleshooting and replacement of components that were affected by thermal-cycling. As an example of sensors troubleshooting, it was discovered that after Test 15 was completed, readings from some of the internal FC HX thermocouples was incorrect or unreliable. Upon inspection of the FC HX internals, the high-temperature leads of some thermocouples sampling temperature at specific location of the graphite matrix failed due to thermal-cycling as expansion and contraction from repeated cold startups physically pulled and corroded some of the thermocouples leads and terminals. As a result, all of the FC HX internal thermocouples were replaced, and the FC HX internal structures designs were modified to enable ample movement of the thermocouples leads resulting from thermal expansion/contraction. As the FC HX was upgraded with new sensors and engineering modifications were implemented to the FC HX structures, data sampling from this component became accurate and repeatable, thus eliminating errors and components failure due to thermal-cycling, these SPM-SS design improvements were also implemented in the full-scale Holos-Quad design.

To compare the PDC prediction of the internal FC HX temperatures with the test data, steady-state conditions for Tests 16 and 18 with air have been analyzed. The internal thermocouples in FC HX are shown in Figure 4.10. Two sets of thermocouples equip the FC HX: a series of heater wall thermocouples located on the outside of the heater rod elements at various axial locations (top figure), and a series of channel wall thermocouples located on the outside surface of coolant tubes. These thermocouples were included in the test to effectively characterize temperature field in the reactor simulation and heat transfer between coolant channels, graphite matrix, and heater rods representing fuel channels. In the PDC steady-state model, temperatures at the graphite block interfaces with the coolant channels and fuel (heater) channels are directly calculated at several axial locations. Note though that PDC uses a one-dimension model of a reactor component (Figure 2.1) such that the three-dimensional effects of the reactor (or FC HX) structure are not simulated in the code, thus the exact azimuthal location of the thermocouples is not necessarily matched by PDC.

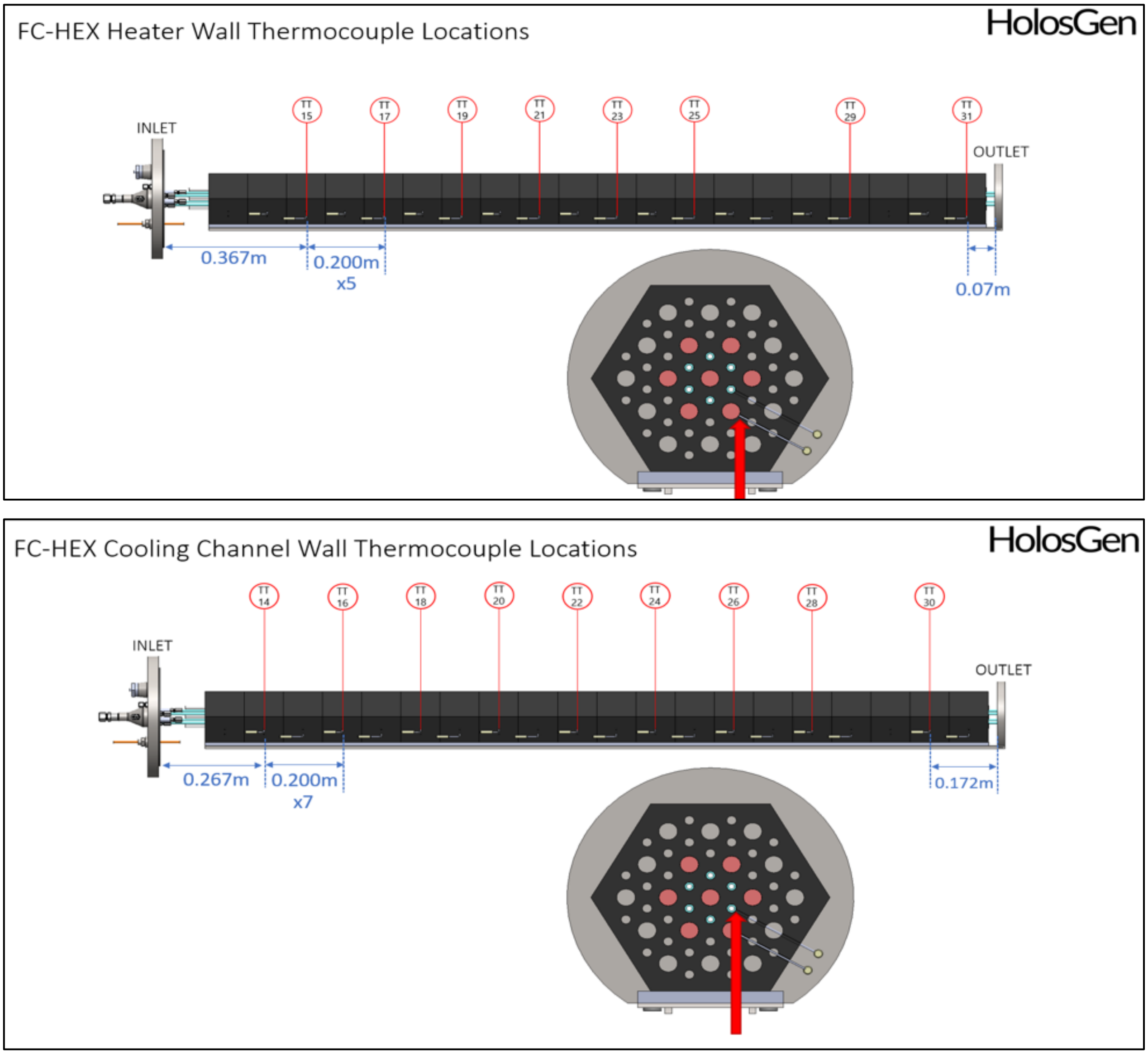

Figure 4.10. FC HX Internal Thermocouples.

4.4.1 *Test 16 with Air*

The long-term steady-state conditions in Test 16 are shown in Figure 4.11 for both the measured data and the PDC steady-state results. In general, both the test conditions and the agreement between the code and the data are very similar to those for Test 15 analyzed in Section 4.1. Therefore, the analysis of this test has focused on the temperatures inside the FC HX.

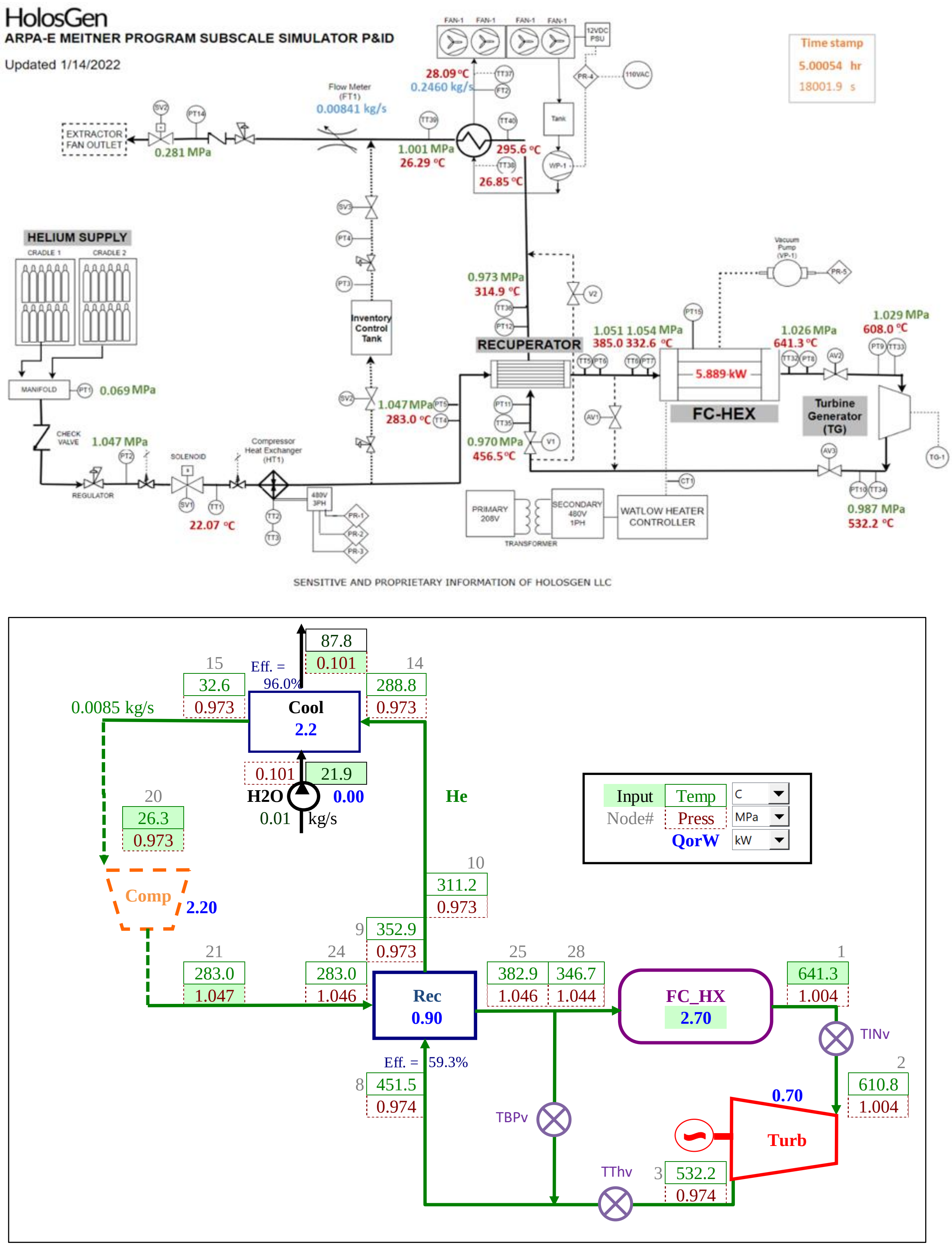

Figure 4.11. PDC Steady-State Results for Test 16 with Air.

The internal FC HX temperatures are compared in Figure 4.12 between the measured data and the PDC predictions. Two sets of internal thermocouples are also shown in Figure 4.10: outside coolant wall in blue and outside heater rod in red at their axial location along the FC HX length. The test data is shown in markers, while the PDC results are presented in lines. Several observations can be made from Figure 4.12. First, there is a noticeable difference, up to 100 °C, between the test results and the code prediction in the middle section of the FC HX. Also, the test data shows a noticeable drop in temperatures towards the end of the HX (a less noticeable drop is also shown at the other, cold, end of the FC HX in the test data). Since the electrical heater power was applied to the entire (2 m) length of the heaters in the FC HX, it is concluded that the reduction in the measured temperatures is attributed to *significant axial heat losses in the testing unit*, such as through the FC HX inlet and outlet flanges-(see Figure 2.2). This observation is confirmed by a greater reduction in temperatures on the hot side where higher temperatures would result in higher heat loss. Also, as shown in Figure 4.10, the outlet flanges are located closer to the graphite blocks than those at the inlet, further increasing heat loss on the hot edge (see "outlet edge" in Figure 2.2) of the FC HX. In PDC calculations, as described in Section 2.3, the heat loss is simulated to be in the radial direction only, and significant axial heat losses at both ends (Figure 2.2 FC HX inlet and outlet edges) could not be simulated in the code. Note though that the code assumes fixed heat transfer coefficient for heat loss and thus the heat loss will be higher for higher temperature – which is evident by the slight curvature of the PDC plots shown in Figure 4.12. However, the curvature is not sufficient to account for the axial heat losses in the test. Since the code could not predict higher axial heat losses at both ends of the FC HX assembly, it could not accurately reproduce the shape of the temperature curves. For the fixed inlet and outlet temperatures, different temperature curves would unavoidably result in the differences between the two curves in the middle of the FC HX, as demonstrated in Figure 4.12.

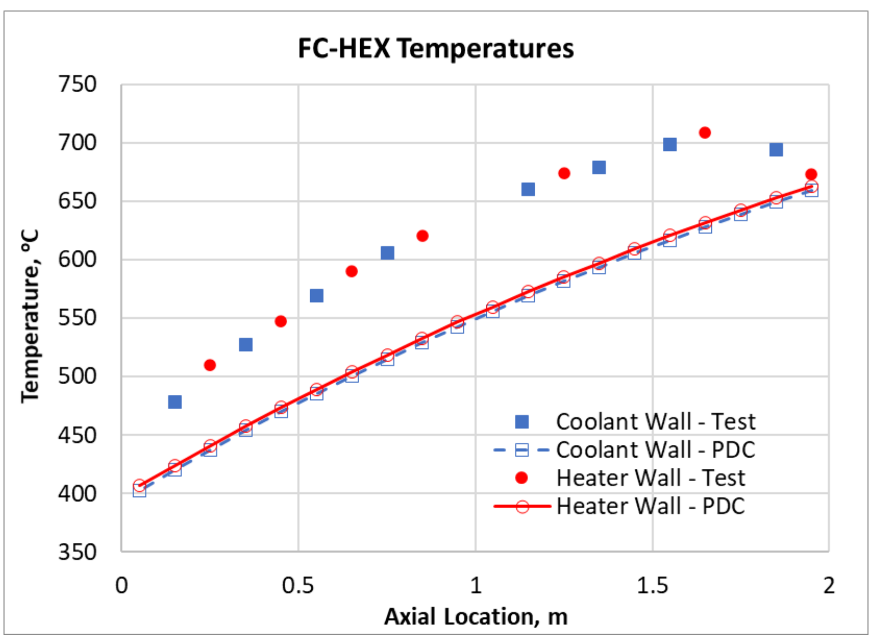

Figure 4.12. Internal FC HX Temperatures in Test 16 with Air.

However, the comparison in Figure 4.12 shows that the code accurately predicts a minimal difference between the coolant channel and the heater rod outside surfaces (difference between red and blues markers and lines). In both the test unit and the actual simulated reactor (SPM-SS FC HX), this difference represents the temperature rise though the graphite matrix. Therefore, the results in Figure 4.12 validate the heat conduction model used in PDC for the graphite matrix, even though it is a rather simplified model, with one-dimensional treatment of two channels in an infinite medium [13].

4.4.2 *Test 18 with Air*

In preparation of the project final helium Test 18, air was first circulated in the SPM-SS to bring the loop to target temperatures from cold start up. As a result, the "air portion" procedures adopted in previous tests was also repeated in Test 18. For this test, there were some modifications to the test loop. First, thermal insulation was improved for some pipes forming the balance of plant, additional thermal insulation was also implemented on the cooler. To eliminate heat losses from loop branches that were not needed for this particular test, the turbine bypass line was physically removed from the loop. This line was suspected to induce part of the heat loss in the recuperator-FC HX pipe (results in Test 18 confirmed small temperature drops in this pipe once the turbine bypass line was removed). The turbine (TG in Figure 1.2) was replaced with an air cooled high-pressure (7MPa) heat exchanger to increase control of the surrogate turbine outlet temperature (although this feature was not actively utilized in this test). Lastly, a measurement of ambient temperature has been added to better characterize heat losses from the SPM-SS loop to its surrounding environment.

The test conditions at the end of steady-state operations with air in Test 18 are shown in Figure 4.13, along with the PDC results. For this simulation, changes to the PDC input were made to reflect changes to the loop described above. Specifically, the heat loss in the recuperator-FC HX piping was re-adjusted to match the new loop configuration without the turbine bypass line (note that the code model still simulates the bypass line, although it will not be activated in the transients). Also, an attempt was made to increase data agreement on the cooler performance. For this part, the compressor inlet temperature was increased from the measured data (under an assumption that the readings from this thermocouple were incorrect) to match the water flow rate in the cooler. Note from Figure 4.13 that to achieve the heat balance in the cooler a significant adjustment to the cooler-outlet temperature, by 5 °C was needed. This temperature change is higher than the specified measurement uncertainty (see Section 1.2) and therefore indicates that the issues with the measured temperatures in the cooler are not justified by measurement uncertainties. As the SPM-SS rig is physically positioned within a closed room and substantial heat losses were identified through various loop components, the environment surrounding the SPM-SS loop was not at constant conditions during testing. Detailed tracing of heat losses and impact of the subsequent heat gains accrued by the closed environment surrounding the SPM-SS was beyond the scope of this project. However, future upgrades of the SPM-SS will include heat loss tracing and stabilizing the ultimate heat sink temperature to increase computer model predictions. Other than the changes in factoring the heat losses in the recuperator and FC HX piping as described above, the results of the PDC predictions for this test are similar to those observed in Tests 15 and 16.

The comparison for the FC HX internal thermocouples in this test is shown in Figure 4.14. These results are very similar to those for Test 16 in Figure 4.12, and no new conclusions or observations are made from these results.

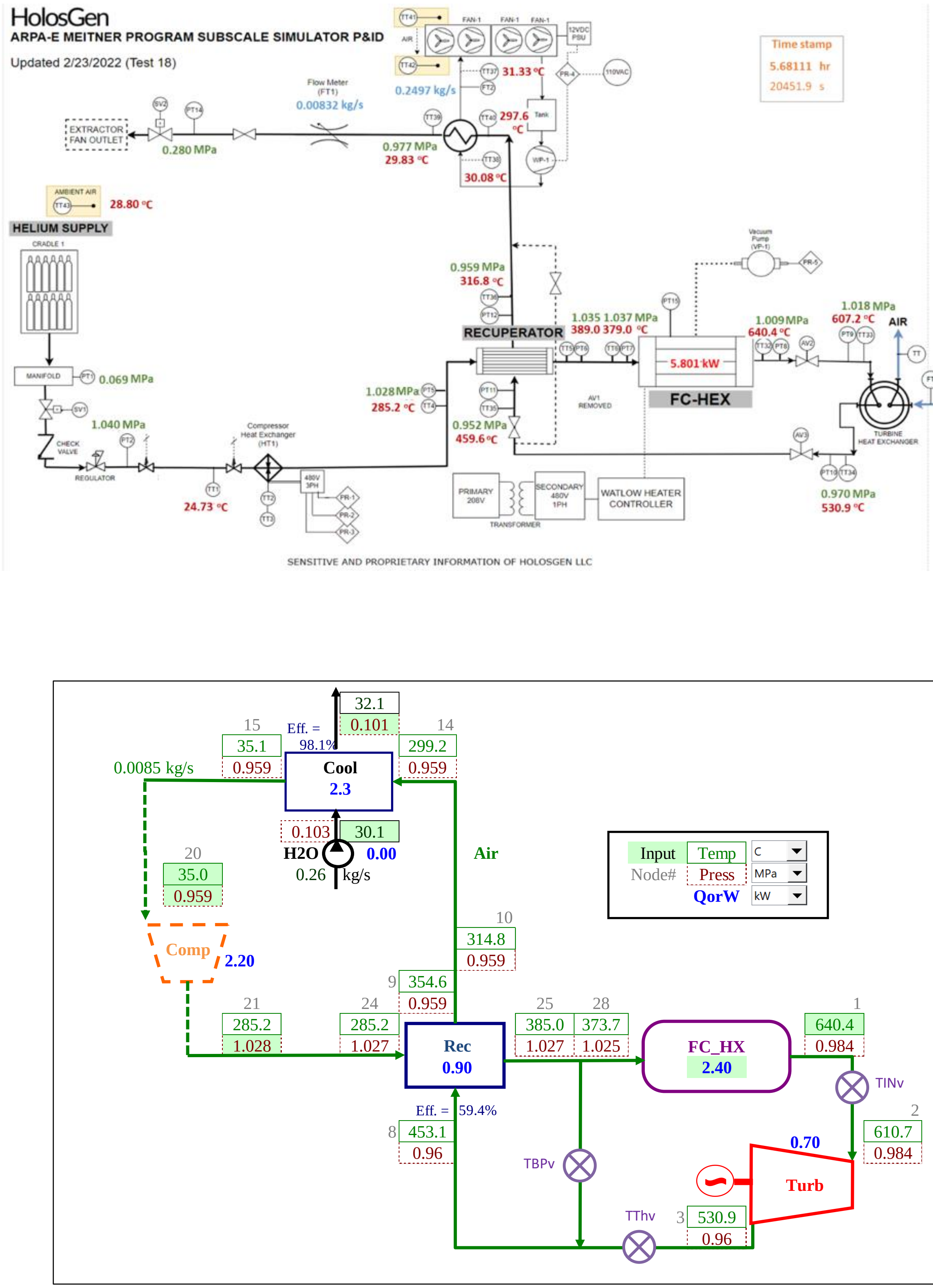

Figure 4.13. PDC Steady-State Results for Test 18 with Air.

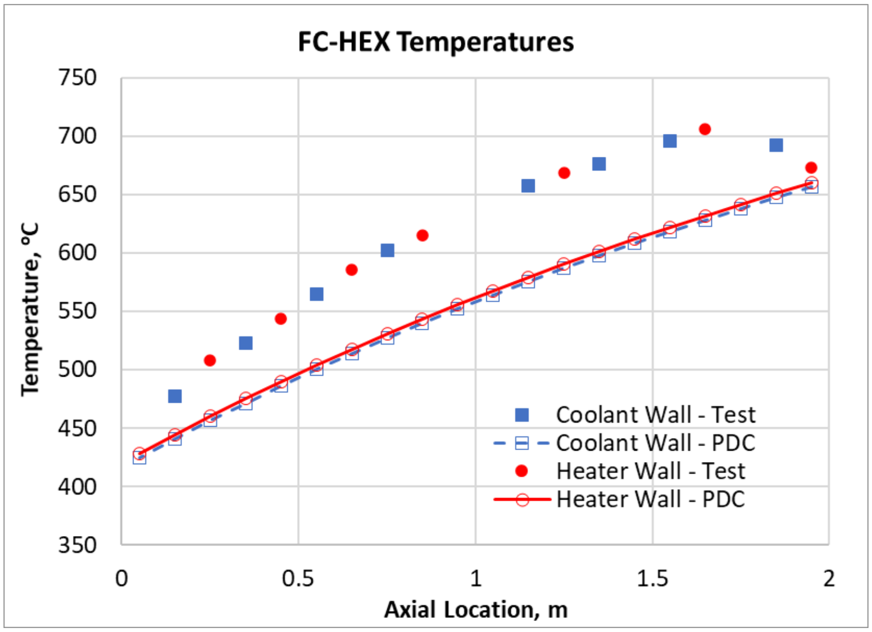

Figure 4.14. Internal FC HX Temperatures in Test 18 with Air.

4.5 Code-to-Code Comparison with SAM

The System Analysis Module (SAM) [18] was used to create a model of the FC HX with increased resolution for comparison with the simplified two-dimensional model used by the PDC. In the SAM model a three-dimensional representation of the FC HX was used to resolve the differing heat removal paths (air coolant channels and environmental heat loss). Coolant channels were modeled with one-dimensional components. As shown in Figure 4.15, the 1D fluid domain was tightly coupled to the 3D solid domain by transferring the calculated wall temperature from the solid domain to the fluid domain, and the fluid temperature and heat transfer calculated by SAM in the 1D fluid domain to the solid domain [19]. This coupling scheme is favored to a full 3D model because of the significant gains in computational efficiency associated with 1D fluid modeling while still producing a fully resolved model of the solid domain where 3D conduction is modeled with relatively low computational costs.

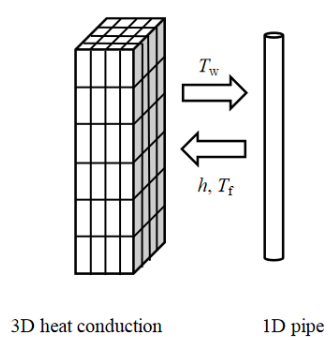

Figure 4.15 Coupling scheme in the 1D fluid-to-3D solid modeling approach. [19]

The solid domain in the SAM model used a true scale representation of the FC HX, shown in Figure 4.16. Axially the model was divided into 40 nodes. The long-term steady-state conditions in Test 16 (Section 4.4.1) were used for the code-to-code comparison between the SAM and PDC predictions. The boundary conditions for the coolant inlet temperature, mass flow rate, and heater power were taken from parameters indicated in Figure 4.11. The heat source was applied assuming a uniform power distribution in the heater rods. As described in section 2.3, the PDC accounted for environmental heat loss by appling a heat loss term, dependent on a prescribed $H{\cdot}P$ coefficient and an assumed environmental temperature, to the graphite matrix energy balance equation. In the SAM model, a convection boundary condition was applied at the outer perimeter with the same environmental temperature and H values that were used in the PDC model. An adiabatic boundary was used at the inlet and outlet faces of the FC HX. The material properties used in the PDC model for the heater elements, graphite matrix, and coolant channel sleeves (tubes) were copied into the SAM model. Air properties from an open source thermophysical property library [20] were used for the equation of state in the coolant domain.

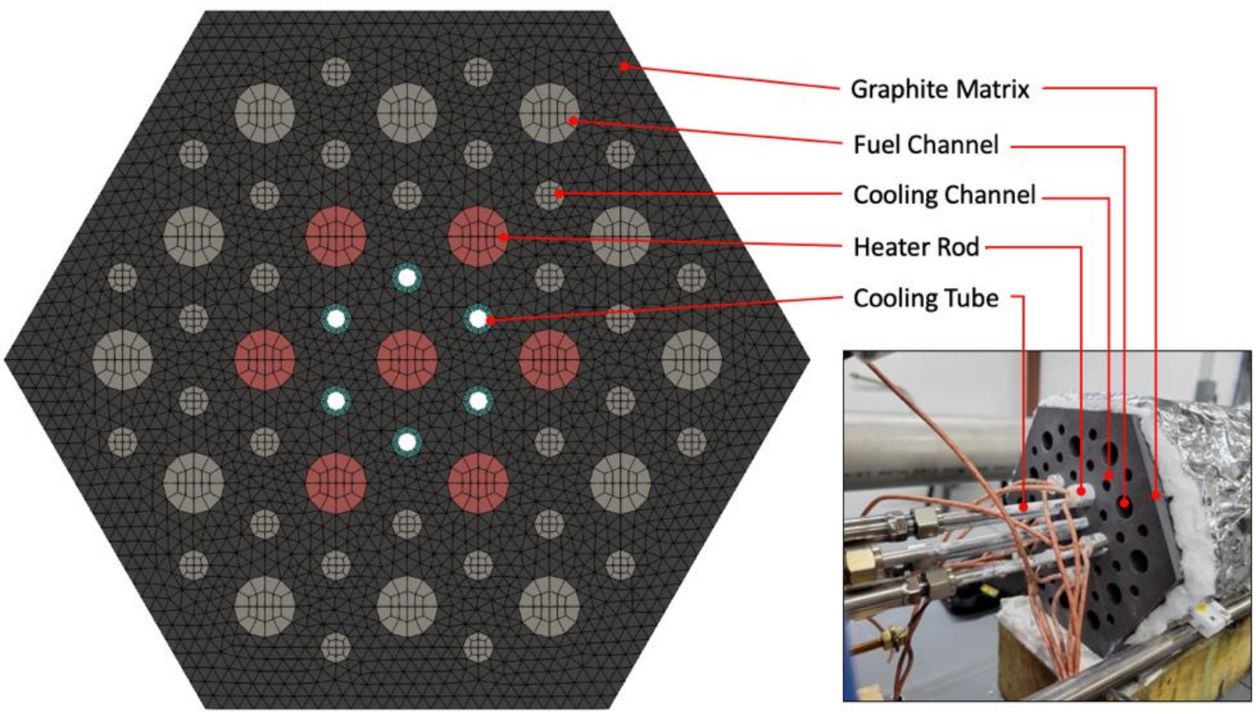

Figure 4.16 Cross Section of the SAM Mesh Used for the Solid Domain Model.

A comparison of the SAM and PDC results for Test 16 with Air as working fluid is shown in Figure 4.17 with temperature sampling locations for SAM results shown in Figure 4.18. In general, the comparison between SAM and PDC results shows a good agreement, especially considering the modeling limitations of the 2D PDC model. Much of this agreement is because the SAM model was created to replicate the physics as implemented in the PDC model to produce a more direct code-to-code comparison. For example, environmental heat losses were limited to the outer perimeter, and not the axial faces where significant losses are expected to occur during testing. In future work, efforts may be made to produce a SAM model that is more representative of the experimental SPM-SS loop by modeling axial heat loss and including the surrounding insulation in the solid domain representation of the FC HX.

At the same time, few differences between the SAM and PDC results can be observed in Figure 4.18. First, although the results for graphite temperatures agree for most of the axial points along the FC HX length, there are noticeable temperature deviations at both active surrogate core edges (see inlet and outlet edges of the FC HX cross-sectional graphite matrix shown in Figure 2.2). This is because the PDC models do not include axial heat transfer in their structures, and this heat transfer mode has the most pronounced effect near the boundaries. The second difference in Figure 4.18 can be seen in the coolant temperatures. This difference was attributed to air properties used in the two codes. As described in Section 2.1, current PDC formulations use a rather simplistic formulation for air properties, while in the SAM model, the equation of state was formulated by equations fit to a wide range of experimental data [21 ,22]. The results in Figure 4.18 demonstrate, though, that the difference in air properties only affects the intermediate results, while the overall heat transfer is consistent between the two codes, as shown by good agreement when comparing the inlet and outlet coolant temperatures. Lastly, a deviation between the predictions is observed on the temperature drop from the heater wall to the outer coolant channel wall (as better seen on the zoomed-in insert in Figure 4.18). At the midplane of the FC HX, the difference calculated by SAM is 1 °C while the PDC model calculates a 3.7 °C temperature drop. This can be explained by the difference in environmental heat loss implementation in each code. Because of the 2D implementation of the PDC code, environmental heat removal must be accounted for in the graphite matrix directly between the heater and coolant, increasing the temperature drop between the two components. In the 3D SAM model, environmental heat removal is accounted for at the outer graphite block surface of the FC HX. The relatively large distance from the outer surface to the interior heater rods and coolant channels decreases the impact of the environmental heat removal on the graphite temperature in this region. It should be noted that in Figure 4.17, the PDC "Outer_surface" curve shows the average graphite matrix temperature while the SAM "Outer_surface" curve shows the graphite temperature calculated at a location on the outer surface of the FC HX.

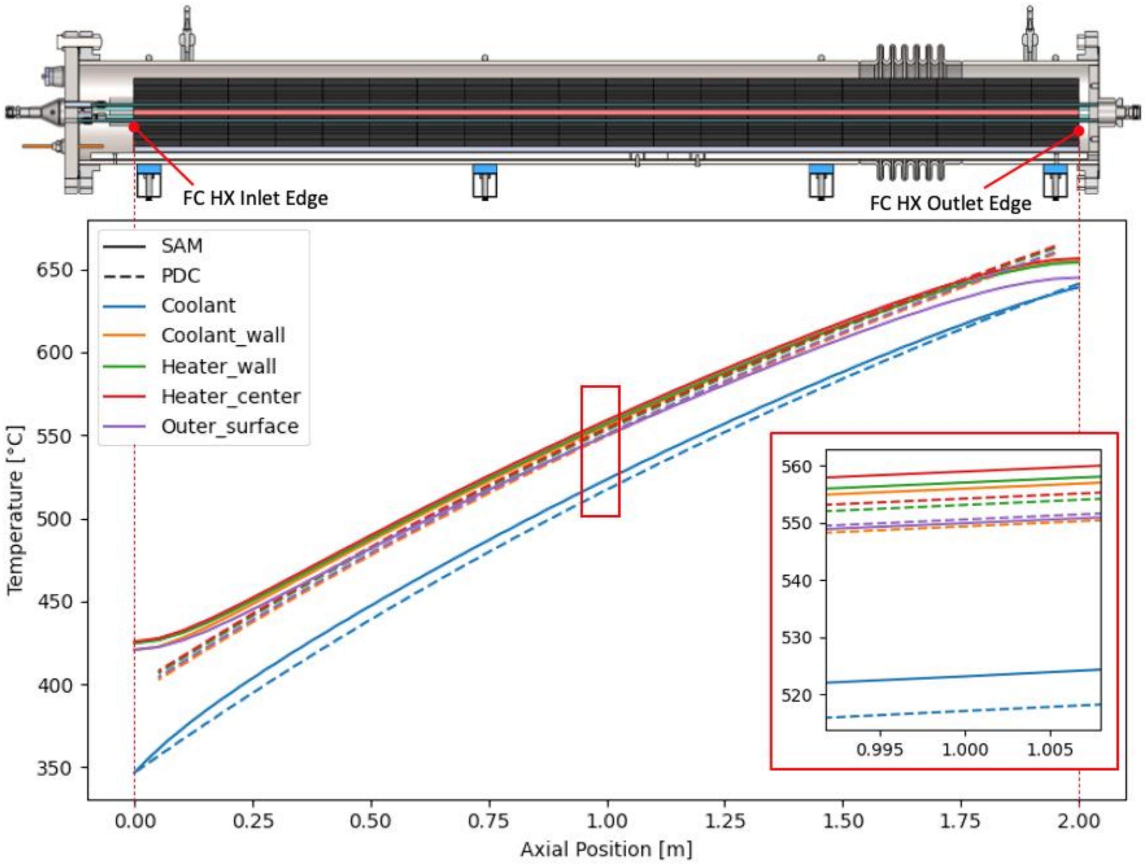

Figure 4.17 Comparison of Internal FC HX Temperatures in Test 16 with Air Calculated by SAM and PDC.

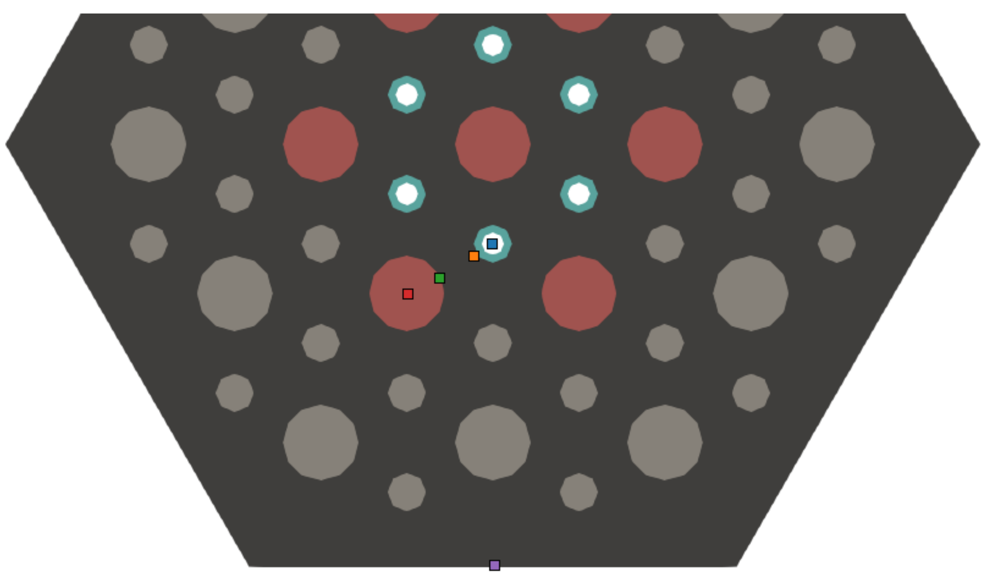

Figure 4.18 Temperature Sampling Locations Used to Measure SAM Results.

5 Analysis of SPM-SS Tests with Helium

As described in the introduction, there were practical limitations on the SPM-SS loop that precluded testing with helium for extended time durations. Testing the loop with air, as described in Chapter 4, demonstrated that the SPM-SS reaches full design conditions (e.g., at max operating temperature) after several hours of operations. In the SPM-SS loop configuration adopted in these tests, helium is provided by high-pressure tanks with the loop equipped with turbine and compressor heat exchangers to mimic the behavior of turbomachinery. As prolonged loop operations with helium were not possible, the following approach was adopted in the test procedure. At start up the loop was operated with air as working fluid circulating through the loop components to achieve desired design/test operating temperatures. Then, the air was evacuated from the loop and a vacuum was applied for some time to ensure that no air was left in the loop. Finally, a controlled helium flow was circulated through the loop at full design mass flow rate and pressure. This procedure effectively "hot swaps" the working fluids. The coolant swap procedure only required a few minutes, with the heaters turned off during this time. Swapping the working fluids causes an unavoidable temperature variation as pressurized helium has different heat transfer characteristics compared to air. Mainly for these reasons, the loop components steady-state conditions obtained with air could not be fully preserved.

The working fluid/coolant change procedure described above could not be simulated with PDC (the code was not designed to model hot swapping of working fluids). Therefore, the air and helium portions of the same test could only be analyzed in PDC as two independent tests. As such, when helium starts to circulate in the hot loop a new steady-state condition as a starting point for transient simulation had to be identified and simulated in PDC. As the helium tanks represent a finite working fluid inventory, the test duration is limited, thus steady-state conditions were not expected to be fully reached during helium tests. The impact of limited helium test time duration on the PDC simulation will be discussed below.

5.1 Test 16 with Helium as working fluid

After filling the loop with helium in Test 16, the helium pressures on the low side of the loop was brought up to 3.5 MPa, this is the Brayton cycle low-pressure of the full scale Holos-Quad design – see Figure 5.1. As this pressure value was reached, the loop was operated at these conditions, with a mass flow rate through the tubes corresponding to the mass flow rate through the sleeves of the full-scale Holos-Quad, until the helium supply tanks exhaust their helium inventory (around 0.3 hr mark in Figure 5.1). At this point, as the thank pressure was decreasing, the loop pressures decreased until it reached approximately 5 bar (0.5MPa), after which the test was terminated. Figure 5.1 also shows the measured helium temperatures at the FC HX inlet and outlet. Once the helium flow was established early in the test, the FC HX heaters were energized for the rest of the test in an automatic mode to reach and maintain the design temperature of 650 °C (measured through an internal heater thermocouple).

The data in Figure 5.1 shows that the helium tanks inventory enabled 0.7 hrs of testing time, with about 0.2 hrs (12 min) of loop operation at "quasi" steady-state. The depressurization phase of the test lasted approximately 0.4 hr (24 min) as part of the last portion of the test. For transient simulation and code predictions validation, the results in Figure 5.1 show that true steady-state conditions were not reached with the inventory of helium available in this test – as shown in this figure, both pressures and temperatures at 0.2 hr are still adjusting. Additionally, the pressure data in Figure 5.1 shows oscillations in the pressure at all measuring points. The inability to reach true steady state conditions with helium has important implications for transient boundary conditions, as shown for the air tests discussed above. In future research the SPM-SS will be equipped with a helium compressor which will enable to preserve the helium inventory in the loop for prolonged testing at true steady state conditions.

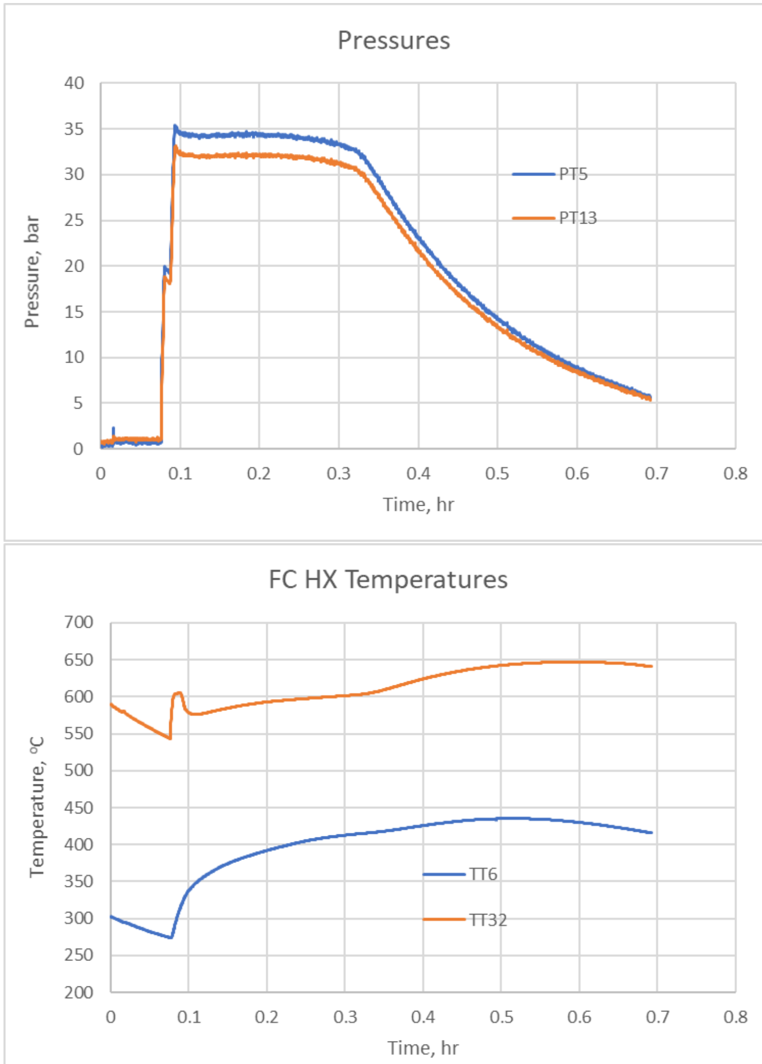

Figure 5.1. Test 16 with Helium.

5.1.1 *Simulation of "Quasi" Steady-State Conditions*

As demonstrated in Figure 5.1 above, true steady-state conditions were not reached in the helium Test 16. Still, PDC calculations require steady-state to define a stable starting point for transient analysis. Therefore, conditions that most accurately reflected steady-state conditions were selected from Test 16 data and simulated as "quasi" instead of "true" steady-state conditions in

PDC. Analysis of Test 16 data shown in Figure 5.1 identified quasi steady state conditions at approximately 0.3 hr into the test. These conditions were utilized for PDC steady-state simulation.

The tests conditions at 0.3 hr are shown in Figure 5.2 along with the PDC steady-state results. For the PDC steady-state simulation, only changes necessary to characterize the actual conditions (working fluid, heater power, boundary temperatures and pressures) were implemented in this analysis. No adjustment to the input, such as for the heat loss, was done in this simulation and all the inputs related to the loop configuration were retained from the analyses conducted on Test 16 with air as described in Section 4.4.1.

Even though true steady-state conditions were not reached in the test (for example, both the FC HX inlet and outlet temperatures in Figure 5.1 were still increasing at 0.3 hr), the results in Figure 5.2 still show a rather good agreement between the code predicted results and test data. By comparison, the most significant difference is an underestimation by the code of the helium flow rate by about 10% (0.0090 vs 0.00986 kg/s).

Still, it is important to note that the lack of true steady-state conditions in this test is expected to induce inaccuracies in the transient simulation. For example, if the internals of the FC HX are hotter than what would be reached in steady-state (as suggested by still increasing FC HX temperatures in Figure 5.1), the stored energy in the FC HX internal components will continue to be transferred to the coolant, thus changing the transient predictions. At the same time, as PDC is not designed to account for the stored energy represented by FC HX internals, the heat addition that would continue to be transferred to the working fluid until the system reaches steady state is not captured in the PDC transient simulation. For these reasons, code predictions validations via test data are more accurate when relied on prolonged testing of the SPM-SS with air as the working fluid reached steady state conditions without inventory and testing time limitations.

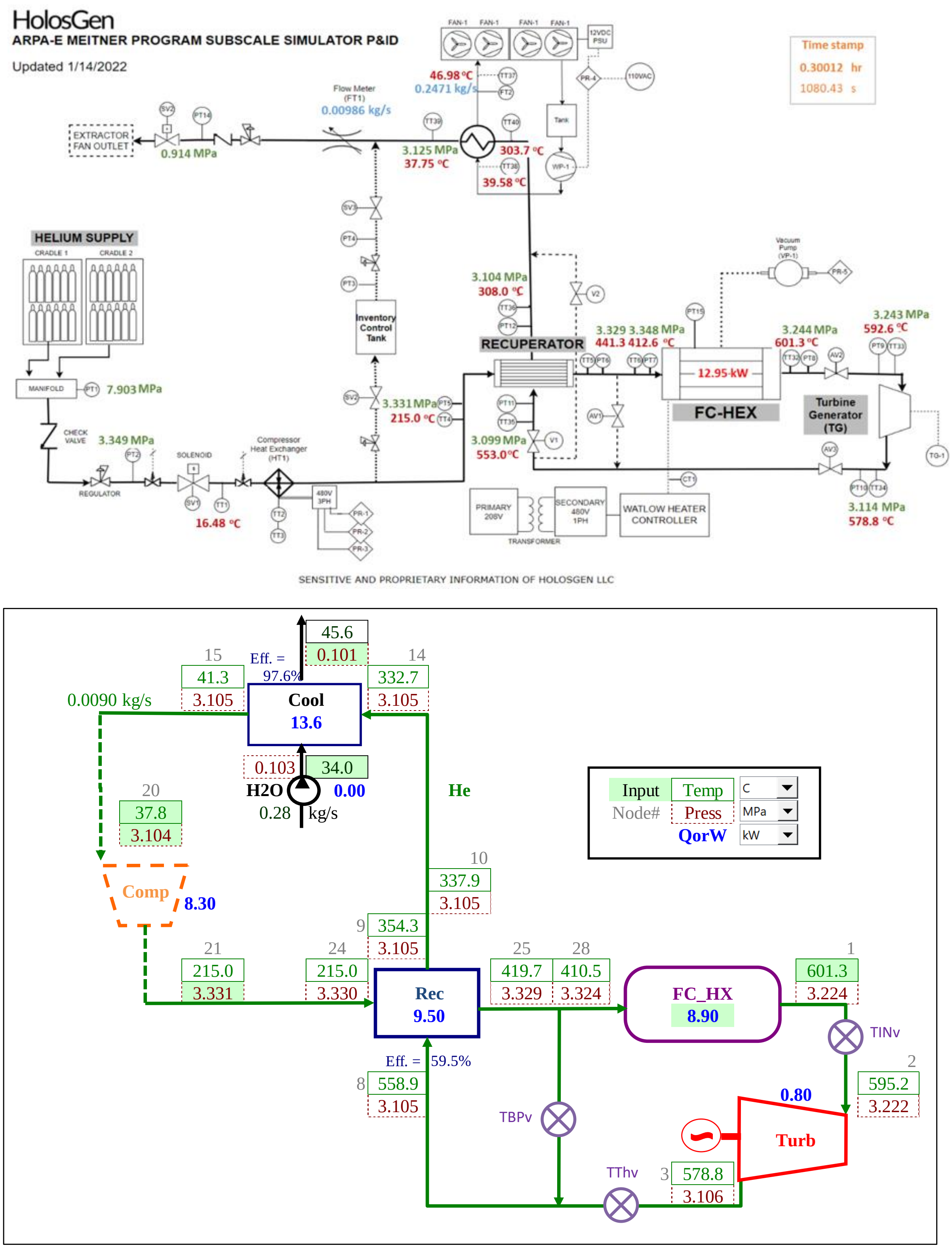

Figure 5.2. PDC Steady-State Results for Test 16 with Helium.

5.1.2 *Transient Simulation*

The transient simulation of Test 16 with helium was initiated in PDC from the starting conditions shown in Figure 5.2 and effectively covered the last depressurization phase of the test. This portion of the test lasted for about 0.4 hours, so the PDC transient simulation was carried out for equivalent 1400 s. The inputs for the transient simulation are the same as described in Section 4.3 for transient with air and shown in Figure 4.6. This input is based on the measured data from Test 16 with helium for this simulation. Note that in this simulation no correction to the component masses (analyzed in Section 4.3.2) was included in the PDC analysis since for this relatively short transient with quasi stable temperatures, the effect of heat capacity of external parts of the components is expected to be small.

The predicted results of the PDC transient simulation of Test 16 with helium are shown in Figure 5.3 in comparison with test data. Because the steady-state model predicted about 10% lower flow rate, the input for the PDC flow rate (Figure 5.3a) had to jump by the same 10% at the beginning of the transient simulation (unlike for the steady-state calculation, flow rate was an input for transient calculations). The rest of the PDC results, however, show that this jump did not significantly affect the rest of the code results. The loop pressures (Figure 5.3b) are accurately predicted during the loop depressurization, and especially for the difference between the orange and green line which represents the pressure drop in the entire loop. Both the recuperator (Figure 5.3c) and cooler (Figure 5.3e) temperatures are accurately predicted by the code.

The biggest difference between the code predictions and test results is shown for the FC HX outlet temperature in Figure 5.3d (red lines). Note that the inlet temperature (blue line) is predicted reasonably well. It is therefore concluded that the difference in the outlet temperature is not due to errors possibly induced by adopting quasi steady-state conditions. The results in Figure 5.3 and the analysis of the test data presented above suggest that there was an additional energy factor stored in the FC HX structures that was released to the coolant (and the loop) during the transient. As explained, the PDC is designed to start transient calculations at steady state conditions and does not capture energy stored in materials, thus the code did not predict an increase in the FC HX outlet temperature. Further supporting this conclusion is the fact that as time elapses during the depressurization phase, the test data starts to show a temperature reduction, thus approaching the temperatures calculated by PDC.

PDC Test

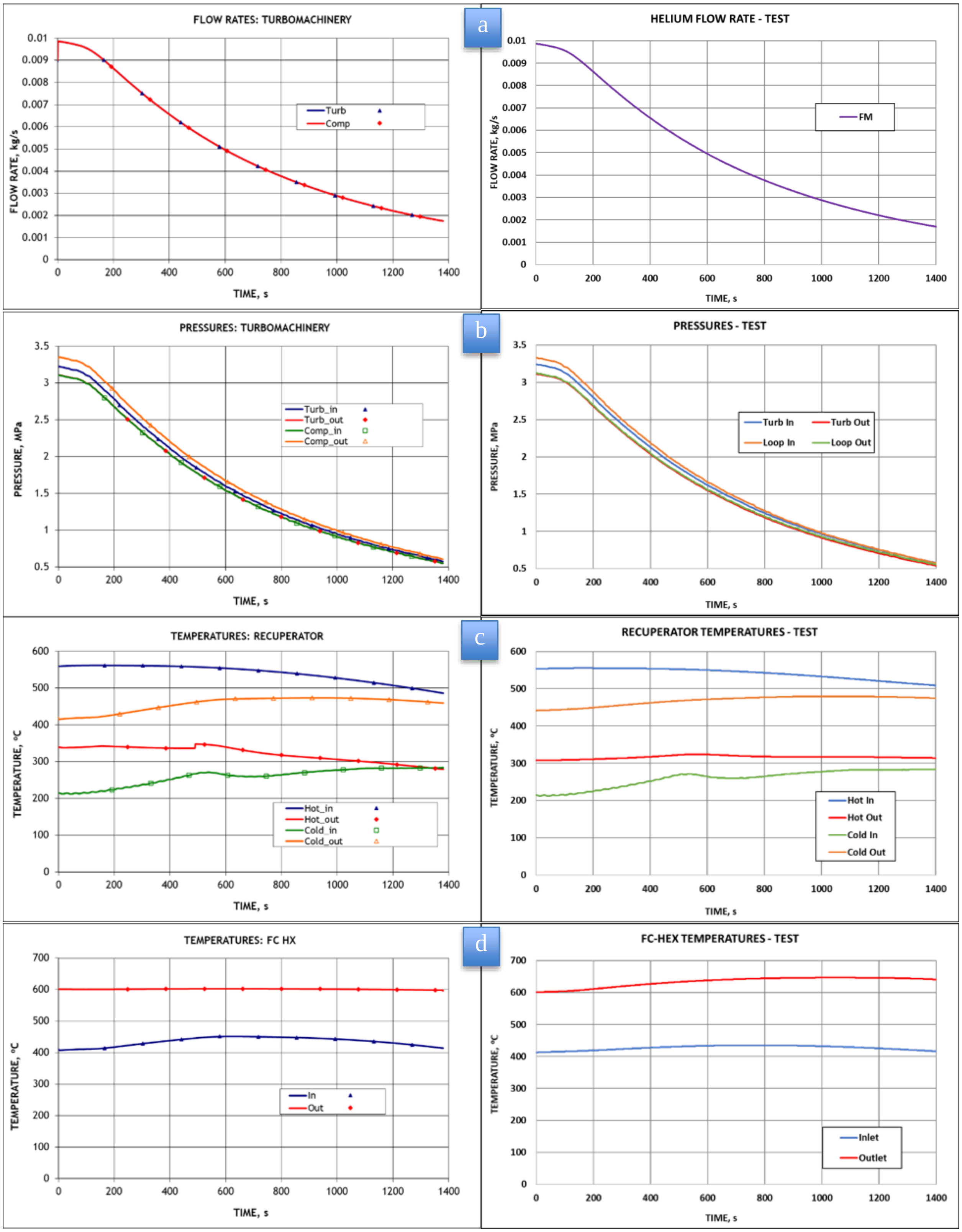
FLOW RATES: TURBOMACHINERY
FLOW RATE, kg/s
TIME, s
Turb
Comp
a
HELIUM FLOW RATE - TEST
FLOW RATE, kg/s
TIME, s
FM
PRESSURES: TURBOMACHINERY
PRESSURE, MPa
TIME, s
Turb_in
Turb_out
Comp_in
Comp_out
b
PRESSURES - TEST
PRESSURE, MPa
TIME, s
Turb In
Turb Out
Loop In
Loop Out
TEMPERATURES: RECUPERATOR
TEMPERATURE, °C
TIME, s
Hot_in
Hot_out
Cold_in
Cold_out
c
RECUPERATOR TEMPERATURES - TEST
TEMPERATURE, °C
TIME, s
Hot In
Hot Out
Cold In
Cold Out
TEMPERATURES: FC HX
TEMPERATURE, °C
TIME, s
In
Out
d
FC-HEX TEMPERATURES - TEST
TEMPERATURE, °C
TIME, s
Inlet
Outlet

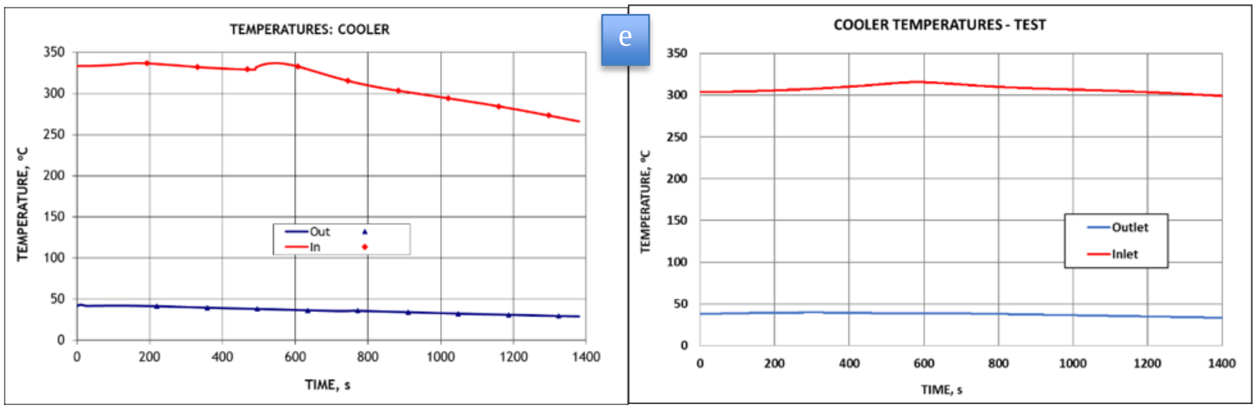

Figure 5.3. PDC Transient Results for Test 16 with Helium.

5.2 Test 18

Test 18 was the last test run with the sub-scale simulator loop at the completion of the HolosGen-ARPA-E project. In general, the results of Test 18 are very similar to Test 16 results. The biggest difference from Test 16 is that Test 18 was run at full scale Holos-Quad Brayton design helium pressure of 7 MPa on the high-pressure side, and a low-pressure side of 3.5 MPa was created by means of a turbine throttle valve. The measured pressures and temperatures in Test 18 with helium are shown in Figure 5.4. In this test, to simulate the turbine effect on the pressure, a throttling valve AV3 was partially closed. The position of this valve was adjusted during the initial 0.15 hrs of the test to obtain the low side pressure of approximately 3.5 MPa. Once the desired full-scale Holos-Quad pressures have been reached, the valve position remained unchanged for the remainder of the test.

Other than these differences, the progression of Test 18 with helium as SPM-SS working fluid is similar to that described for Test 16 described above. In Test 18 the loop was operated at the design conditions until the helium supply was exhausted and the pressures started to decrease. The entire test elapsed for about 0.7 hr. Because higher pressures (and higher helium flow rate) were achieved in Test 18, the limit of helium tank capacity was reached slightly earlier than in Test 16 – at 0.28 hrs instead of 0.3 hrs.

There were also some other (minor) changes to the loop configuration for Test 18. These changes and how they are accounted for in the PDC model are described in Section 4.4.2.

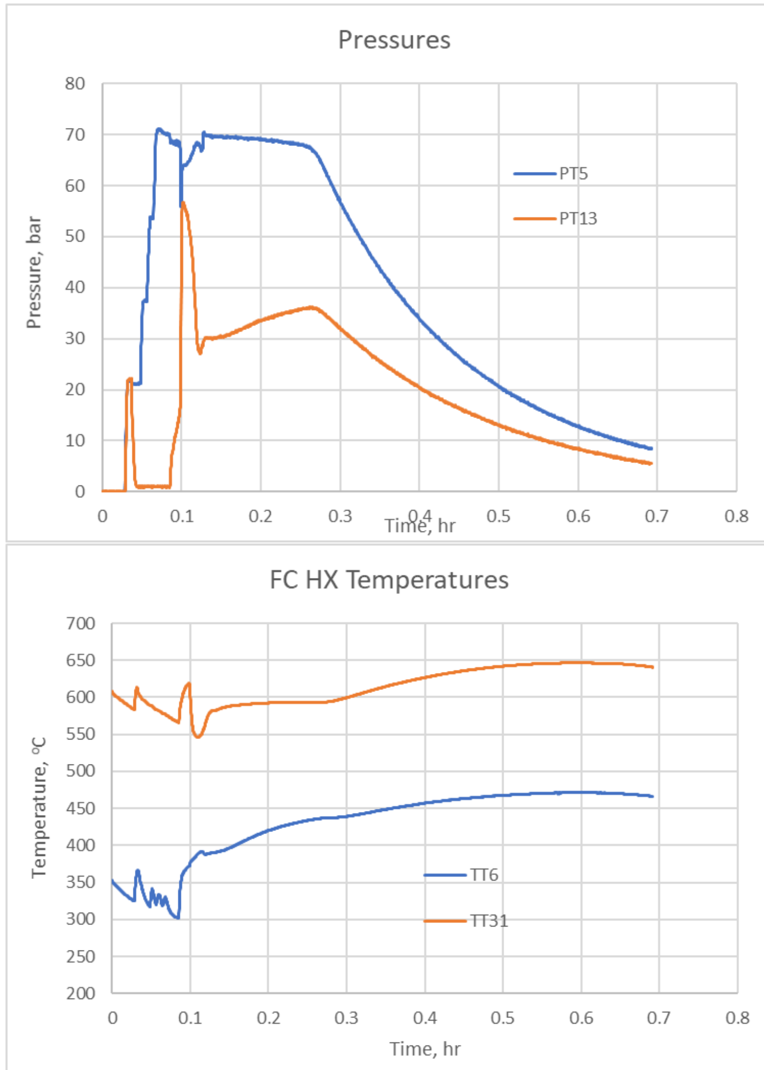

Figure 5.4. Test 18 with Helium.

5.2.1 *Simulation of "Quasi" Steady-State Conditions*

The steady-state simulation of Test 18 in PDC was similar to the simulation of Test 16. The conditions most closely representing steady-state, were identified at 0.28 hrs from the start of the test, and were selected for PDC analysis. Note though that, as shown by test data in Figure 5.4, there were still significant pressure adjustments at this stage, as the low side pressure (PT13) kept increasing until the tank capacity limit was reached. In this test, throttling valve AV3 was actuated and adjusted by an operator via user interface. In future research, the valve actuators will be automatically controlled to minimize off design pressure variations.

The comparison of the test conditions and PDC steady-state results at 0.28 hrs are shown in Figure 5.5. In general, the agreement between PDC predicted results and test data are similar to Test 16 results discussed previously. The most significant difference in Test 18 is in the helium flow rate. This time, the code overpredicted it by about 10%, 0.0123 kg/s in PDC vs 0.01099 kg/s sampled from SPM-SS loop instrumentation.

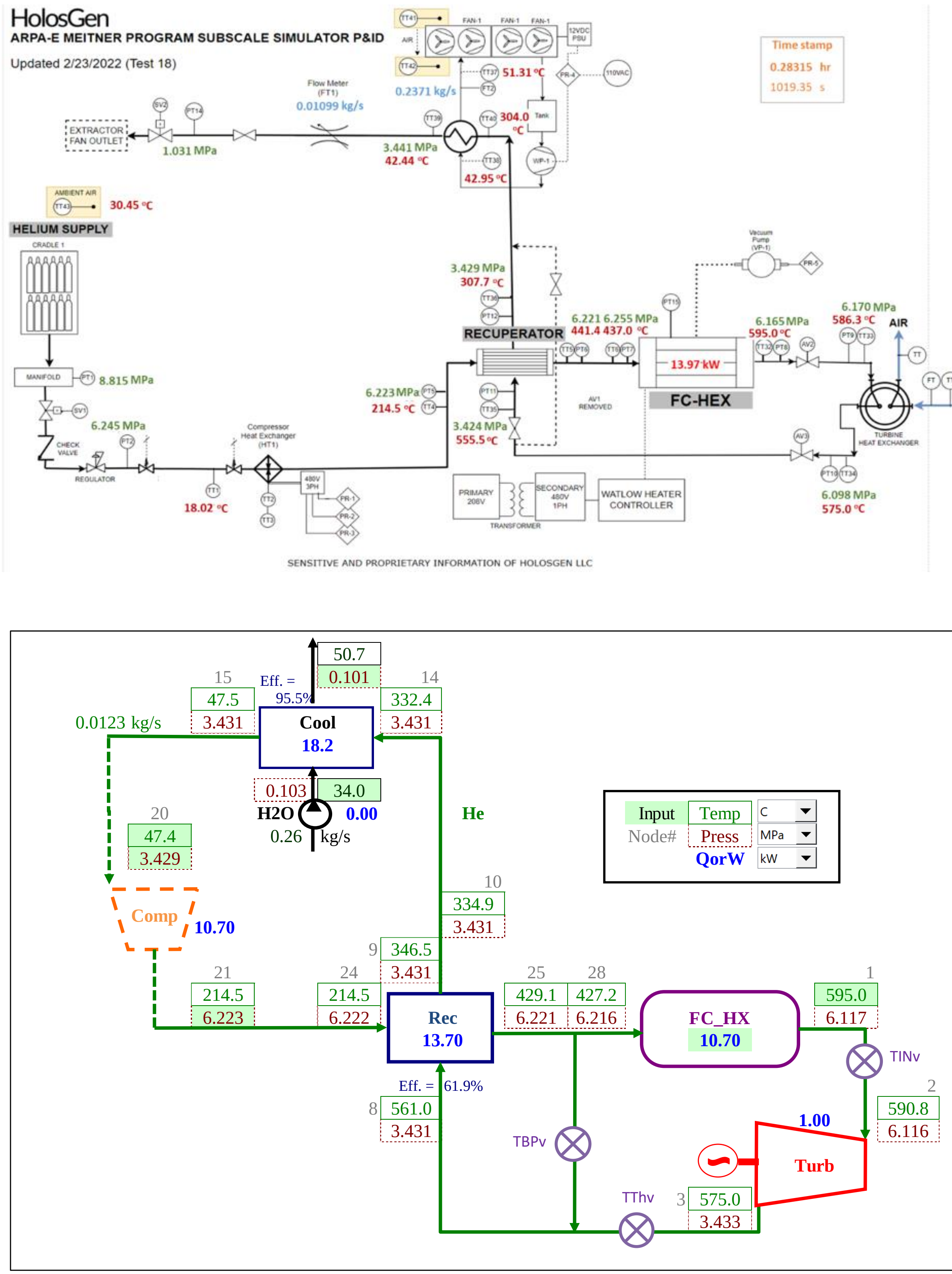

Figure 5.5. PDC Steady-State Results for Test 18 with Helium.

The comparison of the internal FC HX temperatures is shown in Figure 5.6. These results are similar to those obtained when air tests were performed. As shown, there is a larger difference between the code prediction and the test data. This result indicates that the internal FC HX structures are at higher temperature when the transient calculation starts than they would be if true steady-state conditions were obtained.

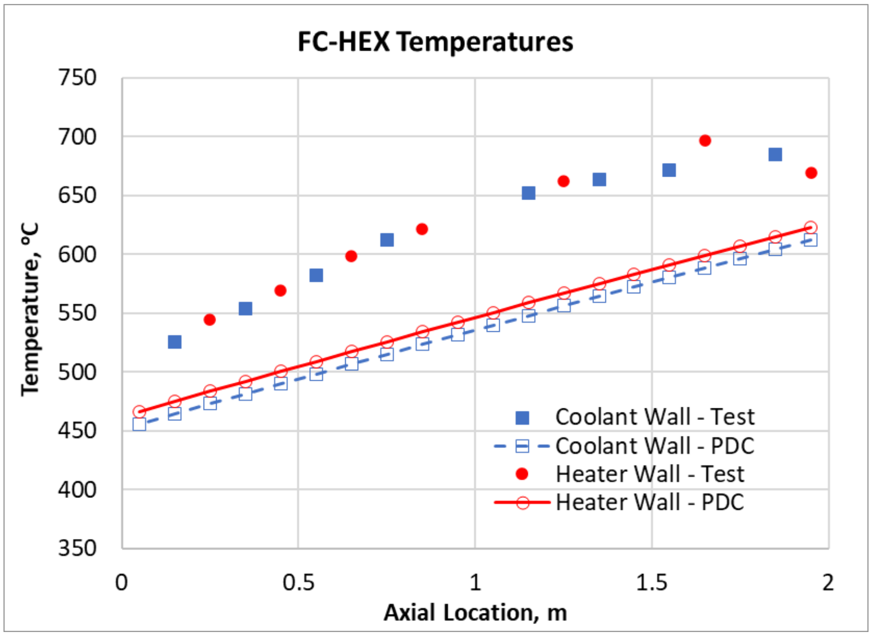

Figure 5.6. Internal FC HX Temperatures in Test 18 with Helium.

5.2.2 *Transient Simulation*

The input for the transient simulation in PDC of Test 18 was generated in a similar manner as for all other tests described in this report. The only difference was that the throttling valve pressure drop was included in the pressure change for the "turbine" map input in PDC (as this valve was used to simulate the pressure drop caused by the turbine).

The results of transient simulation for Test 18 with helium are shown in Figure 5.7. Again, the results are similar to those obtained previously for Test 16, except for higher pressures in the loop (Figure 5.7b). The helium flow rate in this simulation dropped by about 10% at the start of the transient (Figure 5.7a), but again this change has a very limited impact on other results. The FC HX outlet temperature (Figure 5.7c) shows less variation in the PDC results as it does in the test, which is again attributed to the SPM-SS loop not reaching true steady-state condition prior to starting transient calculations.

PDC Test

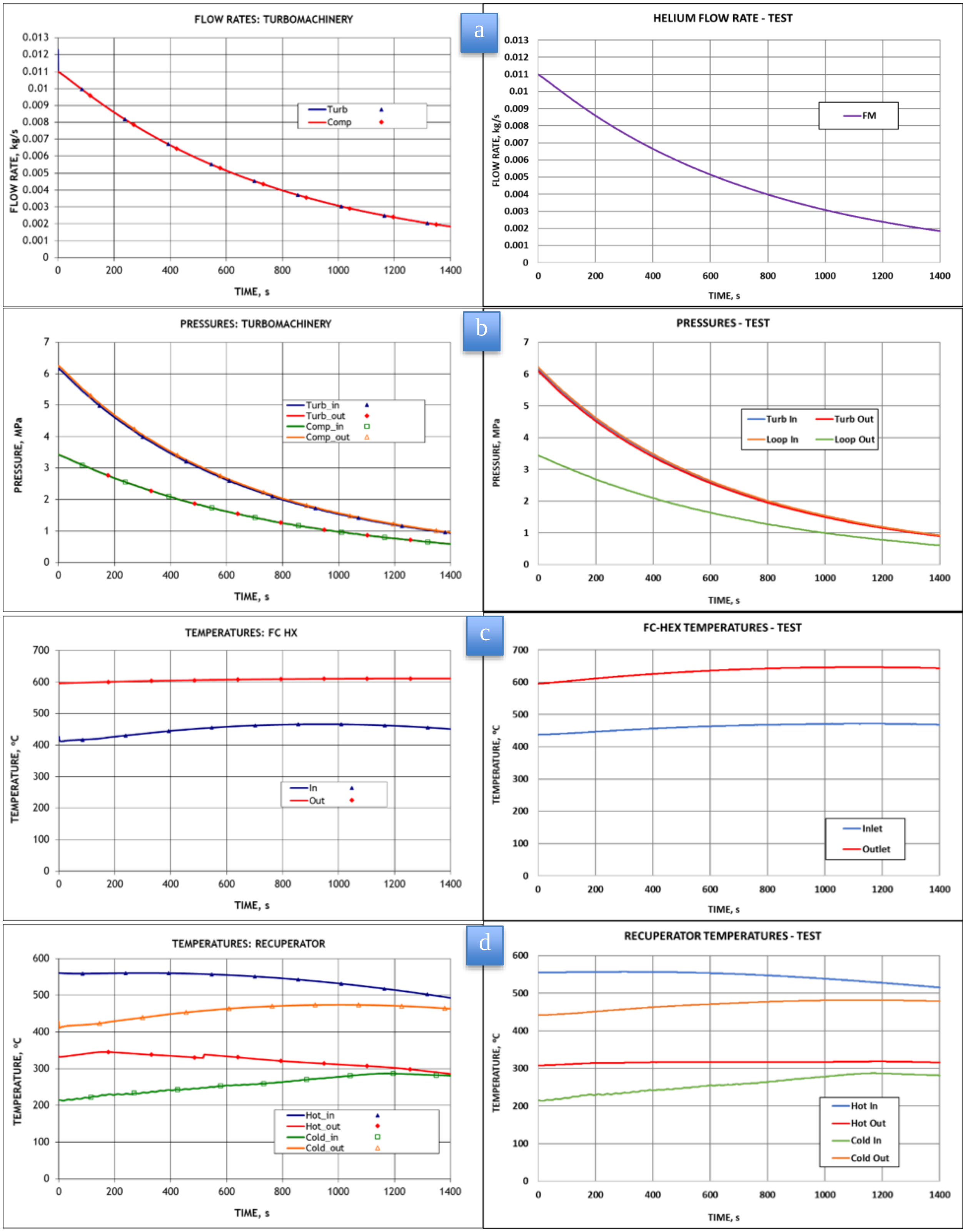
a
FLOW RATES: TURBOMACHINERY
FLOW RATE, kg/s
TIME, s
Turb
Comp
HELIUM FLOW RATE - TEST
FM
b
PRESSURES: TURBOMACHINERY
PRESSURE, MPa
Turb_in
Turb_out
Comp_in
Comp_out
PRESSURES - TEST
Turb In
Turb Out
Loop In
Loop Out
c
TEMPERATURES: FC HX
TEMPERATURE, °C
In
Out
FC-HEX TEMPERATURES - TEST
Inlet
Outlet
d
TEMPERATURES: RECUPERATOR
Hot_in
Hot_out
Cold_in
Cold_out
RECUPERATOR TEMPERATURES - TEST
Hot In
Hot Out
Cold In
Cold Out

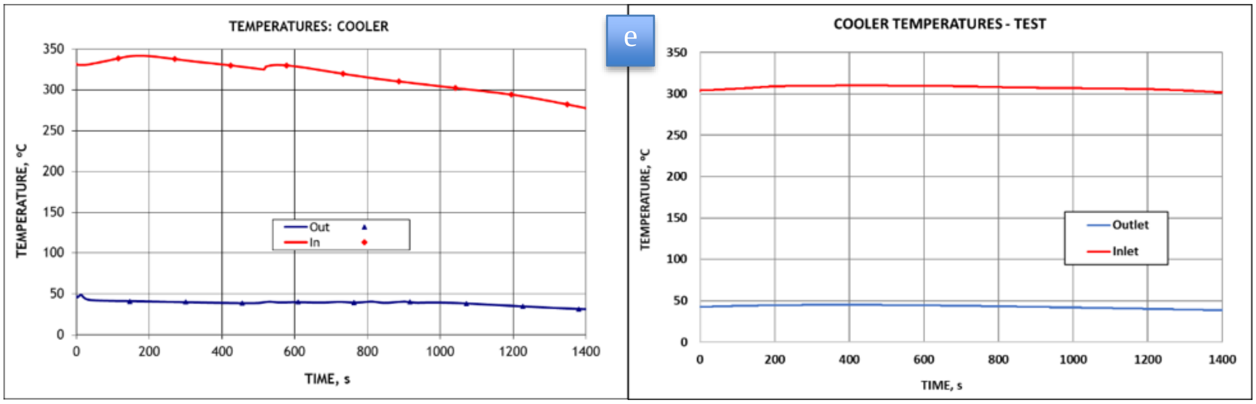

Figure 5.7. PDC Transient Results for Test 18 with Helium.

6 Summary and Interpretation of Results for the Full-Scale Holos-Quad System

A 40-kW level subscale simulator loop was constructed by HolosGen under the ARPA-E MEITNER program to simulate the performance of one of four identical 5.5 MW Holos-Quad sub-critical power modules. The center piece of the loop design is a Fuel Cartridge Heat Exchanger (FC HX) that simulates the reactor component of the full-scale system. The loop was operated with air, nitrogen, and helium to obtain experimental data at temperatures up to 650 °C and pressures up to 7 MPa.

The original intent of the sub-scale simulator was to obtain data to compare test data and validate the Plant Dynamics Code predictions to support the analysis carried out for the full-scale Holos-Quad design. Some specific loop characteristics utilizing limited amounts of helium prevented full code validation with test data for transient analysis when the loop was operated with helium, while code predictions were reasonably in agreement with transient test data when the loop utilized unlimited amounts of air for prolonged testing. Additionally, the small scale and low power rating of the simulator highlighted that heat losses for low power systems can be significant. Additional specific loop limitations were inherent as the lack of actual turbomachinery components, simulated by heat exchangers and actuated valves as the SPM-SS thermodynamic performance was beyond the scope of the project.

This report provides a description of the tests carried out with the Subcritical Power Module Subscale Simulator loop, pressure tested with nitrogen and operated with air and helium, and how these tests were modeled with the Plant Dynamics Code. In some cases, code modifications were introduced to address the specific features and limitations of the small-scale simulator loop. An example of these changes includes provisions for accounting heat losses in the heat exchangers and the reactor simulator, as well as treatment of turbomachinery maps to reflect the loop conditions during transients, to compensate for the lack of actual turbomachinery components.

Overall, a good agreement was obtained between the code predicted results and the test data, both in steady-state and transient simulations. For the steady-state analyses of various test cases, significant code input adjustment was needed to match the test data to properly account for the loop specifics, such as heat losses in pipes and components. During transient analyses, oscillations in measured pressure made it impractical to use the code’s ability to calculate working fluid flow rate based on pressure conditions. Instead, the transient calculations were carried out by providing the flow rate, and the flow equations in the code were indirectly verified by comparing pressure drops in the system (although those pressure drops were within the measurement uncertainty margins).

A brief discussion related to what has been achieved as part of testing and PDC predictions validation activities, and how these results are related to previous analyses of the Holos-Quad reactor design, is provided below.

6.1 Steady-State Design Conditions

As described in previous sections, the SPM-SS loop is designed to operate at the full-scale Holos-Quad design conditions, except for the maximum FC HX temperature, limited to 650°C due to materials limits of the electrical heaters utilized. The components forming the SPM-SS balance of plant and structures were developed in compliance with safety, high-pressure and high temperature requirements. As a result, the heat exchangers' pressure vessels or shells, as well as their flanges, baffles, headers, and internal structures represented relatively large masses with non-negligible thermal inertia with respect to the low power rating of the SPM-SS (<40kW). Additionally, the SPM-SS components' surfaces induced larger heat losses than expected relative to the low power rating. These aspects impacted transient behavior, for example, by increasing the time it takes for the system to achieve steady state conditions. Mainly for these reasons, when a limited inventory of helium was utilized for testing, the SPM-SS did not reach steady state conditions, making it challenging for the PDC to accurately predict transient performance. For the full-scale Holos-Quad SPM with a power rating of approximately 5.5MW, these factors are expected to be less pronounced - for large reactors these aspects are often neglected. The SPM-SS testing results, when compared with computer model's predictions, showed that the computer models of systems with relatively low power rating require detailed accounts of all masses, materials and heat transfer surfaces thermally coupled to the environment surrounding the test loop. As a result, codes originally developed to predict the performance of systems with power sources rated at several MW, require modifications when modeling very low power rating systems. These modifications aim at better capturing and increasing the accuracy of transients and heat loss for very low power rating systems. Modifying the PDC modules to include aspects related to systems with very low power rating was beyond the scope of the project and the effects induced by very low power system are less pronounced at the full-scale Holos-Quad power rating.

By adopting code modifications and considerations that addressed the impact of "robust" components (e.g., to safely operate at high temperature and 70 bar pressure) on heat loss and thermal transient analyses, important results have been achieved in this work. The performance of the Fuel Cartridge Heat Exchanger, which represents a scaled-down version of the full-scale Holos-Quad Subcritical Power Module reactor component, has been successfully simulated in tests and analyzed with PDC. The comparison of the code predictions with test data showed a good agreement for important modeling attributes such as pressure drop in coolant channels as well as for the temperature rise in the coolant channels, through the coolant tubes and in the graphite matrix. In addition, a transient response of the FC HX has mostly been simulated accurately with the code.

A performance of the recuperator (and cooler) heat exchangers, both in steady-state and in transients has also been confirmed by the code results. These results were obtained with a shell-and-tube heat exchanger, rather than a compact diffusion-bonded heat exchanger design selected for the full-scale Holos-Quad design.

The integral response and performance of the entire loop, such as pipe pressure drop and heat transfer in pipes and how the components interact with each other, and calculations of the working fluid flow rates have validated PDC predictions by accurately reflecting the actual test conditions. The code ability to model heat losses from pipes and other components has proven to be an important attribute for the test loop simulation, although the effect of these losses in the full-scale system is expected to be negligible.

The PDC results presented in this report show equally good agreement with the subscale loop test executed for both air and helium and provides high confidence that the code formulations are adequately general and fluid-independent, to scale to other systems, including systems with higher power ratings.

The SPM-SS was not intended to demonstrate the power generation performance of the full-scale Holos-Quad design. The development of turbomachinery components, representing at least one compressor and one turbine rated for a system with <40kW, would not meaningfully scale to the full-scale Holos-Quad SPM design rated at ~ 5.5MW. Mainly for these reasons, the SPM-SS thermodynamic performance was excluded from the scope of the project supported by the ARPA-E MEITNER program. The lack of actual subscale simulator turbomachinery components in the SPM-SS tests executed did not allow confirmation of the cycle efficiency calculations with PDC for the full-scale Holos-Quad design. HolosGen equipped the SPM-SS with a balance of plant and designed all of its components in a manner that allows increasing the power rating, and replacement of the heat exchangers and valves currently simulating turbomachinery, with actual turbomachinery components with higher power rating in future research.

6.2 Load Following Transients

Due to limitations of the subscale loop (rated at less than 40 kW), the exact representation of the load following transients analyzed for the full-scale Holos-Quad (whose individual Subcritical Power Module is rated at 5.5MW) were not carried out with the subscale loop. Scalability of turbomachinery performance from the very low power rating of the subscale simulator to the full-scale Holos-Quad design would have generated results with broad uncertainties. For these reasons, experimental validation of power generation from the subscale simulator was excluded from the scope of this ARPA-E MEITNER project.

However, the depressurization portions of Tests 16 and 18 with helium manifest strong similarities with the inventory control simulated with PDC for the full-scale Holos-Quad load following analysis [16,17]. In both these scenarios, helium is removed from the cycle, leading to a decrease in the system pressures. This pressure decrease resulted in the reduction of the helium flow rate, which was also observed in the subscale simulator loop tests. The load following analysis for the full-scale Holos-Quad design postulated a reactor operation with changing (reducing) power while maintaining the reactor-outlet temperature constant, even if the helium flow rate is decreasing. This reactor operation mode was directly simulated in both Tests 16 and 18, where the FC HX heater power was set to decrease by automatic control to maintain loop target temperatures.

The overall good agreement obtained for all components and the entire loop between the PDC transient results and the test data demonstrate that the code accurately predicts the full-scale Holos-Quad behavior under inventory control action. These results are important because the load following analysis identified the inventory control as the preferable control mechanism for the Holos-Quad load following.

Additionally, the code ability to match the tests data during a long-term heat up transient provides confidence that the code predicts slow transients well, such as operation during decay heat removal mode. The code model of the subscale simulator proved to be capable of predicting the effect of the recuperator bypass flow initialization and termination in the most extreme scenario (from full bypass to zero bypass). This particular result validated the control action modeling in PDC, which is used in every transient simulation by the code.

7 Recommendations for Future Work

Based on the analyses presented in this report, including the analysis of the small-scale loop capabilities, data analysis from multiple test cases with different working fluids, and simulations with the Plant Dynamics Code, the following recommendations for future work are made. These recommendations are separated in terms of the testing and analysis needs, although validation work, testing and analysis produce better results when carried out in close coordination.

7.1 Testing

Turbomachinery components are the components most sensitive to scaling, as turbine and compressor designs (and performance) are expected to be significantly different at kW and MW scales. Operations of a subscale simulator with relatively high-power rating, preferably near 1 MW, including helium-specific turbomachinery components were beyond the scope of the ARPA-E MEITNER project. Adding helium-specific turbomachinery components to the loop will enable full cycle analysis and prolonged loop operations to increase the accuracy of steady-state (cycle efficiency) and transient (cycle control) analyses. Furthermore, uprating the subscale simulator will mitigate or eliminate the effects associated with heat losses and thermal inertia of components' housing and supporting structures generally negligible for large systems.

Therefore, in future testing the subscale simulator should be uprated and equipped with turbomachinery specifically designed to operate with helium at power rating that, although sub-scale with respect to the full-scale Holos-Quad system, minimizes generally large inefficiencies characteristic of kW range systems. Future testing activities should include both the overall turbomachinery performance characterization (efficiency and performance maps), as well as reliability and endurance performance of turbomachinery supporting components such as bearings and seals operating with helium.

In addition to uprating and equipping the loop with turbomachinery equipment, future subscale simulator testing should be conducted by replacing the tube-and-shell heat exchangers with printed circuit heat exchangers (PCHE), designed, fabricated, and tested at power rating that enable accurate scaling to the full-scale Holos-Quad microreactor PCHE. Depending on funding availability, testing should include the full-scale Holos-Quad SPM PCHE units for the recuperator, cooler and intercooler, especially provided that these full-scale units are relatively small (recuperator PCHE size: 0.6 m x 0.6 m x 1 m). The thermal hydraulic performance of these heat exchangers, however, does not necessarily need to be tested with helium, as helium behaves as an ideal gas and its heat transfer characteristics are well known, testing with other working fluids will be possible.

Lastly, future testing will need to include characterization of automatic control elements, such various valve types operating in helium at high-temperature and pressures. These tests should include subjecting these components to repeated thermal cycles to test the ability of these components to reliably execute actuations after several simulated cold start-ups conditions (maximum thermal fatigue).

7.2 Modeling and Analysis

On the analysis side, two important aspects have been identified in this work. First, the assumption that the heat losses in components are small need to be re-evaluated for micro-reactors. Even though the heat losses are still expected to constitute a much smaller fraction of total power compared to those observed in the subscale test, at the ~5 MW level of Holos-Quad, these heat losses may not be negligible. In the tests analyzed in this work, at ~40 kW power rating, losses as high as 70% of the component heat transfer rate were observed. Even though it is expected that the losses would not be scaling linearly with system power, larger external surface areas for larger components, plus higher operating temperatures, may result in losses constituting a larger fraction of total power. Although the full-scale Holos-Quad design is not equipped with a traditional balance of plant, a detailed analysis of expected heat losses for the full-scale system is recommended. If the full-scale analysis reveals that the heat losses are significant, further model development in PDC will need to include considerations of energy loss by subcomponents whose heat loss contribution is normally considered negligible. This development might consist of simple corrections as implemented in this work, or it could include more sophisticated models to calculate and analyze the heat losses of full-scale components and include the effect of such losses on the performance of the full-scale plant. These considerations apply to all microreactors designs, particularly to those relying on traditional balance of plant where the increased distance from the core and power conversion components, combined with these components' masses and heat losses will increasingly impact steady-state and transient behavior of these systems.

The analysis of the heat-up transient revealed that external component masses, as represented by heat exchanger shell, headers and flanges, or reactor vessel, could play a significant role in the progression of transients involving significant temperature changes, such as a cold startup. Analyzing such transients with PDC will require amendments of code formulations to include components structures and their effect on the transient response of the components and the overall plant. These code changes might not only improve predictions of micro-reactors performance, but also that of larger systems.

Acknowledgements

The manuscript has been created by UChicago Argonne, LLC, Operator of Argonne National Laboratory ("Argonne"). Argonne National Laboratory's work is supported by U.S. Department of Energy (DOE) under Contract number DE-AC02-06CH11357. The work described in this report has been funded by ARPA-E MEITNER project under a Resource Team arrangement. The authors are grateful to Rachel Slaybaugh and Robert Ledoux, the MEITNER Program Managers at ARPA-E.

The authors want to express their gratitude to Ryan Cunningham, Nicholas Dodson and the entire HolosGen testing team for their continuous effort during the entire work presented in this report to keep improving the test data and going an extra mile in meeting the requests from the analysis team.

Finally, the authors will be forever grateful of Jim Sienicki of Argonne. Jim passed away during this project, but still made a significant contribution early in this work to define the testing requirements for the Holos-Quad design for modeling validation.

References

1. ARPA-E HolosGen Transportable Modular Reactor project, https://arpa-e.energy.gov/technologies/projects/ transportable-modular-reactor, 2021.

2. Moisseytsev, A., Sienicki, J., Zou, L. and Filippone, C., "Helium Brayton Cycle Design and Analysis for the Holos-Quad Micro Reactor." Proceedings of American Nuclear Society 2020 Winter Meeting and Nuclear Technology Expo, Chicago, IL, November 15-19, 2020.

3. Moisseytsev, A. and Filippone, C., "Load Following Analysis of the Holos-Quad Micro Reactor." Submitted to American Nuclear Society 2021 Winter Meeting and Nuclear Technology Expo, Washington, DC, November 30-December 4, 2021.

4. Moisseytsev, A., Sienicki, J. J., “PDC: Plant Dynamics Code for Design and Transient Analysis of Supercritical Brayton Cycles,” ANL-ART-154, Argonne National Laboratory, September 30, 2018.

5. Moisseytsev, A. and Sienicki, J. J., “Simulation of IST Turbomachinery Power-Neutral Tests with the ANL Plant Dynamics Code,” 6th International Symposium - Supercritical CO_2 Power Cycles, Pittsburgh, PA, March 27-29, 2018.

6. Moisseytsev, A. and Sienicki, J. J., “Simulation of S-CO_2 Integrated System Test with ANL Plant Dynamics Code,” 5th International Symposium - Supercritical CO_2 Power Cycles, San Antonio, TX, March 28-31, 2016.

7. Moisseytsev, A. and Sienicki, J. J., “Lessons Learned and Improvements in ANL Plant Dynamics Code Simulation of Experimental S-CO_2 Loops,” PowerEnergy2015-49182**,** Proceedings of ASME Power & Energy 2015, San Diego, CA, June 28-July 2, 2015.

8. Moisseytsev, A. and Sienicki, J. J., “Validation of the ANL Plant Dynamics Code with the SNL S-CO_2 Loop Transient Data,” GT2013-94893, *Proceedings of ASME Turbo Expo 2013, GT2013*, San Antonio, Texas, USA, June 3-7, 2013.

9. Moisseytsev, A. and Sienicki, J. J., “Progress Report on Dynamic Simulation of the Sandia Small-Scale Supercritical Carbon Dioxide Brayton Cycle Test Loop with the ANL Plant Dynamics Code,” ANL-ARC-249, Argonne National Laboratory, September 25, 2012.

10. Moisseytsev, A., Sienicki, J. J., Cho, D. H., and Thomas, M. R., “Comparison of Heat Exchanger Modeling with Data from CO_2-to-CO_2 Printed Circuit Heat Exchanger Performance Tests,” 2010 International Congress on Advances in Nuclear Power Plants (ICAPP 10), San Diego, CA, June 13-17, 2010, paper 10123.

11. Moisseytsev, A. and Sienicki, J. J., “Analysis of SNL Compressor Tests,” ANL-GenIV-136, Argonne National Laboratory, June 9, 2010.

12. Moisseytsev, A. and Sienicki, J. J., "Analysis of Small Scale S-CO_2 Compressor Tests for ANL Plant Dynamics Model Validation," ANL-GenIV-118, Argonne National Laboratory, June 1, 2009.

13. Moisseytsev, A., "PDC Modifications for Analysis of Gas-Cooled Reactors with Direct Helium Brayton Cycle," ANL/NSE-21/31, Argonne National Laboratory, May 9, 2021.

14. The Engineering Tool Box, Air Properties, http://www.engineeringtoolbox.com/22_156.html

15. Thermal Design: Heat Sinks, Thermoelectrics, Heat Pipes, Compact Heat Exchangers, and Solar Cells by HoSung Lee, John Wiley & Sons, Inc., 2010.

16. Moisseytsev, A., "Load Following Analysis of HolosGen Reactor with Plant Dynamics Code," ANL/NSE-21/32, I Argonne National Laboratory, May 10, 2022.

17. Moisseytsev, A. and Filippone, C., "Load Following Analysis of the Holos-Quad Micro Reactor." Submitted to American Nuclear Society 2021 Winter Meeting and Nuclear Technology Expo, Washington, DC, November 30-December 4, 2021.

18. Hu, R., et al., "SAM Theory Manual," ANL/NE-17/4, Rev. 1, Argonne National Laboratory (2021).

19. Zou, L and Hu, R., "Recent SAM Code Improvement to Heat Transfer Modeling Capabilities," ANL/NSE-19/46, Argonne National Laboratory, December 2019.

20. Bell, I. H.; Wronski, J.; Quoilin, S.; Lemort, V. Pure and Pseudo-pure Fluid Thermophysical Property Evaluation and the Open-Source Thermophysical Property Library CoolProp. Ind. Eng. Chem. Res. 2014, 53, 2498−2508.

21. CoolProp, Air Properties, http://www.coolprop.org/fluid_properties/fluids/Air.html

22. Lemmon, E., et al., Thermodynamic Properties of Air and Mixtures of Nitrogen, Argon, and Oxygen from 60 to 2000 K at Pressures to 2000 MPa. *J. Phys. Chem. Ref. Data*, 29(3):331–385, 2000. doi:10.1063/1.1285884.

Nuclear Science and Engineering Division
Argonne National Laboratory
9700 South Cass Avenue, Bldg. 208
Argonne, IL 60439-4842

www.anl.gov

Argonne National Laboratory is a U.S. Department of Energy
laboratory managed by UChicago Argonne, LLC